On the Power of Randomization in Big Data Analytics

Phạm Đăng Ninh

Theoretical Computer Science Section

IT University of Copenhagen, Denmark

A thesis submitted for the degree of

Doctor of Philosophy

31/08/2014

Acknowledgements

No guide, no realization.

First of all I am deeply grateful to Rasmus Pagh, a very conscientious advisor that I could ever ask or even hope for. He is patient enough to take the time to listen to my ideas, good as well as bad, and to share his thoughts, basic as well as advanced. He is open-minded enough to guide me to find such a good balance between computational algorithms and data analysis, which inspired the principle of the thesis contribution. Rasmus is not only a superb teacher but also a great colleague.

A special thank you goes to Hoàng Thanh Lâm, a very enthusiastic friend, who provided me constant support and encouragement, from comments on finding the PhD scholarship and preparing specific research background - to discussions about data mining challenges and advices on how to grow scientific research network. Without his help my PhD would have remained incomplete.

I also thank to my colleagues, Thore Husfeldt, Jesper Larsson, Konstantin Kutzkov, Nina Sofia Taslaman, Andrea Campagna, Morten Stöckel, Troels Bjerre Sørensen, Francesco Silvestri, Tobias Lybecker Christiani. It is my pleasure to discuss with you about both research topics and life experience.

A big thank you goes to my co-author Michael Mitzenmacher for letting me work with him and learn from him.

I gratefully acknowledge IT University of Copenhagen, which provided me a very nice working environment and the Danish National Research Foundation, which gave me the financial support.

I am also grateful to John Langford for his hospitality during my visit at NYC Microsoft research. I also thank the Center for Urban Science and Progress (CUSP) for being my host at New York City and receiving me so well.

I would like to express my gratitude to my close friends, Lê Quang Lộc, Nguyễn Quốc Việt Hùng, Mai Thái Sơn for sharing their PhD

experience, and my Vietnamese friends from Technical University of Denmark, University of Copenhagen, and Liễu Quán temple, who made my PhD journey pleasant and memorable.

I would like to thank Aristides Gionis and Ira Assent for accepting to be the external members of my assessment committee and Dan Witzner Hansen for chairing the committee.

Last, but not least, I would like to thank my parents, Phạm Sỹ Hỷ and Lê Thị Thanh Hà, with their great upbringing and support throughout my life.

Ninh Pham,
Copenhagen, July 3, 2014

Abstract

We are experiencing a big data deluge, a result of not only the internetization and computerization of our society, but also the fast development of affordable and powerful data collection and storage devices. The explosively growing data, in both size and form, has posed a fundamental challenge for big data analytics. That is how to efficiently handle and analyze such big data in order to bridge the gap between data and information.

In a wide range of application domains, data are represented as high-dimensional vectors in the Euclidean space in order to benefit from computationally advanced techniques from numerical linear algebra. The computational efficiency and scalability of such techniques have been growing demands for not only novel platform system architectures, but also efficient and effective algorithms to address the fast-paced big data needs.

In the thesis we will tackle the challenges of big data analytics in the algorithmic aspects. Our solutions have leveraged simple but fast randomized numerical linear algebra techniques to approximate fundamental data relationships, such as data norm, pairwise Euclidean distances and dot products, etc. Such relevant and useful approximation properties will be used to solve fundamental data analysis tasks, including outlier detection, classification and similarity search.

The main contribution of the PhD dissertation is the demonstration of the power of randomization in big data analytics. We illustrate a happy marriage between randomized algorithms and large-scale data analysis in data mining, machine learning and information retrieval. In particular,

- We introduced *FastVOA*, a near-linear time algorithm to approximate the variance of angles between pairs of data points, a robust outlier score to detect high-dimensional outlier patterns.
- We proposed *Tensor Sketching*, a fast random feature mapping for approximating non-linear kernels and accelerating the training kernel machines for large-scale classification problems.

- We presented *Odd Sketch*, a space-efficient probabilistic data structure for estimating high Jaccard similarities between sets, a central problem in information retrieval applications.

The proposed randomized algorithms are not only simple and easy to program, but also well suited to massively parallel computing environments so that we can exploit distributed parallel architectures for big data. In future we hope to exploit the power of randomization not only on the algorithmic aspects but also on the platform system architectures for big data analytics.

Contents

Chapter 1

Introduction

We are experiencing a big data deluge, a result of not only the internetization and computerization of our society, but also the fast development of affordable and powerful data collection and storage devices. Recently e-commerce companies worldwide generate petabytes of data and handle millions of operations every day. Google search engine has indexed trillions of websites, and received billions of queries per month. Developed economies make increasing use of data-intensive technologies and applications. From now on there are more than 2 billion of Internet users, and the global backbone networks need to carry tens of petabytes of data traffic each day.

The explosively growing data, in both size and form, has posed a fundamental challenge of how to handle and analyze such tremendous amounts of data, and to transform them into useful information and organized knowledge. Big data analytics to bridge the gap between data and information has become a major research topic in recent years due to its benefits in both business and society. With more information, businesses can efficiently allocate credit and labor, robustly combat fraud, and significantly improve the profit. Large-scale analysis of geospatial data has been used for urban planning, predicting natural disaster, and optimizing energy consumption, benefiting society as a whole.

Finding elements that meet a specified criterion and modeling data for useful information discovery are the most fundamental operations employed in big

data analytics. Scanning and evaluating the entire massive data sets to find appropriate elements or to learn predictive models are obviously infeasible due to the high cost of I/O and CPU. In addition, such big data can only be accessed sequentially or in a small number of times using limited computation and storage capabilities in many applications, such as intrusion detection in network traffic, Internet search and advertising, etc. Therefore the efficiency and scalability of big data analytics have been growing demands for not only novel platform system architectures but also computational algorithms to address the fast-paced big data needs.

In this thesis we will tackle the challenges of big data analytics in the algorithmic aspects. We design and evaluate scalable and efficient algorithms that are able to handle complex data analysis tasks, involving big data sets without excessive use of computational resources. In wide range of application domains, data are represented as high-dimensional vectors in the Euclidean space in order to benefit from computationally advanced techniques from numerical linear algebra. Our solutions have leveraged simple but fast randomized numerical linear algebra techniques to approximate fundamental properties of data, such as data norm, pairwise Euclidean distances and dot products. These relevant and useful approximation properties will be used to solve fundamental data analysis tasks in data mining, machine learning and information retrieval.

The proposed randomized algorithms are very simple and easy to program. They are also well suited to massively parallel computing environments so that we can exploit distributed parallel architectures for big data. This means that we can trade a small loss of accuracy of results in order to achieve substantial parallel and sequential speedups. Although the found patterns or learned models may have some probability of being incorrect, if the probability of error is sufficiently small then the dramatic improvement in both CPU and I/O performance may well be worthwhile. In addition, such results can help to accelerate interacting with the domain experts to evaluate or adjust new found patterns or learned models.

The thesis consists of two parts. The first one will present fundamental background of high-dimensional vector in the Euclidean space, and core randomized techniques. The second part contains three chapters corresponding to the three contributions of the PhD dissertation. It illustrates the power of randomization in

wide range applications of big data analytics. We show how advanced randomized techniques, e.g. sampling and sketching, can be applied to solve fundamental data analysis tasks, including outlier detection, classification, and similarity search. In particular,

- In Chapter 3, we show how to efficiently approximate angle relationships in high-dimensional space by the combination between random hyperplane projection and sketching techniques. These relationships will be used as the outlier scores to detect outlier patterns in very large high-dimensional data sets.

- Chapter 4 represents how advanced randomized summarization techniques can speed up Support Vector Machine algorithm for massive classification tasks. We introduced *Tensor Sketching*, a fast and scalable sketching approach to approximate the pairwise dot products in the kernel space for accelerating the training of kernel machines.

- Chapter 5 demonstrates how advanced sampling technique can improve the efficiency of the large-scale web applications. We introduce *Odd Sketch*, a space-efficient probabilistic data structure to represent text documents so that their pairwise Jaccard similarity are preserved and fast computed. We evaluated the efficiency of the novel data structure on association rule learning and web duplicate detection tasks.

Besides the basic background presented in the first part, each chapter of the second part requires more advances in randomized techniques which will be provided correspondingly in each chapter.

Chapter 2

Background

This section presents basic definitions of high-dimensional vectors in the Euclidean space, and fundamental concepts widely used in data analysis applications. These concepts, including nearest neighbor search, outlier detection and classification, are challenging problems in data analysis that the thesis aims at solving. We then introduce core randomized techniques including random projection, sampling and sketching via hashing mechanism. These randomized techniques are used as powerful algorithmic tools to tackle the data analysis problems presented in the thesis.

2.1 High-dimensional Vectors in the Euclidean Space

In a wide range of application domains, object data are represented as high-dimensional points (vectors) where each dimension corresponds to each feature of the objects of interest. For example, genetic data sets consist of thousands of dimensions corresponding to experimental conditions. Credit card data sets contain hundreds of features of customer transaction records. A data set S consisting of n points of d features can be viewed as n d-dimensional vectors in the Euclidean space $\mathbb{R}^d$. We often represent S as the matrix $A \in \mathbb{R}^{n \times d}$ in order to explore innumerable powerful techniques from numerical linear algebra. As the standard Euclidean structure, the data relationships are expressed by the Euclidean distance between points or the angle between lines. Such relationships are dominantly used in fundamental concepts in data analysis, and briefly described as follows.

Definition 2.1. *Given any two points $x = \{x_1, \cdots, x_d\}, y = \{y_1, \cdots, y_d\} \in S \subset \mathbb{R}^d$, the Euclidean norm and pairwise relationships including Euclidean distance, dot product, angle are defined as follows:*

- *Euclidean norm:* $\|x\| = \sqrt{\sum_{i=1}^{d} x_i^2}$.
- *Euclidean distance:* $d(x, y) = \|x - y\| = \sqrt{\sum_{i=1}^{d} (x_i - y_i)^2}$.
- *Dot product (or inner product):* $x \cdot y = \langle x, y \rangle = \sum_{i=1}^{d} x_i y_i$.
- *Angle:* $\theta_{xy} = \arccos\left(\frac{\langle x,y \rangle}{\|x\|\|y\|}\right)$, *where* $0 \leq \theta_{xy} \leq \pi$.

2.2 Fundamental Concepts in Data Analysis

This section describes some fundamental concepts widely used in data analysis applications, including nearest neighbor search, outlier detection and classification. These concepts are also basic data analysis problems that the thesis aims at solving. We discuss challenges and solutions corresponding to each concept.

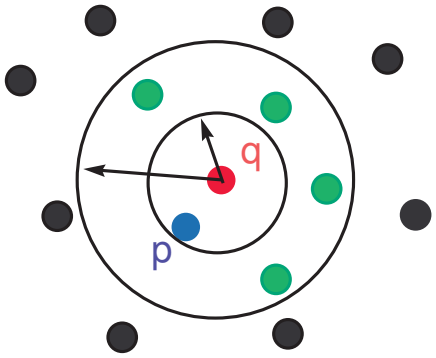

Figure 2.1: An illustration of the NNS. Given the query point q in red color, we retrieve the point p in blue color as the 1-NN of q, and the green points together the blue point as the 5-NN points of q.

2.2.1 Nearest Neighbor Search

Nearest neighbor search (NNS) or similarity search is an optimization problem for finding the closest point in a point set given a query point and a similarity measure. Mathematically, given a point set S in the Euclidean space $\mathbb{R}^d$, a query point $q \in \mathbb{R}^d$, and a similarity measure (e.g. Euclidean distance) $d(.,.)$, we would like to find the closest point $p \in S$ such that $d(p, q)$ has the smallest value. A generalization of NNS is the k-NN search, where we need to find the top-k closest points, as illustrated in Figure 2.1

When the data dimensionality increases, the data become sparse due to the exponential increase of the space volume. This phenomenon, called "curse of dimensionality", affects a broad range of data distributions. The sparsity in high-dimensional space is problematic for concepts like distance or nearest neighbor due to the poor discrimination between the nearest and farthest neighbors [9, 35]. The problem worsens for data containing irrelevant dimensions (e.g. noise) which might obscure the influence of relevant ones.

The effects of "curse of dimensionality" prevent many approaches to find *exact* nearest neighbor from being efficient. That is because the performance of convex indexing structures in high-dimensional space degenerates into scanning the whole data set. To avoid this problem, one can resort to *approximate* search.

This is due to the fact that the choice of dimensions and the use of a similarity measure are often mathematical approximations of users in many data mining applications [37]. Thus a fast determining approximate NNS will suffice and benefit for most practical problems. This approach turns out to be the prominent solution for alleviating the effects of the "curse of dimensionality".

Chapter 5 continues the line of research on *approximate* similarity search. The chapter introduces *Odd Sketch*, a compact binary sketch for efficiently estimating the Jaccard similarity of two sets, which is one of the key research challenge in many information retrieval applications.

2.2.2 Outlier Detection

Detecting outliers is to identify the objects that considerably deviate from the general distribution of the data. Such the objects may be seen as suspicious objects due to the different mechanism of generation. A conventional unsupervised approach is to assign to each object a outlier score as the outlierness degree, and retrieve the top-k objects which have the highest outlier scores as outliers. Such outlier scores (e.g. distance-based [42], density-based [11]) are frequently based the Euclidean distance to the k-nearest neighbors in order to label objects of interest as outliers or non-outliers. Figure 2.2 shows an illustration of non-outliers (inner points and border points) and outliers.

Due to the aforementioned "curse of dimensionality", detecting outlier patterns in high-dimensional space poses a huge challenge. As the dimensionality increases, the Euclidean distance between objects are heavily dominated by noise. Conventional approaches which use implicit or explicit assessments on differences in Euclidean distance between objects are deteriorated in high-dimensional data [43].

An alternative solution is to develop new heuristic models for outlier detection that can alleviate the effects of the "curse of dimensionality". Such new models should not have many input parameters (ideally free-parameter) and are scalable so that incorrect settings of parameters or the high computational complexity cannot cause the algorithm to fail in finding outlier patterns in large-scale high-dimensional data sets.

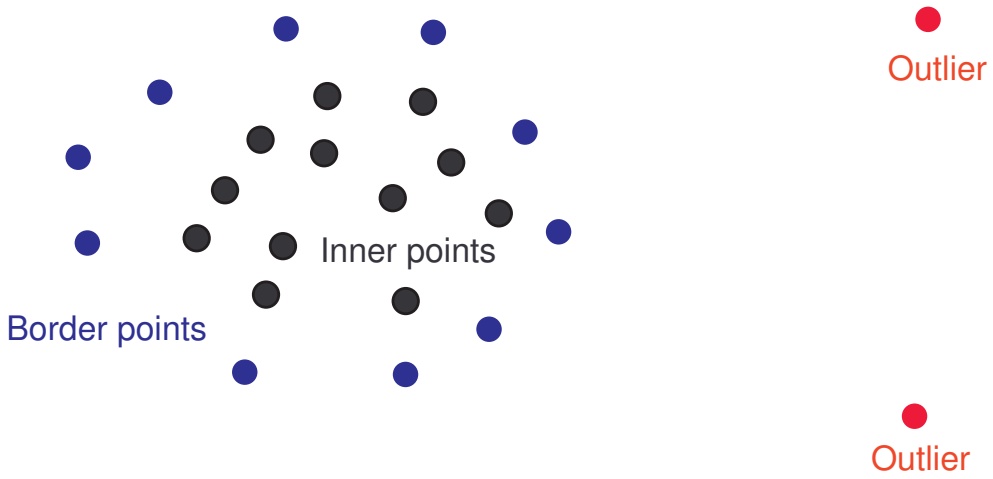

Figure 2.2: An illustration of different types of points: inner points in black color, border points in blue color and outliers in red color.

Chapter 3 considers a recent approach named *angle-based outlier detection* [43] for detecting outlier patterns in high-dimensional space. Due to the high computational complexity of this approach (e.g. cubic time), the chapter proposes *FastVOA*, a near-linear time algorithm for estimating the variance of angle, an angle-based outlier score for outlier detection in high-dimensional space.

2.2.3 Classification

Classification is the process of learning a predictive model given a set of training samples with categories so that the predictive model can accurately assign any new sample into one category. Such model often represents samples as high-dimensional vectors and learns a mathematical function as a classifier such that it is able to separate well samples in each category by a wide gap. New samples will be assigned into a category based on which side of the gap they belong to.

It often happens that the classifier in the data space is non-linear, which is very difficult to learn. The ubiquitous technique called Support Vector Machine (SVM) [62] performs a non-linear classification using the so-called *kernel trick*. Kernel trick is an implicit non-linear data mapping from original data space into

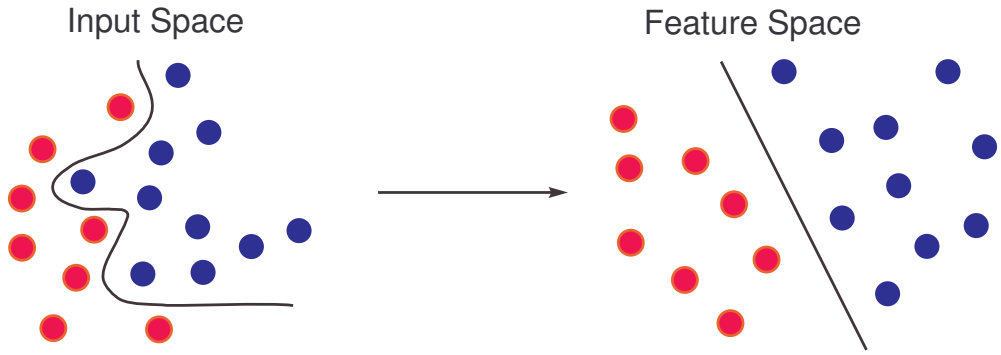

Figure 2.3: A schematic illustration of Support Vector Machine for classification. Often, the classifier in the data space (left picture) is a non-linear function and difficult to learn. By mapping data into the feature space (right picture), we can easily learn a linear function as a classifier.

high-dimensional feature space, where each coordinate corresponds to one feature of the data points. In that space, one can perform well-known data analysis algorithms without ever interacting with the coordinates of the data, but rather by simply computing their pairwise dot products. This operation can not only avoid the cost of explicit computation of the coordinates in feature space, but also handle general types of data (such as numeric data, symbolic data). The basic idea of SVM classification is depicted in Figure 2.3.

Although SVM methods have been used successfully in a variety of data analysis tasks, their scalability is a bottleneck. Kernel-based learning algorithms usually scale poorly with the number of the training samples (cubic running time and quadratic storage for direct methods). In order to apply kernel methods to large-scale data sets, recent approaches [60, 76] have been proposed for quickly approximating the kernel functions by explicitly mapping data into a relatively low-dimensional random feature space. Such techniques then apply existing fast linear learning algorithms [27, 39] to find nonlinear data relations in that random feature space.

Chapter 4 continues the line of research on approximating the kernel functions. The chapter introduces *Tensor Sketching*, a fast random feature mapping for

approximating polynomial kernels and accelerating the training kernel machines for large-scale classification problems.

2.3 Core Randomized Techniques

2.3.1 Tools from Probability Theory

The randomized algorithms described in the thesis are approximate and probabilistic. They need two parameter, $\varepsilon > 0$ and $0 < \delta < 1$ to control the probability of error of result. Often, we need to bound the probability δ that the result exceeds its expectation by a certain amount ε or within a factor of ε. The basic tools from probability theory, Chebyshev's inequality and Chernoff bound, are used to analyze the randomized algorithms throughout the thesis.

Lemma 2.1 (Chebyshev's inequality). *Let X be a random random variable with expectation $\mathbf{E}[X]$ and variance $\mathbf{Var}[X]$. For any $\varepsilon > 0$,*

$$\mathbf{Pr}[|X - \mathbf{E}[X]| \geq \varepsilon] \leq \frac{\mathbf{Var}[X]}{\varepsilon^2} \ .$$

Lemma 2.2 (Chernoff bound). *Let $X = \sum_{i=1}^{t} X_i$ be a sum of independent random variables X_i with values in $[0, 1]$. For any $\varepsilon > 0$,*

$$\mathbf{Pr}[|X - \mathbf{E}[X]| \geq \varepsilon] \leq 2e^{-2\varepsilon^2/t} \ .$$

2.3.2 Random Projection

Random projection has recently emerged as a powerful technique for dimensionality reduction to achieve theoretical and applied results in high-dimensional data analysis. This technique simply projects data in high-dimensional space onto random lower-dimensional space but still preserves fundamental properties of the original data, such as pairwise Euclidean distances and dot products. So, instead of performing our analysis on the original data, we work on low-dimensional ap-

proximate data. That reduces significantly the computational time and yet yields good approximation results.

Let $A \in \mathbb{R}^{n \times d}$ be the original data matrix and a random projection matrix $R \in \mathbb{R}^{d \times k}$ ($k << d$), containing independent and identically distributed (i.i.d.) normal distribution $\mathbf{N}(0, 1)$ entries. We obtain a projected data matrix:

$$B = \frac{1}{\sqrt{k}} AR \in \mathbb{R}^{n \times k} \quad .$$

The much smaller matrix B preserves *all* pairwise Euclidean distances of A within an arbitrarily small factor with high probability according to Johnson-Lindenstrauss lemma [23, 40].

Lemma 2.3 (Johnson-Lindenstrauss). *Given a point set S of n points in $\mathbb{R}^d$, a real number $0 < \varepsilon < 1$, and a positive integer $k \leq \mathcal{O}(\varepsilon^{-2} \log n)$. There is a linear map $f : \mathbb{R}^d \to \mathbb{R}^k$ such that for all $x, y \in S$,*

$$(1 - \varepsilon) \|x - y\|^2 \leq \|f(x) - f(y)\|^2 \leq (1 + \varepsilon) \|x - y\|^2 \quad .$$

The choice of the random matrix R is one of the key points of interest because it affects to the computational time complexity. A sparse or well-structured R [1, 3] can speed up the process of computing matrix vector product. In addition to the preservation of all pairwise Euclidean distances, the pairwise dot product, $x \cdot y$, and angle, θ_{xy}, between two points x and y are also retained well under random projections [16, 69]. The following lemmas will justify the statement.

Lemma 2.4 (Dot product preservation). *Given any two points $x, y \in \mathbb{R}^d$, a positive integer $k \leq \mathcal{O}(\varepsilon^{-2} \log n)$. Let $f = \frac{1}{\sqrt{k}} Ru$ where R is a $k \times d$ matrix, where each entry is sampled i.i.d. from a normal distribution $\mathbf{N}(0, 1)$. Then,*

$$\mathbf{Pr}[|x \cdot y - f(x) \cdot f(y)| \geq \varepsilon] \leq 4e^{-(\varepsilon^2 - \varepsilon^3)k/4} \quad .$$

Lemma 2.5 (SimHash). *Let θ_{xy} be the angle between two points $x, y \in \mathbb{R}^d$, and $sign(.)$ be the sign function. Given a random vector $r \in \mathbb{R}^d$, where each entry is*

sampled i.i.d. from a normal distribution $\mathbf{N}(0,1)$*, then,*

$$\mathbf{Pr}[sign(r \cdot u) = sign(r \cdot v)] = 1 - \frac{\theta_{xy}}{\pi} \ .$$

In general, random projection can preserve essential characteristics of data in the Euclidean space. Therefore, it is beneficial in applications to dimensionality reduction on high-dimensional data where answers rely on the assessments on concepts like Euclidean distance, dot product, and angle between points.

Chapter 3 leverages the angle preservation of random projections to estimate the angle relationships among data points. Such angle relationships will be used to estimate the angle-based outlier factor for outlier detection in high-dimensional space.

2.3.3 Hashing

Hashing is a technique using hash functions with certain properties for performing insertions, deletions, and lookups in constant average time (i.e. $\mathcal{O}(1)$). A hash function maps data of arbitrary size to data of fixed size. The values returned by the hash function are called hash values. Depending on the certain properties of hash functions, we can use hashing techniques to differentiate between data or to approximate basic properties of data. Typically we use a family of k-wise independent hash functions because it provides a good average case performance in randomized algorithms [72]. The mathematical definition of k-wise independent family of hash functions is as follows:

Definition 2.2. *A family of hash functions* $\mathcal{F} = \{f : [\Omega] \to [d]\}$ *is* k*-wise independent if for any* k *distinct hash keys* $(x_1, \cdots, x_k) \in [\Omega]^k$ *and* k *hash values (not necessarily distinct)* $(y_1, \cdots, y_k) \in [d]^k$*, we have:*

$$\mathbf{Pr}_{f \in \mathcal{F}}[f(x_1) = y_1 \wedge \cdots \wedge f(x_k) = y_k] = d^{-k} \ .$$

A practical implementation of k-wise independent hash function $f : [\Omega] \to [d]$ is the so-called *CW-trick* [66, 72], proposed by Carter and Wegman by using only

shifts and bit-wise Boolean operations. Refer to Appendix A for a pseudo-code of 4-wise independent hash function generation.

In the thesis we primarily use hashing techniques with k-wise independent hash functions (small k) for summarizing data in high-dimensional space such that the summary can approximate well data fundamentals, including frequency moments, pairwise distances and dot products. We now describe how to use hashing techniques for advanced randomized algorithms, including sketching and min-wise hashing to summarize high-dimensional data.

Sketching

Over the past few years there has been significant research on developing compact probabilistic data structures capable of representing a high-dimensional vector (or a data stream). A family of such data structures is the so-called *sketches* which can make a pass over the whole data to approximate fundamental properties of data. Typically sketches maintain the linear projections of a vector with the number of random vectors defined implicitly by simple independent hash functions. Based on these random projection values, we are able to estimate data fundamentals, such as frequency moments, pairwise Euclidean distances and dot products, etc. In addition, sketches can easily process inserting or deleting in the form of additions or subtractions to dimensions of the vectors because of the property of linearity.

AMS Sketch Alon et al. [4] described and analyzed AMS Sketches to estimate the frequency moments of a data stream by using 4-wise independent hash functions. Viewing a high-dimensional data as a stream, we can apply AMS Sketches to approximate the second frequency moments (i.e. the squared norm) of such data.

Definition 2.3 (AMS Sketch). *Given a high-dimensional vector* $x = \{x_1, \cdots, x_d\}$, *take a 4-wise independent hash function* $s : [d] \to \{+1, -1\}$. *The AMS Sketch of* x *is the value* $\mathbf{Z} = \sum_{i=1}^{d} s(i)x_i$.

Lemma 2.6. *Let* $\mathbf{Z}$ *be the AMS Sketch of* $x = \{x_1, \cdots, x_d\}$*, and define* $\mathbf{Y} = \mathbf{Z}^2$*, then,*

$$\mathbf{E}[\mathbf{Y}] = \sum_{i=1}^{d} x_i^2, \text{ and } \mathbf{Var}[\mathbf{Y}] \leq 2\left(\mathbf{E}[\mathbf{Y}]\right)^2.$$

We usually use the *median trick*, a technique relying on Chebyshev's inequality and Chernoff bound in order to boost the success probability of Y as argued in [4]. That is, we output the median of s_2 random variables $Y_1, \cdots, Y_{s_2}$ as the estimator, where each Y_i is the mean of s_1 i.i.d. random variables $Y_{ij} : 1 \leq j \leq s_1$.

In Chapter 3 we leverage this property of AMS Sketches together with angle preservation of random projections for fast approximating the variance of angle between pairs of data points. Such value will be used as outlier score to detect outliers in high-dimensional data.

Count Sketch Charikar et al. [17] introduced Count Sketch to find frequent items in data streams by using 2-wise independent hash functions. Again, consider a high-dimensional data as a stream data, we view Count Sketch as a specific random projection technique because it maintains linear projections of a vector with the number of random vectors defined *implicitly* by simple independent hash functions.

Definition 2.4 (Count Sketch). *Given two 2-wise independent hash functions* $h : [d] \to [k]$ *and* $s : [d] \to \{+1, -1\}$*. Count Sketch of a point* $x = \{x_1, \cdots, x_d\} \in \mathbb{R}^d$ *is denoted by* $Cx = \{(Cx)_1, \cdots, (Cx)_k\} \in \mathbb{R}^k$ *where* $(Cx)_j = \sum_{i:h(i)=j} s(i)x_i$*.*

The following lemma shows that the pairwise dot product is well preserved with Count Sketches.

Lemma 2.7. *Given two points* $x, y \in \mathbb{R}^d$*, we denote by* $Cx, Cy \in \mathbb{R}^k$ *their respective Count Sketches using the same hash functions* h, s*.*

$$\mathbf{E}[\langle Cx, Cy \rangle] = \langle x, y \rangle \quad .$$

It is worth noting that Count Sketch might provide low distortion on sparse vectors. This is due to the fact that non-zero elements are retained after sketching

with high probability. In addition, Count Sketch requires $\mathcal{O}(nd)$ operations for n points in d-dimensional space. Therefore, Count Sketch might provide better performance than traditional random projections in applications dealing with sparse vectors.

In Chapter 4 we exploit the fast computation of Count Sketches on tensor domains to introduce *Tensor Sketching*, an efficient algorithm for approximating polynomial kernels, accelerating the training kernel machines.

MinHash

MinHash (or minwise hashing) is a powerful algorithmic technique to estimate Jaccard similarities of two sets, originally proposed by Broder et al. [12, 13]. It uses the *min-wise independent* permutation to pick up one element in a set such that all the elements of the set have the same probability to be the minimum element after permuting the set. A min-wise independent family of permutations is defined as follows:

Definition 2.5. *Given a set $\mathbb{S} \subset [n]$, a set element $x \in \mathbb{S}$, and a minwise independent permutation $\pi : [n] \to [n]$ such that*

$$\mathbf{Pr}[\min(\pi(\mathbb{S})) = \pi(x)] = \frac{1}{|\mathbb{S}|} \ .$$

Apply such independent random permutations, we can estimate the Jaccard similarity between two sets $\mathbb{S}_1$ and $\mathbb{S}_2$ by the following lemma

Lemma 2.8 (MinHash). *Given any two sets $\mathbb{S}_1, \mathbb{S}_2 \subset [n]$, and a minwise independent permutation $\pi : [n] \to [n]$, then*

$$\mathbf{Pr}[\min(\pi(\mathbb{S}_1)) = \min(\pi(\mathbb{S}_2))] = \frac{|\mathbb{S}_1 \cap \mathbb{S}_2|}{|\mathbb{S}_1 \cup \mathbb{S}_2|} = J(\mathbb{S}_1, \mathbb{S}_2) \ .$$

Typically we get an estimator for J by considering a sequence of permutations $\pi_1, \ldots, \pi_k$ and storing the annotated minimum values (called "minhashes").

$$S_1 = \{(i, \min(\pi_i(\mathbb{S}_1))) \mid i = 1, \ldots, k\},$$
$$S_2 = \{(i, \min(\pi_i(\mathbb{S}_2))) \mid i = 1, \ldots, k\}.$$

We estimate J by the fraction $\hat{J} = |S_1 \cap S_2|/k$. This estimator is unbiased, and by independence of the permutations it can be shown that $\mathbf{Var}[\hat{J}] = \frac{J(1-J)}{k}$.

In Chapter 5 we combine the minwise hashing technique with a hash table to introduce *Odd Sketch*, a highly space-efficient data structure for estimating set similarities, a central problem in many information retrieval applications.

Chapter 3

Angle-based Outlier Detection

Outlier mining in d-dimensional point sets is a fundamental and well studied data mining task due to its variety of applications. Most such applications arise in high-dimensional domains. A bottleneck of existing approaches is that implicit or explicit assessments on concepts of distance or nearest neighbor are deteriorated in high-dimensional data. Following up on the work of Kriegel et al. (KDD'08), we investigate the use of angle-based outlier factor in mining high-dimensional outliers. While their algorithm runs in cubic time (with a quadratic time heuristic), we propose a novel random projection-based technique that is able to estimate the angle-based outlier factor for all data points in time near-linear in the size of the data. Also, our approach is suitable to be performed in parallel environment to achieve a parallel speedup. We introduce a theoretical analysis of the quality of approximation to guarantee the reliability of our estimation algorithm. The empirical experiments on synthetic and real world data sets demonstrate that our approach is efficient and scalable to very large high-dimensional data sets.

*This work was published as an article, "**A near-linear time approximation algorithm for angle-based outlier detection in high-dimensional data**" in Proceedings of 18th ACM SIGKDD Conference on Knowledge Discovery and Data Mining (KDD), 2012.*

3.1 Introduction

Outlier mining is a fundamental and well studied data mining task due to the variety of domain applications, such as fraud detection for credit cards, intrusion detection in network traffic, and anomaly motion detection in surveillance video, etc. Detecting outliers is to identify the objects that considerably deviate from the general distribution of the data. Such the objects may be seen as suspicious objects due to the different mechanism of generation. For example, consider the problem of fraud detection for credit cards and the data set containing the card owners' transactions. The transaction records consist of usage profiles of each customer corresponding the purchasing behavior. The purchasing behavior of customer usually changes when the credit card is stolen. The abnormal purchasing patterns may be reflected in transaction records that contain high payments, high rate of purchase or the orders comprising large numbers of duplicate items, etc.

Most such applications arise in very high-dimensional domains. For instance, the credit card data set contains transaction records described by over 100 attributes [74]. To detect anomalous motion trajectories in surveillance videos, we have to deal with very high representational dimensionality of pixel features of sequential video frames [50]. Because of the notorious "*curse of dimensionality*", most proposed approaches so far which are explicitly or implicitly based on the assessment of differences in Euclidean distance metric between objects in full-dimensional space do not work efficiently. Traditional algorithms to detect distance-based outliers [42, 61] or density-based outliers [11, 58] suffer from the high computational complexity for high-dimensional nearest neighbor search. In addition, the higher the dimensionality is, the poorer the discrimination between the nearest and the farthest neighbor becomes [9, 35]. That leads to a situation where most of the objects in the data set appear likely to be outliers if the evaluation relies on the neighborhood using concepts like distance or nearest neighbor in high-dimensional space.

In KDD 2008, Kriegel et al. [43] proposed a novel outlier ranking approach based on the variance of the angles between an object and all other pairs of objects. This approach, named Angle-based Outlier Detection (ABOD), evaluates

the degree of outlierness of each object on the assessment of the broadness of its angle spectrum. The smaller the angle spectrum of a object to other pairs of objects is, the more likely it is an outlier. Because "*angles are more stable than distances in high-dimensional space*" [44], this approach does not substantially deteriorate in high-dimensional data. In spite of many advantages of alleviating the effects of the "curse of dimensionality" and being a parameter-free measure, the time complexity taken to compute ABOD is significant with $\mathcal{O}(dn^3)$ for a data set of n objects in d-dimensional space. To avoid the cubic time complexity, the authors also proposed heuristic approximation variants of ABOD for efficient computations. These approximations, however, still rely on nearest neighbors and require high computational complexity with $\mathcal{O}(dn^2)$ used in sequential search for neighbors. Moreover, there is no analysis to guarantee the accuracy of these approximations.

In this chapter we introduce a near-linear time algorithm to approximate the variance of angle for all data points. Our proposed approach works in $\mathcal{O}(n \log n(d + \log n))$ time for a data set of size n in d-dimensional space, and outputs an unbiased estimator of variance of angles for each object. The main technical insight is the combination between random hyperplane projections [16, 31] and AMS Sketches on product domains [10, 36], which enables us to reduce the computational complexity from cubic time complexity in the naïve approach to near-linear time complexity in the approximation solution. Another advantage of our algorithm is the suitability for parallel processing. We can achieve a nearly linear (in the number of processors used) parallel speedup of running time. We also give a theoretical analysis of the quality of approximation to guarantee the reliability of our estimation algorithm. The empirical experiments on real world and synthetic data sets demonstrate that our approach is efficient and scalable to very large high-dimensional data.

3.2 Related Work

A good outlier measure is the key aspect for achieving effectiveness and efficiency when managing the outlier mining tasks. A great number of outlier measures have

been proposed, including global and local outlier models. Global outlier models typically take the complete database into account while local outlier models only consider a restricted surrounding neighborhood of each data object.

Knorr and Ng [42] proposed a simple and intuitive distance-based definition of outlier as an earliest global outlier model in the context of databases. The outliers with respect to parameter k and λ are the objects that have less than k neighbors within distance λ. A variant of the distance-based notion is proposed in [61]. This approach takes the distance of a object to its k^{th} nearest neighbor as its outlier score and retrieve the top m objects having the highest outlier scores as the top m outliers. The distance-based approaches are based on the assumption, that the lower density region that the data object is in, the more likely it is an outlier. The basic algorithm to detect such distance-based outliers is the nested loop algorithm [61] that simply computes the distance between each object and its k^{th} nearest neighbor and retrieve top m objects with the maximum k^{th} nearest neighbor distances. To avoid the quadratic worst case complexity of nested loop algorithm, several key optimizations are proposed in the literature. Such optimizations can be classified based on the different pruning strategies, such as the approximate nearest neighbor search [61], data partitioning strategies [61] and data ranking strategies [7, 30, 71]. Although these optimizations may improve performance, they scale poorly and are therefore inefficient as the dimensionality or the data size increases, and objects become increasingly sparse [2].

While global models take the complete database into account and detect outliers based on the distances to their neighbors, local density-based models evaluate the degree of outlierness of each object based on the local density of its neighborhood. In many applications, local outlier models give many advantages such as the ability to detect both global and local outliers with different densities and providing the boundary between normal and abnormal behaviors [11]. The approaches in this category assign to each object a local outlier factor as the outlierness degree based on the local density of its k-nearest neighbors [11] or the multi-granularity deviation of its ε-neighborhood [58]. In fact, these approaches implicitly rely on finding nearest neighbors for every object and typically use indexing data structures to improve the performance. Therefore, they are unsuitable for the requirements in mining high-dimensional outliers.

Due to the fact that the measures like distance or nearest neighbor may not be qualitatively meaningful in high-dimensional space, recent approaches focus on subspace projections for outlier ranking [2, 55]. In other words, these approaches take a subset of attributes of objects as subspaces into account. However, these approaches suffer from the difficulty of choosing meaningful subspaces [2] or the exponential time complexity in the data dimensionality [55]. As mentioned above, Kriegel at al. [43] proposed a robust angle-based measure to detect high-dimensional outliers. This approach evaluates the degree of outlierness of each data object on the assessment of the variance of angles between itself and other pairs of objects. The smaller the variance of angles between a object to the residual objects is, the more likely it is outlier. Because the angle spectrum between objects is more stable than distances as the dimensionality increases [44], this measure does not substantially deteriorate in high-dimensional data. However, the naïve and approximation approaches suffer from the high computational complexity with cubic time and quadratic time, respectively.

3.3 Angle-based Outlier Detection (ABOD)

As elaborated above, using concepts like distance or nearest neighbor for mining outlier patterns in high-dimensional data is unsuitable. A novel approach based on the variance of angles between pairs of data points is proposed to alleviate the effects of "curse of dimensionality" [43]. Figure 3.1 shows an intuition of angle-based outlier detection, where points have small angle spectrum are likely outliers. Figure 3.2 depicts the angle-based outlier factor, the variance of angles for three kinds of points.

The figures show that the border and inner points of a cluster have very large variance of angles whereas this value is much smaller for the outliers. That is, the smaller the angle variance of a point to the residual points is, the more likely it is an outlier. This is because the points inside the cluster are surrounded by other points in all possible directions while the points outside the cluster are positioned in particular directions. Therefore, we use the variance of angles (VOA) as an outlier factor to evaluate the degree of outlierness of each point

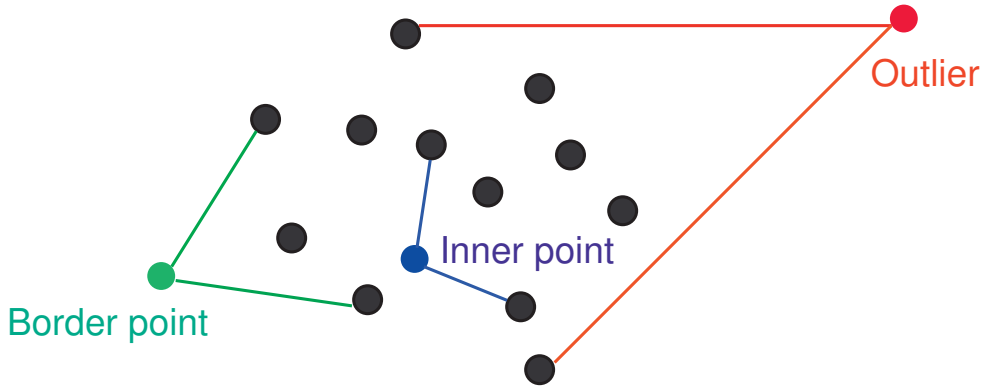

Figure 3.1: An intuition of angle-based outlier detection.

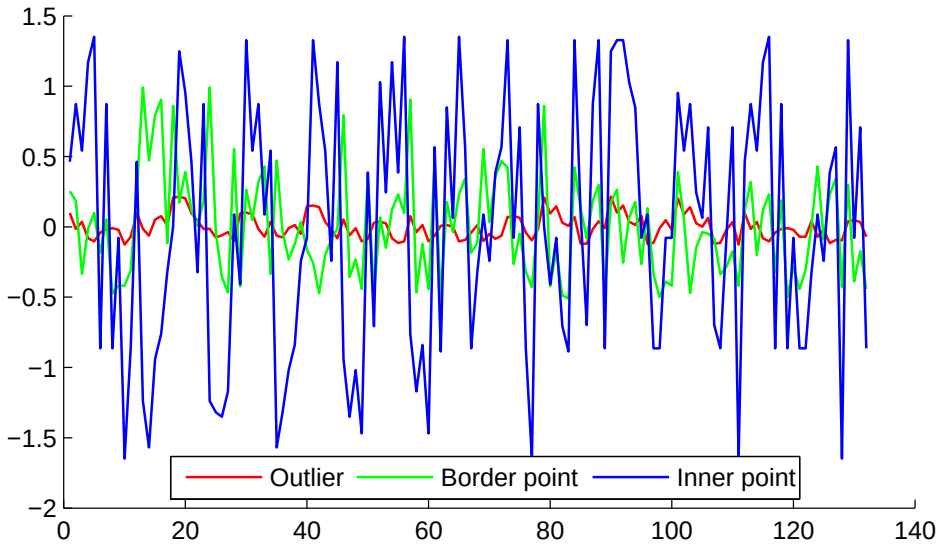

Figure 3.2: Variance of angles of outlier, border point, and inner point.

of the data set. The proposed approaches in [43] do not deal directly with the variance of angles but variance of cosine of angles weighted by the corresponding distances of the points instead. We argue that the weighting factors are less and less meaningful in high-dimensional data due to the "curse of dimensionality". We expect the outlier rankings based on the variance of cosine spectrum with or

without weighting factors and the variance of angle spectrum are likely similar in high-dimensional data. We therefore formulate the angle-based outlier factor using the variance of angles as follows:

Definition 3.1. *Given a point set $S \subseteq \mathbb{R}^d$, $|S| = n$ and a point $p \in S$. For a random pair of different points $a, b \in S \setminus \{p\}$, let Θ_{apb} denote the angle between the difference vectors $a - p$ and $b - p$. The angle-based outlier factor VOA(p) is the variance of Θ_{apb}:*

$$VOA(p) = \mathbf{Var}[\Theta_{apb}] = MOA_2(p) - (MOA_1(p))^2,$$

where MOA_2 and MOA_1 are defined as follows:

$$MOA_2(p) = \frac{\sum_{\substack{a,b \in S\setminus\{p\} \\ a \neq b}} \Theta_{apb}^2}{\frac{1}{2}(n-1)(n-2)} \;\; ; \;\; MOA_1(p) = \frac{\sum_{\substack{a,b \in S\setminus\{p\} \\ a \neq b}} \Theta_{apb}}{\frac{1}{2}(n-1)(n-2)} \;\; .$$

It is obvious that the VOA measure is entirely free of parameters and therefore is suitable for unsupervised outlier detection methods. The naïve ABOD algorithm computes the VOA for each point of the data set and return the top m points having the smallest VOA as top m outliers. However, the time complexity of the naïve algorithm is in $\mathcal{O}(dn^3)$. The cubic computational complexity means that it will be very difficult to mine outliers in very large data sets.

3.4 Algorithm Overview and Preliminaries

3.4.1 Algorithm Overview

The general idea of our approach is to efficiently compute an unbiased estimator of the variance of the angles for each point of the data set. In other words, the expected value of our estimate is equal to the variance of angles, and we show that it is concentrated around its expected value. These estimated values are then used to rank the points. The top m points having the smallest variances of angles are retrieved as top m outliers of the data set.

In order to estimate the variance of angles between a point and all other pairs of points, we first project the data set on the hyperplanes orthogonal to random vectors whose coordinates are i.i.d. chosen from the standard normal distribution $\mathbf{N}(0,1)$. Based on the partitions of the data set after projection, we are able to estimate the unbiased mean of angles for each point (i.e. MOA_1). We then approximate the second moment (i.e. MOA_2) and derive its variance (i.e. VOA) by applying the AMS Sketches to summarize the frequency moments of the points projected on the random hyperplanes. The combination between random hyperplane projections and AMS Sketches on product domains enables us to reduce the computational complexity to $\mathcal{O}(n \log n(d + \log n))$ time. In the following we start with some basic notions of random hyperplane projection and AMS Sketch, then propose our approach to estimate the variance of angles for each point of the data set.

3.4.2 Preliminaries

Random Hyperplane Projection

As elaborated in Chapter 2, the angle between two points are preserved under random projection, see Lemma 2.5. We now apply this technique for the angle between a triple of points and show that this value is also well retained. Taking t random vectors r_1,..., $r_t \in \mathbb{R}^d$ such that each coordinate is i.i.d. chosen from the standard normal distribution $\mathbf{N}(0,1)$, for $i = 1, \ldots, t$ and any triple of points $a, b, p \in S$, we consider the independent random variables

$$X_{apb}^{(i)} = \begin{cases} 1 & \text{if } a \cdot r_i < p \cdot r_i < b \cdot r_i \\ 0 & \text{otherwise} \end{cases}$$

For a vector r_i we see that $X_{apb}^{(i)} = 1$ only if the vectors $a - p$ and $b - p$ are on different sides of the hyperplane orthogonal to r_i, and in addition $(a - p) \cdot r_i < 0$. The probability that this happens is proportional to Θ_{apb}, as exploited in the seminal papers of Goemans and Williamson [31] and Charikar [16]. More precisely we have:

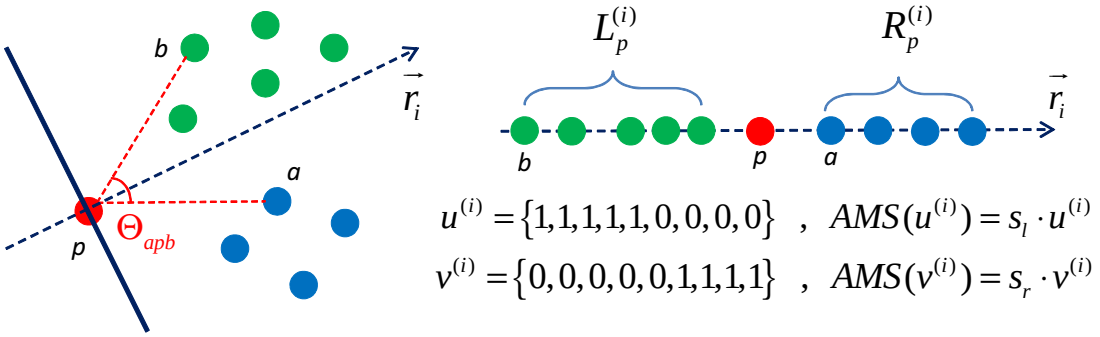

Figure 3.3: An illustration of FastVOA for the point p using one random projection r_i. We project all points into the hyperplane orthogonal to r_i and sort them by their dot products. We present each partition $\mathbf{L}_p^{(i)}, \mathbf{R}_p^{(i)}$ as binary vectors $u^{(i)}, v^{(i)}$, respectively. Applying AMS Sketches on product domains of these vectors, we can approximate $\left\|u^{(i)} \otimes v^{(i)}\right\|_F$, which is then used to estimate $VOA(p)$.

Lemma 3.1. *For all* a, b, p, i, $\mathbf{Pr}[X_{apb}^{(i)} = 1] = \Theta_{apb}/(2\pi)$.

Note that we also have $\mathbf{Pr}[X_{bpa}^{(i)} = 1] = \Theta_{apb}/(2\pi)$ due to symmetry [31]. By using t random vectors r_i, we are able to boost the accuracy of the estimator of Θ_{apb}. In particular, we have $\Theta_{apb} = \frac{2\pi}{t}\sum_{i=1}^{t} X_{apb}^{(i)}$. The analysis of accuracy for random projections will be presented in Section 3.6.

AMS Sketch on Product Domains

As mentioned in Chapter 2, AMS Sketch can be used to estimate the second frequency moments of a high-dimensional vector by considering such vector as a stream. In this work we use AMS Sketch on product domains, which are recently analyzed by Indyk and McGregor [36] and Braverman et al. [10]. That is, given two vectors $u = \{u_1, \cdots, u_d\}, v = \{v_1, \cdots, v_d\}$, we view an outer product matrix $(uv) = u \otimes v$, where by definition $(uv)_{ij} = u_i v_j$ as a vector of matrix elements. We apply AMS Sketches with two different 4-wise independent vectors for the outer product (uv) in order to estimate its squared Frobenius norm. The following lemma justifies the statement.

Lemma 3.2. *Given two different 4-wise independent vectors* $r, s \in \{\pm 1\}^d$. *The AMS Sketch of an outer product* $(uv) \in \mathbb{R}^{d \times d}$, *where by definition* $(uv)_{ij} = u_i v_j$,

is:

$$\mathbf{Z} = \sum_{(i,j)\in[d]\times[d]} r_i s_j (uv)_{ij} = \left(\sum_{i=1}^{d} r_i u_i\right)\left(\sum_{j=1}^{d} s_j v_j\right).$$

Define $\mathbf{Y} = \mathbf{Z}^2$ *then* $\mathbf{E}[\mathbf{Y}] = \sum_{ij}(u_i v_j)^2$ *or squared Frobenius norm of the outer product* (uv) *and* $\mathbf{Var}[\mathbf{Y}] \leq 8\left(\mathbf{E}[\mathbf{Y}]\right)^2$.

That is, the AMS sketch of the outer product is simply the product of the AMS sketches of the two vectors (using different 4-wise independent random vectors). This means that we can estimate the Frobenius norm of an outer product matrix without ever interacting with matrix elements. In addition, we can use the *median trick* to boost the success probability of the estimator.

3.5 Algorithm Description

To avoid the cubic time complexity, we propose a near-linear time algorithm named *FastVOA* to estimate the variance of angles for each data point based on random hyperplane projections. Figure 3.3 shows the high level illustration of FastVOA using one random projection.

3.5.1 First Moment Estimator

Given a random vector r_i and a point $p \in S$, we estimate $MOA_1(p)$ using Lemma 3.1 as follows:

$$\begin{aligned} F_1(p) &= \tfrac{2}{(n-1)(n-2)}\left(2\pi \sum_{\substack{a,b\in S\setminus\{p\}\\ a\neq b}} \mathbf{E}[X^{(i)}_{apb}]\right) \\ &= \tfrac{2}{(n-1)(n-2)} \sum_{\substack{a,b\in S\setminus\{p\}\\ a\neq b}} \pi\left(\mathbf{E}[X^{(i)}_{apb}] + \mathbf{E}[X^{(i)}_{bpa}]\right) \text{(due to the symmetry)} \\ &= \tfrac{2\pi}{(n-1)(n-2)} |\mathbf{L}^{(i)}_p||\mathbf{R}^{(i)}_p| \ , \end{aligned}$$

where the sets $\mathbf{L}_p^{(i)} = \{x \in S \backslash \{p\} \mid x \cdot r_i < p \cdot r_i\}$ and $\mathbf{R}_p^{(i)} = \{x \in S \backslash \{p\} \mid x \cdot r_i > p \cdot r_i\}$ consist of the points on each side of p under the random projection.

Note that this value is an unbiased estimator of mean of angles between the point p and the other pairs of points. We boost the accuracy of the estimation by using t random projections, and obtain a more accurate unbiased estimator of $MOA_1(p)$ as follows:

$$F_1(p) = \frac{2\pi}{t(n-1)(n-2)} \sum_{i=1}^{t} |\mathbf{L}_p^{(i)}||\mathbf{R}_p^{(i)}| \ . \tag{3.1}$$

3.5.2 Second Moment Estimator

Since estimation of the second moment is more complicated, we first present the general idea by considering a less efficient approach and then propose an efficient algorithm to compute the unbiased second moment estimator. Focus on a single point p, suppose that we fix an arbitrary ordering of the set $S\backslash\{p\}$ as $x_1, x_2, \cdots, x_{n-1}$. For each projection using the random vector r_i, we take the two vectors $u^{(i)}, v^{(i)} \in \{0,1\}^{n-1}$ such that their k^{th} coordinate corresponds to the k^{th} point of the set $S\backslash\{p\}$. The k^{th} coordinate of $u^{(i)}$ (or $v^{(i)}$) is 1 if the k^{th} point of the set locates on the left (or right) partition, and 0, otherwise. As shown in Figure 3.3, $u^{(i)} = \{1,1,1,1,1,0,0,0,0\}$ corresponds to the left partition $\mathbf{L}_p^{(i)}$ and $v^{(i)} = \{0,0,0,0,0,1,1,1,1\}$ corresponds to the right partition $\mathbf{R}_p^{(i)}$.

We now consider the matrix $\mathbf{P} = \sum_{i=1}^{t} u^{(i)} \otimes v^{(i)}$ where $u^{(i)} \otimes v^{(i)}$ is the outer product between $u^{(i)}$ and $v^{(i)}$. Note that all diagonal elements of $\mathbf{P}$ are 0. Consider any pair of points $a, b \in S\backslash\{p\}$ where $a = x_k$ and $b = x_l$, we observe that $\mathbf{P}_{kl}$ is the number of times that a locates on the left side and b locates on the right side after t projections. We can therefore estimate Θ^2_{apb}, the squared

angle between p and a, b based on the element $\mathbf{P}_{kl}$ of the matrix $\mathbf{P}$.

$$\mathbf{P}_{kl}^2 = \left(\sum_{i=1}^{t} X_{apb}^{(i)}\right)^2 = \sum_{i=1}^{t}\left(X_{apb}^{(i)}\right)^2 + 2\sum_{\substack{i,j=1\\ i\neq j}}^{t} X_{apb}^{(i)} X_{apb}^{(j)}$$

$$\begin{aligned}\mathbf{E}[\mathbf{P}_{kl}^2] &= \sum_{i=1}^{t}\mathbf{E}\left[\left(X_{apb}^{(i)}\right)^2\right] + 2\sum_{\substack{i,j=1\\ i\neq j}}^{t}\mathbf{E}[X_{apb}^{(i)}]\mathbf{E}[X_{apb}^{(j)}] \\ &= t\tfrac{\Theta_{apb}}{2\pi} + t(t-1)\left(\tfrac{\Theta_{apb}}{2\pi}\right)^2 \ .\end{aligned}$$

So we have an unbiased estimator:

$$\Theta_{apb}^2 = \tfrac{(2\pi)^2}{t(t-1)}\left(\mathbf{E}[\mathbf{P}_{kl}^2] - \tfrac{t}{2\pi}\Theta_{apb}\right) \ . \tag{3.2}$$

Now we can compute $MOA_2(p)$ based on all elements of $\mathbf{P}$ as follows:

$$\begin{aligned}MOA_2(p) &= \tfrac{2}{(n-1)(n-2)}\sum_{\substack{a,b\in S\setminus\{p\}\\ a\neq b}}\Theta_{apb}^2 \\ &= \tfrac{1}{(n-1)(n-2)}\sum_{\substack{a,b\in S\setminus\{p\}\\ a\neq b}}\left(\Theta_{apb}^2 + \Theta_{bpa}^2\right) && \text{(due to the symmetry)} \\ &= \tfrac{4\pi^2}{t(t-1)(n-1)(n-2)}\left(\sum_{k,l=1}^{n-1}\mathbf{E}[\mathbf{P}_{kl}^2] - \tfrac{t}{2\pi}\sum_{\substack{a,b\in S\setminus\{p\}\\ a\neq b}}\left(\Theta_{apb}+\Theta_{bpa}\right)\right) && \text{(based on 3.2)} \\ &= \tfrac{4\pi^2}{t(t-1)(n-1)(n-2)}\left(\mathbf{E}[\|\mathbf{P}\|_F^2] - \tfrac{t(n-1)(n-2)}{2\pi}MOA_1(p)\right) \\ &= \tfrac{4\pi^2}{t(t-1)(n-1)(n-2)}\mathbf{E}[\|\mathbf{P}\|_F^2] - \tfrac{2\pi}{t-1}MOA_1(p) \ .\end{aligned}$$

From the equation above, we can estimate $MOA_2(p)$:

$$F_2'(p) = \tfrac{4\pi^2}{t(t-1)(n-1)(n-2)}\|\mathbf{P}\|_F^2 - \tfrac{2\pi}{t-1}F_1(p) \ . \tag{3.3}$$

However, the squared Frobenius norm $\|\mathbf{P}\|_F^2$ will not be computed exactly, since

we do not know how to achieve this in less than quadratic time. Instead, it will be estimated using AMS Sketches on product domains. Let $AMS(\mathbf{L}_p^{(i)})$ and $AMS(\mathbf{R}_p^{(i)})$ be the AMS Sketches of the vectors $u^{(i)}$ and $v^{(i)}$ (using different 4-wise independent random vectors), respectively. Due to linearity the sketch of sum of distributions is equal to the sum of sketches of the distributions, so:

$$\|\mathbf{P}\|_F^2 = \left\| \sum_{i=1}^{t} u^{(i)} \otimes v^{(i)} \right\|_F^2 = \mathbf{E}\left[\left(\sum_{i=1}^{t} AMS(\mathbf{L}_p^{(i)}) AMS(\mathbf{R}_p^{(i)}) \right)^2 \right] .$$

We therefore estimate the second moment estimator $F_2(p)$ as:

$$F_2(p) = \frac{4\pi^2 \left(\sum_{i=1}^{t} AMS(\mathbf{L}_p^{(i)}) AMS(\mathbf{R}_p^{(i)}) \right)^2}{t(t-1)(n-1)(n-2)} - \frac{2\pi F_1(p)}{t-1} . \tag{3.4}$$

3.5.3 FastVOA - A Near-linear Time Algorithm for ABOD

Based on the estimators of $MOA_1(p)$ and $MOA_2(p)$ for any point p described above, we now present *FastVOA*, a near-linear time algorithm to estimate the variance of angles for all points of the data set. The pseudo-code in Algorithm 1 shows how FastVOA works.

At first, we project the data set S on the hyperplanes orthogonal to random projection vectors (Algorithm 2). *RandomProjection()* returns a data structure $\mathcal{L}$ containing the information of the partitions of S under t random projections. Using $\mathcal{L}$, we are able to compute the values $|\mathbf{L}_p^{(i)}|$ and $|\mathbf{R}_p^{(i)}|$ corresponding to each point p and r_i. The pseudo-code in Algorithm 3 computes the first moment estimator for each point. Similarly, we also make use of $\mathcal{L}$ to compute the Frobenius norm $\|\mathbf{P}\|_F$ for each point p in Algorithm 4. To boost the accuracy of AMS Sketch, we need to use the *median trick*. That is, we repeat the computation of *FrobeniusNorm()* $s_1 s_2$ times, and output F_{norm} as the median of s_2 random variables $\mathbf{Y}_1, \cdots, \mathbf{Y}_{s_2}$, each being the average of s_1 values (lines 3 - 6). After that, the second moment estimator and variance estimator for each point are computed in lines 9 - 10.

Algorithm 1 FastVOA(S, t, s_1, s_2)

Ensure: Return the variance estimator for all points

$VAR \leftarrow [0]^n, F_2 \leftarrow [0]^n$
$\mathcal{L} \leftarrow RandomProjection(S, t)$
$F_1 \leftarrow FirstMomentEstimator(\mathcal{L}, t, n)$
for $i = 1 \rightarrow s_2$ **do**
  $\mathbf{Y}_i \leftarrow \sum_{j=1}^{s_1} \left(FrobeniusNorm(\mathcal{L}, t, n)\right)^2 / s_1$
end for
$F_{norm} \leftarrow median\left\{\mathbf{Y}_1, \cdots, \mathbf{Y}_{s_2}\right\}$
for $j = 1 \rightarrow n$ **do**
  $F_2[j] = \frac{4\pi^2}{t(t-1)(n-1)(n-2)} F_{norm}[j] - \frac{2\pi F_1[j]}{t-1}$
  $VAR[j] = F_2[j] - (F_1[j])^2$
end for
return VAR

Algorithm 2 RandomProjection(S, t)

Ensure: Return a list $\mathcal{L} = L_1 L_2 \cdots L_t$ where L_i is a list of point IDs ordered by their dot product with r_i

$\mathcal{L} \leftarrow \emptyset$
for $i = 1 \rightarrow t$ **do**
  Generate a random vector r_i whose coordinates are independently chosen from $\mathbf{N}(0, 1)$
  $L_i \leftarrow \emptyset$
  for $j = 1 \rightarrow n$ **do**
    Insert $(x_j, x_j \cdot r_i)$ into the list L_i
  end for
  Sort L_i based on the dot product order
  Insert L_i into $\mathcal{L}$
end for
return $\mathcal{L}$

3.5.4 Computational Complexity and Parallelization

It is clear that the computational complexity of FastVOA depends on Algorithms 2 - 4. We note that Algorithm 2 takes $O(tn(d + \log n))$ time in computing dot products and sorting for all points while both Algorithm 3 and 4 run in $O(tn)$ time. Since we have to repeat the Algorithm 4 in $s_1 s_2$ times, the total running time is $O(tn(d + \log n + s_1 s_2))$. To guarantee the accuracy of FastVOA, we have to

Algorithm 3 FirstMomentEstimator($\mathcal{L}, t, n$)

Ensure: Return the first moment estimator for all points

```
F_1 ← [0]^n
for i = 1 → t do
    C_l ← [0]^n, C_r ← [0]^n
    L_i ← L[i]
    for j = 1 → n do
        idx = L_i[j].pointID
        C_l[idx] = j − 1
        C_r[idx] = n − 1 − C_l[idx]
    end for
    for j = 1 → n do
        F_1[j] = F_1[j] + C_l[j]C_r[j]
    end for
end for
return 2π/(t(n−1)(n−2)) F_1
```

choose $t = \mathcal{O}(\log n)$ and $s_1 s_2$ sufficiently large to boost the accuracy of estimation as analyzed later in Section 3.6. In the experiment the running time is usually dominated by the AMS Sketch computational time. That means FastVOA runs in $O(s_1 s_2 n \log n)$ time.

It is worth noting that Algorithms 2 - 4 use the **for** loop with t random vectors that performs the same independent operations for each random vector. Therefore, we can simply parallelize this loop in those three algorithms to achieve a nearly linear (in the number of processors used) speedup.

3.6 Error Analysis

It has already been argued that our estimators are unbiased, i.e., produce the right first and second moments in expectation: $\mathbf{E}[F_1(p)] = MOA_1(p)$ and $\mathbf{E}[F_2(p)] = MOA_2(p)$. In this section we analyze the precision, showing bounds on the number of random projections and AMS sketches needed to achieve a given precision ε. This will imply that the variance is estimated within an additive error of $\mathcal{O}(\varepsilon^2)$.

For $MOA_1(p)$ we get this directly with high probability, whereas for $MOA_2(p)$ the basic success probability of the estimator $F_2(p)$ is only 8/9 where $s_1 = \mathcal{O}(\varepsilon^{-2})$

Algorithm 4 FrobeniusNorm($\mathcal{L}, t, n$)

Ensure: Return an estimator of $\|\mathbf{P}\|_F$ for each point p

```
F_norm ← [0]^n
Initialize 4-wise independent vectors S_l[n], S_r[n] whose entries are in {±1} with equal probability
for i = 1 → t do
    AMS_l ← [0]^n, AMS_r ← [0]^n
    L_i ← L[i]
    for j = 2 → n do
        idx1 = L_i[j − 1].pointID
        idx2 = L_i[j].pointID
        AMS_l[idx2] = AMS_l[idx1] + S_l[idx1]
    end for
    for j = n − 1 → 1 do
        idx1 = L_i[j].pointID
        idx2 = L_i[j + 1].pointID
        AMS_r[idx1] = AMS_r[idx2] + S_r[idx2]
    end for
    for j = 1 → n do
        F_norm[j] = F_norm[j] + AMS_l[j]AMS_r[j]
    end for
end for
return F_norm
```

as justified later. By repeating the second moment estimation procedure $s_2 = \mathcal{O}(\log(1/\delta))$ times and taking the median value for each point, the success probability can be magnified to $1-\delta$, for any $\delta > 0$ as argued in [4]. We will use tools from probability theory described in Chapter 2 to justify these statements.

3.6.1 First Moment Estimator

Consider the probability (over choice of vectors $r_1, \cdots, r_t$) that $F_1(p)$ deviates from $MOA_1(p)$ by more than ε. We splitting the sum $\frac{F_1(p)t}{\pi}$ into t terms, each of which is $Y^{(i)} = \frac{F_1(p)}{\pi} = \frac{2}{(n-1)(n-2)}|\mathbf{L}_p^{(i)}||\mathbf{R}_p^{(i)}|$, and $0 \leq Y^{(i)} \leq 1$. We apply Chernoff

bound (Lemma 2.2) with the deviation error $\varepsilon t/\pi$,

$$\mathbf{Pr}[|\frac{F_1(p)t}{\pi} - \frac{MOA_1(p)t}{\pi}| \geq \frac{\varepsilon t}{\pi}] \leq 2e^{-2\left(\frac{\varepsilon t}{\pi}\right)^2/t}$$
$$\mathbf{Pr}[|F_1(p) - MOA_1(p)| \geq \varepsilon] \leq 2e^{-2\varepsilon^2 t/\pi^2}$$

If we choose $t > \varepsilon^{-2}\pi^2 \ln(n)$ the probability that $F_1(p)$ deviates from $MOA_1(p)$ by more than ε is at most $2/n^2$. So the probability that all of n first moment estimators have error at most ε is $1 - \mathcal{O}(1/n)$.

3.6.2 Second Moment Estimator

Recall that the second moment estimator bases on the two estimate from equation (3.3) and equation (3.4),

$$F_2'(p) = \frac{4\pi^2}{t(t-1)(n-1)(n-2)} \|\mathbf{P}\|_F^2 - \frac{2\pi}{t-1} F_1(p) \ ,$$
$$F_2(p) = \frac{4\pi^2 \left(\sum_{i=1}^{t} AMS(\mathbf{L}_p^{(i)}) AMS(\mathbf{R}_p^{(i)})\right)^2}{t(t-1)(n-1)(n-2)} - \frac{2\pi F_1(p)}{t-1} \ .$$

We will show error bounds on the first estimator $F_2'(p)$ over choice of random vectors $r_1, \ldots, r_t$, and on the second estimator $F_2(p)$ over choice of random hash functions of AMS Sketches. Note that the expectation of $F_2'(p)$ over choice of random vectors is $MOA_2(p)$ where the expectation of $F_2(p)$ over the choice of random hash functions of AMS Sketches is $F_2'(p)$.

Now, consider the probability (again over choice of vectors $r_1, \ldots, r_t$) that the first version of the second moment estimator, $F_2'(p)$, deviates from its expectation by more than ε, given that $F_1(p)$ deviates by at most ε from its expectation. We can see that this happens when $||\mathbf{P}||_F^2$ deviates from its expectation by at least $\binom{n-1}{2}\binom{t}{2}\varepsilon/\pi^2$ because the error caused by $\frac{2\pi}{t-1}F_1(p)$ is smaller than $o(1)$. Thus, it suffices to show that each squared entry $\mathbf{P}_{kl}^2$ deviates by at most $\frac{1}{4}\varepsilon t^2/\pi^2$ from its expectation with high probability because $\mathbf{P}$ has $2\binom{n-1}{2}$ non-zero entries. Recall that $\mathbf{P}_{kl} = \sum_{i=1}^{t} X_{apb}^{(i)}$, a sum of independent indicator random variables, which

means that we can apply Chernoff bound again,

$$\mathbf{Pr}[|\mathbf{P}_{kl} - \mathbf{E}[\mathbf{P}_{kl}]| \geq \frac{1}{4}\varepsilon t/\pi^2] \leq 2e^{-\varepsilon^2 t/8\pi^4} \ .$$

For $t > 8\varepsilon^{-2}\pi^4 \ln(n)$ we get that $\mathbf{P}_{kl}$ deviates from its expectation by at most $\frac{1}{4}\varepsilon t/\pi^2$ with probability $1 - \mathcal{O}(1/n^2)$. Since $\mathbf{P}_{kl} \leq t$ this implies that $\mathbf{P}_{kl}^2$ deviates by at most $\frac{1}{4}\varepsilon t^2/\pi^2$, as desired. The total error for $F_2'(p)$, accounting for all $2\binom{n-1}{2}$ entries of $\mathbf{P}$, is therefore bounded by ε with probability $1 - \mathcal{O}(1/n^2)$.

Finally, we should account for the error caused by the use of AMS Sketches in the second estimator $F_2(p)$. Note that the error caused by the second term of $F_2'(p)$, $\frac{2\pi}{t-1}F_1(p)$, is smaller than $o(1)$. Therefore it suffices to consider only the error caused by the first term of $F_2'(p)$, which is estimated by AMS Sketch. By Lemma 3.2 we have $\mathbf{Var}[F_2(p)]$ is bounded by $8F_2'(p)^2$. Taking the average of s_1 sketches the variance is reduced to at most $\frac{8F_2'(p)^2}{s_1}$. By applying Chebyshev's inequality (Lemma 2.1), we have

$$\begin{aligned}\mathbf{Pr}[|F_2(p) - F_2'(p)| \geq \varepsilon F_2'(p)] &\leq \frac{\mathbf{Var}[F_2(p)]}{\varepsilon^2 F_2'(p)^2} \\ &\leq \frac{8F_2'(p)^2}{s_1\varepsilon^2 F_2'(p)^2} = \frac{8}{s_1\varepsilon^2} \ .\end{aligned}$$

For $s_1 > 72\varepsilon^{-2}$ the probability that $F_2(p)$ deviates by $\varepsilon F_2'(p)$ from its expectation is less than $1/9$. As stated above, by repeating the estimation $s_2 = \mathcal{O}(\log(1/\delta))$ times and taking the median value, the success probability can be magnified to $1 - \delta$, where $\delta < 1$.

3.6.3 Variance Estimator

From aforementioned bounds on errors caused by the first moment and second moment estimations, we can conclude the error analysis by the following lemma.

Lemma 3.3. *Given $0 < \delta < 1$ and $\varepsilon > 0$, using $t = \mathcal{O}(\varepsilon^{-2}\log(n))$ random vectors and the AMS Sketch size $s_1 = \mathcal{O}(\varepsilon^{-2})$ and $s_2 = \mathcal{O}(\log(1/\delta))$, the probability*

that an unbiased estimator of VOA of a point deviates from its expectation by at most $\mathcal{O}(\varepsilon^2)$ *is at most* $1 - \mathcal{O}(n^{-2})$.

3.7 Experiments

We implemented all algorithms in C++ and conducted experiments in a 2.67 GHz core i7 Windows platform with 3GB of RAM on both synthetic and real world data sets. All results are over 5 runs of the algorithms.

3.7.1 Data Sets

For the sake of fair comparison, we made use of the same synthetic data generation process as the ABOD approach [43]. We generated a Gaussian mixture including 5 equally weighted clusters having random means and variances as normal points and employed a uniform distribution as the outliers. All points were generated in full-dimensional space. For each synthetic data set, we generated 10 outliers which are independent on the Gaussian mixture. We evaluated the performance of all algorithms on synthetic data sets with varying sizes and dimensions.

For the real world high-dimensional data sets, we picked three data sets (Isolet, Multiple Features and Optical Digits) designed for classification and machine learning tasks from UCI machine learning repository [29]. Isolet contains the pronunciation data of 26 letters of the alphabet while Multiple Features and Optical Digits consist of the data of handwritten numerals ('0' - '9'). For each data set, we picked all data points from some classes having common behaviors as normal points and 10 data points from another class as outliers. For instance, we picked points of classes C, D, and E of Isolet that share the "e" sound as normal points and 10 points from class Y as outliers. Similarly, we picked points of classes 6 and 9 of Multiple Features, classes 3 and 9 of Optical Digits as normal points because of the similar shapes and 10 points of class 0 as outliers. It is worth noting that there are some outliers that probably locate on the region covered by the normal points. This means that we are not able to isolate exactly all outliers. Instead, we expect our algorithms to rank all outliers into sufficiently high positions.

3.7.2 Accuracy of Estimation

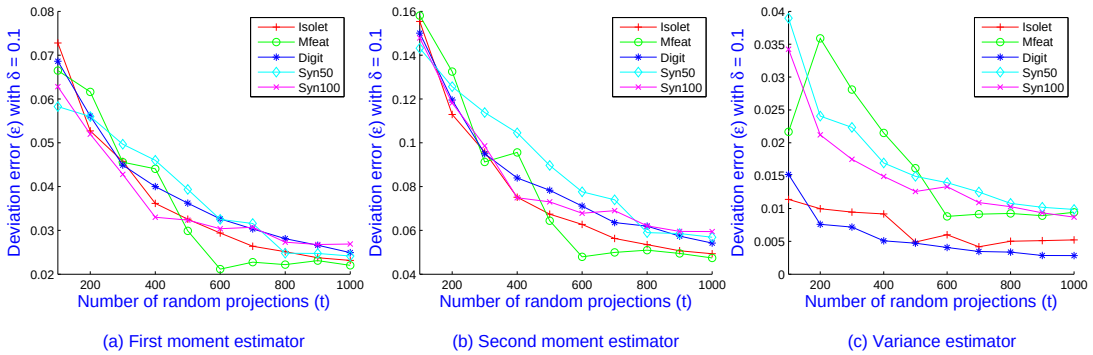

Figure 3.4: Deviation error of random projection based estimators on 5 data sets.

This subsection presents the accuracy experiments to evaluate the reliability of our estimation algorithm. As analysis in the Section 3.6, the estimators $F_1(p)$, $F_2'(p)$, and $F_2(p)$ for any point p of the data set can deviate from their expectations by more than ε with probability at most δ by using a sufficiently large number of random projections and AMS Sketch sizes. Note that $F_2(p)$ is the second moment estimator using AMS Sketch while $F_2'(p)$ is based on only random projections.

At first, we carried out experiments to measure the accuracy of estimators based on only random projections. We measured the deviation error ε of $F_1(p)$ and $F_2'(p)$ from their expectations with probability $\delta = 0.1$. That is, we considered 90% data points and computed the error between the estimators and the true values. We took t in ranges [100, 1000] and conducted experiments on 2 synthetic data sets having 1000 points on 50 and 100 dimensions, namely Syn50 and Syn100, as well as the three real world data sets, namely Isolet, Mfeat and Digit.

Figures 3.4.a and 3.4.b display the deviation errors (ε) from expectation of the estimators $F_1(p)$ and $F_2'(p)$ with probability $\delta = 0.1$. Using these two estimators, we derived the variance estimator and measured its deviation from expectation, as shown in Figure 3.4.c. Although the theoretical analysis requires a sufficiently large number of random projections t to achieve the small ε, the results on 5 data sets surprisingly show that with a rather small t, we are able to estimate exactly the variance of angles for all points. With $t = 600$, 90% number of points of 5 data sets have the first moment, the second moment and the derived

variance estimators deviating from their expectations at most 0.035, 0.08 and 0.015 respectively. When t increases to 1000, 90% of points of 5 data sets have the variance estimator deviate from its expectation by at most 0.01. Therefore, for such data sets having large difference between VOA of outliers and VOA of border points, the use of random projections to estimate VOA can achieve good performance on detecting outliers.

To quantify the relative error of estimate and the quality of outlier ranking, we measured the error probability δ of the variance estimator using AMS Sketches with parameter settings $t = 1000, s_1 = 7200, s_2 = 50, \varepsilon = 0.1$ on all data sets. Concretely, we computed the number of points p of the data set such that its variance estimator by using AMS Sketch deviates by more than $\varepsilon VOA(p)$ from its expectation $VOA(p)$. Table 3.1 presents the error probability of variance estimators on 5 data sets.

Table 3.1: Error probability of variance estimator using AMS Sketch on 5 data sets

Isolet	Mfeat	Digit	Syn50	Syn100
0.75	0.19	0.35	0.04	0.03

It is clear that the two synthetic data sets obtain very small errors while the real world data sets take rather large errors, especially on Isolet. This is because the variance estimator of all points of the data set may be underestimated or overestimated by using AMS Sketch. To guarantee the capability of our approximation approach on detecting outliers, we analyzed the accuracy of outlier ranking between the brute force algorithm called SimpleVOA and the approximate algorithm FastVOA. The accuracy of outlier ranking is defined as $\frac{|A \cap B|}{m}$ where A and B are the top m positions retrieved by SimpleVOA and FastVOA algorithms, respectively. Figure 3.5 shows the accuracy of outlier ranking between SimpleVOA and FastVOA where m is in ranges 10 - 100.

The results of outlier ranking indicate that FastVOA provided a rather high accurate ranking on all data sets. While the two synthetic data sets and the Multiple Feature dataset show a highly accurate ranking for all ranges of top positions, the other data sets offered a medium accurate ranking when $m < 30$ but more accurate when $m > 40$. Although the use of AMS Sketch may lead to

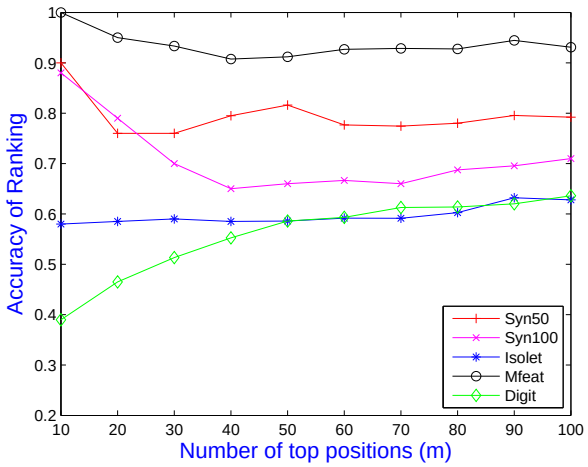

Figure 3.5: The accuracy of outlier ranking between SimpleVOA and FastVOA on 5 data sets.

underestimate or overestimate of the variance estimator, FastVOA still introduces good performance on ranking data points based on VOA.

3.7.3 Effectiveness

It is obvious that our approaches are dealing directly with the variance of angles (VOA) while the approaches in [43] compute the variance of cosine of angles weighted by distances (ABOF). This subsection demonstrates experiments to measure the effectiveness of both measures on detecting outliers. For each measure, we compared the quality of outlier ranking provided by brute force (SimpleVOA and ABOD) and approximation algorithms (FastVOA and FastABOD). For the sake of fair comparison, we used the precision-recall graph to evaluate the capability of each algorithm to retrieve the most likely outliers. The precision is the number of retrieved points that are indeed outliers. For each precision level, we measured the recall as the percentage of the number of outliers in the retrieved set.

For synthetic data sets, we generated 4 data sets with varying sizes of 1000 and 5000 points and dimensions of 50 and 100. We observed that the differences of VOA between outliers and border points on synthetic data sets become large when

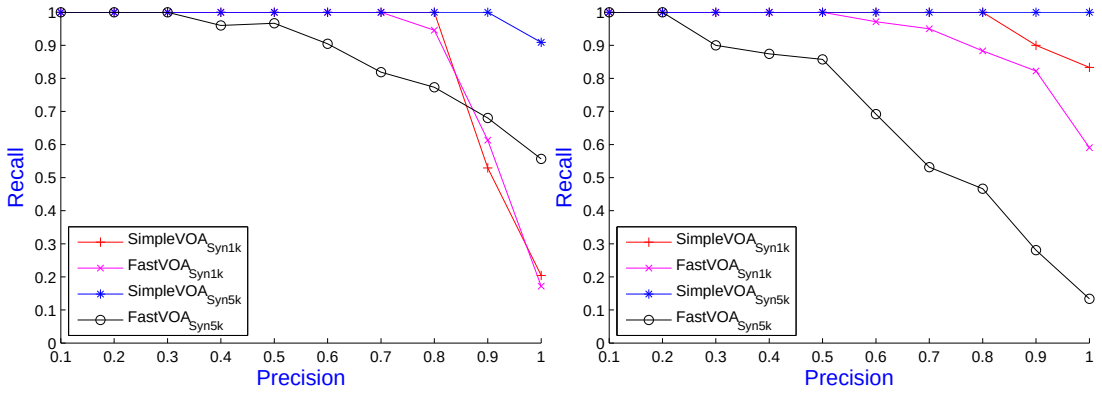

(a) 50 dimensional synthetic datasets

(b) 100 dimensional synthetic datasets

Figure 3.6: Precision-Recall Graph for 4 synthetic data sets. Each graph describes the behavior on 1000 and 5000 points.

the size increases. Therefore we adjusted the parameter settings for FastVOA on synthetic data sets of size 5000 points to reduce the time complexity. In particular, we determined $t = 100$, $s_1 = 1600$, $s_2 = 10$. We kept the same parameter setting as Section 3.7.2 for the other data sets. The sample size of FastABOD was chosen as $0.1n$ as [43]. Let us note that both ABOD and FastABOD offered perfect results on 4 synthetic data sets. That means all 10 outliers were ranked into the top 10 positions. So we did not show the results of ABOD and FastABOD on synthetic data sets.

Figure 3.6 depicts the precision-recall graph for synthetic data sets. Figure 3.6.a shows the results of brute force ($\text{SimpleVOA}_{\text{Syn1k}}$ and $\text{SimpleVOA}_{\text{Syn5k}}$) and approximation algorithms ($\text{FastVOA}_{\text{Syn1k}}$ and $\text{FastVOA}_{\text{Syn5k}}$) on the 2 data sets of 50 dimensions and varying sizes of 1000 and 5000 points. For the medium dimensionality of 50, VOA did not work well in the small data set size but achieved almost perfect performance in the large data set by ranking all 10 outliers between top 11 retrieved points. It is clear that the better performance of SimpleVOA leads to the better performance of FastVOA. Results of 2 synthetic data sets with 100 dimensions are displayed in Figure 3.6.b. Since the effect of weighting factors in ABOF is not meaningful in high-dimensional data, SimpleVOA shows competitive results with ABOD with almost perfect performance. FastVOA on

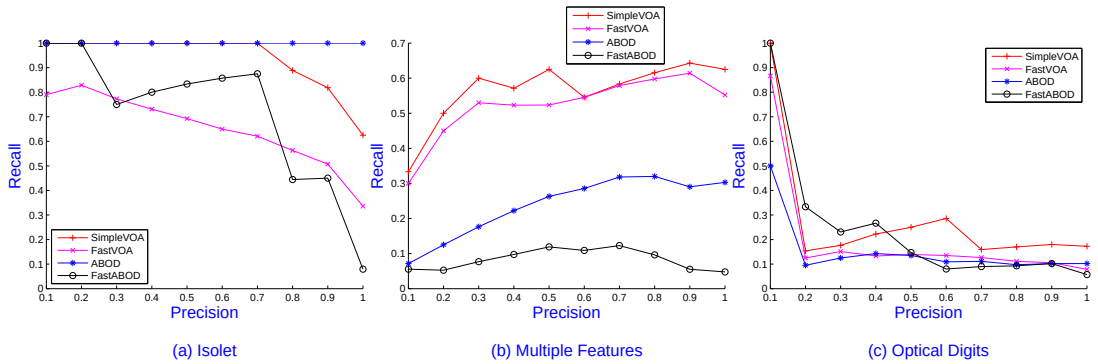

Figure 3.7: Precision-Recall Graph for 3 real world data sets.

the data set Syn1k achieves better performance than that of Syn5k. This is due to the fact that we use the different parameter settings, which is $t = 100$ for Syn5k and $t = 1000$ for Syn1k.

Figure 3.7 shows the observed precision-recall graphs for the 3 real world data sets. On the Isolet dataset, SimpleVOA and ABOD obtained high accuracy by ranking 10 outliers in top 10 and top 16 positions, respectively. FastABOD provided better outlier ranking than FastVOA on detecting 7 outliers in top 10 positions. However, on ranking all 10 outliers, both of them did not work well and required large recall levels. Both SimpleVOA and FastVOA performed rather well on the Multiple Features dataset by ranking all outliers on the top 16 positions while both ABOD and FastABOD suffered from low accuracy. All approaches had difficulties to detect outliers on the Optical Digits dataset although the VOA-based approaches clearly offered better results than the ABOF-based ones.

3.7.4 Efficiency

This section compares the running time of 3 algorithms, namely FastVOA, LB_ABOD [43] and FastABOD [43] on the large high-dimensional data sets. In fact, there are very few large real world data sets where the outliers are identified exactly in advance. Therefore we decided to evaluate the efficiency of these 3 approaches on synthetic data sets. We carried out experiments measuring the CPU time of each approach on data sets with varying both size and dimensions in ranges 10,000 - 100,000 points and 100 - 1000 respectively.

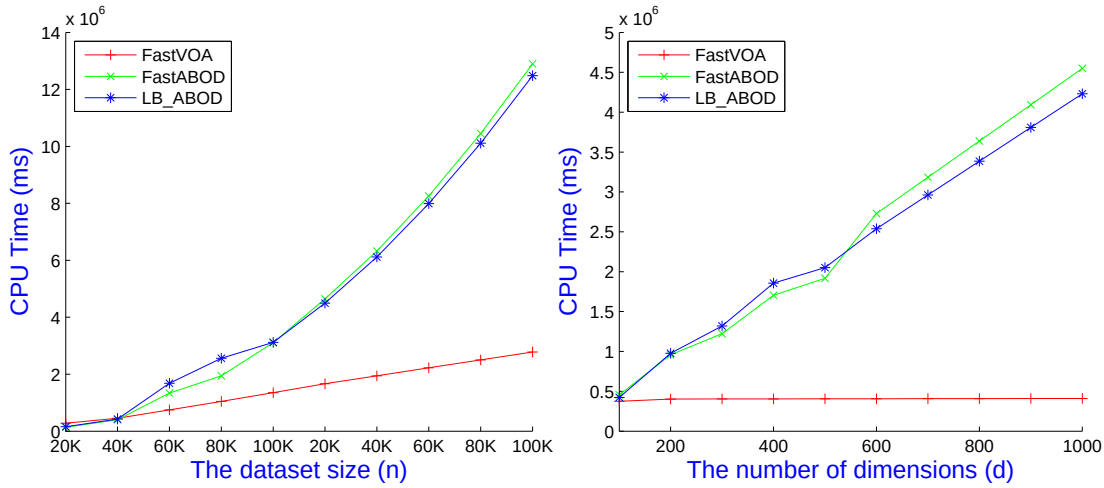

(a) 100 dimensional synthetic datasets

(b) Datasets of 20,000 points

Figure 3.8: Comparison of CPU time of FastVOA, FastABOD and LB_ABOD.

Note that both LB_ABOD and FastABOD run in $\mathcal{O}(dn^2)$ time while the running time of FastVOA depends on the parameters t, s_1, s_2. As mentioned in Subsection 3.7.3, we can use rather small parameter settings for FastVOA in very large high-dimensional synthetic data sets without reducing the accuracy. Therefore we set $t = 100$, $s_1 = 1600$, $s_2 = 10$ for FastVOA and the sample size of FastABOD was chosen as $0.1n$. It is worth noting that the value $0.1n$ for ABOD-based approaches becomes rather large when the data set size increases while FastVOA still needs rather small number of random projections and the AMS Sketch sizes. As analysis in the Section 3.6, the total running time of FastVOA is $\mathcal{O}(tn(d + \log n + s_1 s_2))$. With the choice of parameters above, the total running time of FastVOA is still dominated by the computational time of AMS Sketches, which is in $\mathcal{O}(ts_1 s_2 n)$ time.

Figure 3.8.a shows the CPU time in (ms) of FastVOA, LB_ABOD and FastABOD for data sets having 100 dimensions and sizes of 10,000 - 100,000 points while Figure 3.8.b displays the CPU time in (ms) for data sets having size of 20,000 points and dimensions of 100 - 1000. It is clear that the running time of FastVOA is linear time in the size of data set and independent on number of dimensions. In contrast, both LB_ABOD and FastABOD run in quadratic time

in the size of data set and linear time in the number of dimensions.

We conclude the efficiency evaluation of FastVOA by illustrating its suitability for parallel processing. We made use of Open Multi-Processing API (OpenMP) supporting multi-platform shared memory multiprocessing programming in C++ to parallelize the **for** loop of random projection vectors in Algorithms 2 - 4 of Subsection 3.5.3. We measured the parallel speedup when running on 4 processors of Core i7 machine. Table 3.2 illustrates a nearly linear parallel speedup of FastVOA (in the number of processors used) on synthetic data sets with size of 10,000 points on 100 dimensions.

Table 3.2: Parallel speedup of FastVOA

Number of processors	1	2	4
Speedup	1	2.3	3.7

3.8 Conclusion

In this chapter we introduced a random projection-based algorithm to approximate the variance of angles between pairs of points of the data set, a robust outlier score to detect high-dimensional outlier patterns. By combining random projections and AMS Sketches on product domains, our approximation algorithm runs in near-linear time in the size of data set and is suited for parallel processing. We presented a theoretical analysis of the quality of approximation to guarantee the reliability of our estimation algorithm. The empirical experiments on synthetic and real world data sets demonstrate the scalability, effectiveness and efficiency of our approach on detecting outliers in very large high-dimensional data sets. In future, we plan to deploy MapReduce framework [24] to exploit the parallel capability of the proposed approach for very large-scale high-dimensional data sets.

Chapter 4

Large-scale SVM Classification

*Approximation of non-linear kernels using random feature mapping has been successfully employed in large-scale data analysis applications, accelerating the training of kernel machines. While previous random feature mappings run in $\mathcal{O}(ndD)$ time for n training samples in d-dimensional space and D random feature maps, we propose a novel randomized tensor product technique, called **Tensor Sketching**, for approximating any polynomial kernel in $\mathcal{O}(n(d + D\log D))$ time. Also, we introduce both absolute and relative error bounds for our approximation to guarantee the reliability of our estimation algorithm. Empirically, Tensor Sketching achieves higher accuracy and often runs orders of magnitude faster than the state-of-the-art approach for large-scale real-world datasets.*

*This work was published as an article, "**Fast and Scalable Polynomial Kernels via Explicit Feature Maps**" in Proceedings of 19th ACM SIGKDD Conference on Knowledge Discovery and Data Mining (KDD), 2013.*

4.1 Introduction

Kernel machines such as Support Vector Machines (SVMs) have recently emerged as powerful approaches for many machine learning and data mining tasks. One of the key properties of kernel methods is the capability to efficiently find non-linear structure of data by the use of kernels. A kernel can be viewed as an *implicit* non-linear data mapping from original data space into high-dimensional feature space, where each coordinate corresponds to one feature of the data points. In that space, one can perform well-known data analysis algorithms without ever interacting with the coordinates of the data, but rather by simply computing their pairwise dot products. This operation can not only avoid the cost of explicit computation of the coordinates in feature space, but also handle general types of data (such as numeric data, symbolic data).

While kernel methods have been used successfully in a variety of data analysis tasks, their scalability is a bottleneck. Kernel-based learning algorithms usually scale poorly with the number of the training samples (a cubic running time and quadratic storage for direct methods). This drawback is becoming more crucial with the rise of big data applications [19, 51]. Recently, Joachims [39] proposed an efficient training algorithm for *linear* SVMs that runs in time linear in the number of training examples. Since one can view *non-linear* SVMs as *linear* SVMs operating in an appropriate feature space, Rahimi and Recht [60] first proposed a random feature mapping to approximate shift-invariant kernels in order to combine the advantages of both linear and non-linear SVM approaches. This approach approximates kernels by an *explicit* data mapping into relatively low-dimensional random feature space. In this random feature space, the kernel of any two points is well approximated by their dot product. Therefore, one can apply existing fast linear learning algorithms to find data relations corresponding to non-linear kernel methods in the random feature space. That leads to a substantial reduction in training time while obtaining similar testing error.

Following up this line of work, many randomized approaches to approximate kernels are proposed for accelerating the training of kernel machines [41, 51, 68, 70]. While the training algorithm is linear, existing kernel approximation mappings require time proportional to the product of the number of dimensions

d and the number of random features D. This means that the mapping itself is a bottleneck whenever dD is not small. In this work we address this bottleneck, and present a near-linear time mapping for approximating any polynomial kernel.

Particularly, given any two points of a dataset S of n points, $x = \{x_1, \cdots, x_d\}$, $y = \{y_1, \cdots, y_d\} \in S \subset \mathbb{R}^d$ and an implicit *feature space* mapping $\phi : \mathbb{R}^d \to \mathcal{F}$, the dot product between these points in the feature space $\mathcal{F}$ can be quickly computed as $\langle \phi(x), \phi(y) \rangle = \kappa(x, y)$ where $\kappa()$ is an easily computable kernel. An *explicit* random feature mapping $f : \mathbb{R}^d \to \mathbb{R}^D$ can efficiently approximate a kernel $\kappa()$ if it satisfies:

$$\mathbf{E}\left[\langle f(x), f(y) \rangle\right] = \langle \phi(x), \phi(y) \rangle = \kappa(x, y) \ .$$

So we can transform data from the original data space into a low-dimensional explicit random feature space and use any linear learning algorithm to find non-linear data relations.

Rahimi and Recht [60] introduced a random projection-based algorithm to approximate shift-invariant kernels (e.g. the Gaussian kernel $\kappa(x, y) = \exp\left(\frac{-\|x-y\|^2}{2\sigma^2}\right)$, for $\sigma > 0$). Vempati et al. [70] extended this work to approximate generalized radial-basic function (RBF) kernels (e.g. the exponential-χ^2 kernel $\kappa(x, y) = \exp(-\chi^2(x, y)/2\sigma^2)$, where $\sigma > 0$ and χ^2 is the Chi-squared distance measure). Recently, Kar and Karnick [41] made use of the Maclaurin series expansion to approximate dot product kernels (e.g. the polynomial kernel $\kappa(x, y) = (\langle x, y \rangle + c)^p$, for $c \geq 0$ and an integer p).

These approaches have to maintain D random vectors $\omega_1, \cdots \omega_D \in \mathbb{R}^d$ in $\mathcal{O}(dD)$ space and need $\mathcal{O}(ndD)$ operations for computing D random feature maps. That incurs significant (quadratic) computational and storage costs when $D = \mathcal{O}(d)$ and d is rather large. When the decision boundary of the problem is rather smooth, the computational cost of random mapping might dominate the training cost. In addition, the *absolute* error bounds of previous approaches are not tight. Particularly, the Maclaurin expansion based approach [41] suffers from large error because it approximates the homogeneous polynomial kernel $\kappa(x, y) = \langle x, y \rangle^p$ by $\prod_{i=1}^{p} \langle \omega_i, x \rangle \prod_{i=1}^{p} \langle \omega_i, y \rangle$ where $\omega_i \in \{+1, -1\}^d$. Our experiments show that large estimation error results in either accuracy degradation or negligible reduction in training time.

In this work we consider the problem of approximating the commonly used polynomial kernel $\kappa(x, y) = (\langle x, y \rangle + c)^p$ to accelerate the training of kernel machines. We develop a fast and scalable randomized tensor product technique, named *Tensor Sketching*, to estimate the polynomial kernel of any pair of points of the dataset. Our proposed approach works in $\mathcal{O}(np(d + D \log D))$ time and requires $\mathcal{O}(pd \log D)$ space for random vectors. The main technical insight is the connection between tensor product and fast convolution of Count Sketches [17, 57], which enables us to reduce the computational complexity and space usage. We introduce both *absolute* and *relative* error bounds for our approximation to guarantee the reliability of our estimation algorithm. The empirical experiments on real-world datasets demonstrate that Tensor Sketching achieves higher accuracy and often runs orders of magnitude faster than the state-of-the-art approach for large-scale datasets.

4.2 Related Work

Traditional approaches for solving non-linear SVMs on large datasets are *decomposition methods* [15, 56]. These methods divide the training set into two sets, named working set and fixed set; and iteratively solve the optimization problem with respect to the working set while *freezing* the fixed set. In other words, they iteratively update a subset of kernel methods' coefficients by performing coordinate ascent on subsets of the training set until KKT conditions have been satisfied to within a certain tolerance. Although such approaches can handle the memory restrictions involving the dense kernel matrix, they still involve numerical solutions of optimization subproblems and therefore can be problematic for large-scale datasets.

In order to apply kernel methods to large-scale datasets, many approaches have been proposed for quickly approximating the kernel matrix, including the Nyström methods [25, 75], sparse greedy approximation [65] and low-rank kernel approximation [28]. These approximation schemes can reduce the computational and storage costs of operating on a kernel matrix while preserving the quality of results. An assumption of these approaches is that the kernel matrix has many

zero eigenvalues. This might not be true in many datasets. Furthermore, there is a lack of experiments to illustrate the efficiency of these approaches on large-scale datasets [60].

Instead of approximating the kernel matrix, recent approaches [41, 46, 51, 60, 68, 70, 76] approximate the kernels by explicitly mapping data into a relatively low-dimensional random feature space. The explicit mapping transforms data into a random feature space where the pairwise dot products of transformed data points are approximately equal to kernels in feature space. Therefore, we can apply existing fast linear learning algorithms [27, 39, 64] to find non-linear data relations in that random feature space. While previous such approaches can efficiently accelerate the training of kernel machines, they incur significant computational cost (quadratic in the dimensionality of data). That results in performance degradation on large-scale high-dimensional datasets.

4.3 Background and Preliminaries

4.3.1 Count Sketch

As elaborated in Chapter 2, Count Sketch is a probabilistic data structure that can preserve the pairwise dot products within an arbitrarily small factor. Recently, the machine learning community has used Count Sketch as a feature hashing technique for large-scale multitask learning [73]. In this work we make use Count Sketch as a specific random projection technique, and we recall its definition and properties as follows:

Definition 4.1 (Count Sketch). *Given a 2-wise independent hash function* $h : [d] \to [k]$ *and a 4-wise independent hash function* $s : [d] \to \{+1, -1\}$. *Count Sketch of a point* $x = \{x_1, \cdots, x_d\} \in \mathbb{R}^d$ *is denoted by* $Cx = \{(Cx)_1, \cdots, (Cx)_k\} \in \mathbb{R}^k$ *where* $(Cx)_j = \sum_{i:h(i)=j} s(i)x_i$.

Note that the hash function s is *4-wise* independent, which is different from the original definition. The two Count Sketches $C^{(1)}x, C^{(2)}x$ of a point x are different if they use different hash functions $h_1 \neq h_2$ and $s_1 \neq s_2$. The following lemma provides the bias and variance of the pairwise dot product of Count Sketches.

Lemma 4.1. *Given two points $x, y \in \mathbb{R}^d$, we denote by $Cx, Cy \in \mathbb{R}^k$ the respective Count Sketches of x, y on the hash functions $h : [d] \to [k]$ and $s : [d] \to \{+1, -1\}$, we have*

$$\begin{aligned}\mathbf{E}[\langle Cx, Cy\rangle] &= \langle x, y\rangle \,, \\ \mathbf{Var}[\langle Cx, Cy\rangle] &= \frac{1}{k}\left(\sum_{i\neq j} x_i^2 y_j^2 + \sum_{i\neq j} x_i y_i x_j y_j\right).\end{aligned}$$

Proof. See Appendix B. □

We derive an upper bound of variance of any pairwise dot product of Count Sketches as follows:

Lemma 4.2. *Given two points $x, y \in \mathbb{R}^d$, we denote by $Cx, Cy \in \mathbb{R}^k$ the respective Count Sketches of x, y on the same hash functions h, s.*

$$\mathbf{Var}[\langle Cx, Cy\rangle] \leq \frac{1}{k}\left(\langle x, y\rangle^2 + \|x\|^2 \|y\|^2\right).$$

Proof. Given any two points $x = \{x_1, \cdots, x_d\}, y = \{y_1, \cdots, y_d\}$, we have:

$$\begin{aligned}\|x\|^2\|y\|^2 &= \sum_i x_i^2 y_i^2 + \sum_{i\neq j} x_i^2 y_j^2 \;\;, \\ \langle x, y\rangle^2 &= \sum_i x_i^2 y_i^2 + \sum_{i\neq j} x_i y_i x_j y_j \;\;.\end{aligned}$$

By Lemma 4.1, we have:

$$\begin{aligned}\mathbf{Var}[\langle Cx, Cy\rangle] &= \frac{1}{k}\left(\sum_{i\neq j} x_i^2 y_j^2 + \sum_{i\neq j} x_i y_i x_j y_j\right) \\ &= \frac{1}{k}\left(\langle x, y\rangle^2 + \|x\|^2 \|y\|^2\right) - \frac{2}{k}\sum_i x_i^2 y_i^2 \\ &\leq \frac{1}{k}\left(\langle x, y\rangle^2 + \|x\|^2 \|y\|^2\right).\end{aligned}$$

□

It is worth noting that Count Sketch might provide low distortion on sparse vectors. This is due to the fact that non-zero elements will always be hashed into a cell of Count Sketch. In other words, they are retained after sketching with high probability. In addition, Count Sketch requires $\mathcal{O}(nd)$ operations for n points in d-dimensional space. Therefore, Count Sketch might provide better performance than traditional random projections in applications dealing with sparse vectors.

4.3.2 Tensor Product

Given a vector $x = \{x_1, \cdots, x_d\} \in \mathbb{R}^d$, the 2-level tensor product or outer product $x^{(2)} = x \otimes x$ is defined as follows:

$$x^{(2)} = x \otimes x = \begin{bmatrix} x_1x_1 & x_1x_2 & \cdots & x_1x_d \\ x_2x_1 & x_2x_2 & \cdots & x_2x_d \\ \vdots & \vdots & \ddots & \vdots \\ x_dx_1 & x_dx_2 & \cdots & x_dx_d \end{bmatrix} \in \mathbb{R}^{d^2} \quad .$$

Given an integer p, we consider a p-level tensor product $\Omega^p : \mathbb{R}^d \to \mathbb{R}^{d^p}$ given by

$$x \to x^{(p)} = x \underbrace{\otimes \cdots \otimes}_{p \text{ times}} x \quad .$$

The following lemma justifies that tensor product is an explicit feature mapping for the homogeneous polynomial kernel.

Lemma 4.3. *Given any pair of points x, y and an integer p, we have:*

$$\left\langle x^{(p)}, y^{(p)} \right\rangle = \langle x, y \rangle^p \quad .$$

Proof. See [62, Proposition 2.1]. □

By taking $y = x$ on Lemma 4.3, we have:

Lemma 4.4. *Given any point x and an integer p, we have:*

$$\|x^{(p)}\|^2 = \|x\|^{2p}.$$

It is obvious that the tensor product requires d^p dimensions to comprise the polynomial feature space. Therefore, it fails for realistically sized applications.

4.4 Tensor Sketching Approach

As elaborated above, it is infeasible to directly perform any learning algorithm in the polynomial feature space. In this section, we introduce an efficient approach to randomly project the images of data without ever computing their coordinates in that polynomial feature space. The proposed approach runs in $\mathcal{O}(np(d + D\log D))$ time for n training examples in d-dimensional space and D random projections, and outputs unbiased estimators of the degree-p polynomial kernel of any pair of data points.

4.4.1 The Convolution of Count Sketches

Recently, Pagh [57] has introduced a fast algorithm to compute Count Sketch of an outer product of two vectors. Instead of directly computing the outer product, the approach compresses these vectors into their Count Sketches and then computes the Count Sketch of their outer product by those sketches. Due to the fact that the outer product of two different Count Sketches can be efficiently computed by the polynomial multiplication (using FFT), we can compute the Count Sketch of an outer product of any two vectors in time near-linear in the dimensionality of the sketches.

More precisely, given a vector $x \in \mathbb{R}^d$, we denote by $C^{(1)}x, C^{(2)}x \in \mathbb{R}^D$ its two different Count Sketches using *2-wise* independent hash functions $h_1, h_2 : [d] \to [D]$ and *4-wise* independent hash functions $s_1, s_2 : [d] \to \{+1, -1\}$. We consider the outer product $x \otimes x \in \mathbb{R}^{d^2}$ and its Count Sketch $Cx^{(2)} \in \mathbb{R}^D$ using independent and *decomposable* hash functions $H : [d^2] \to [D]$ and $S : [d^2] \to \{+1, -1\}$. We

decompose H and S as follows:

$$H(i,j) = h_1(i) + h_2(j) \bmod D \text{ and } S(i,j) = s_1(i)s_2(j).$$

We note that the hash functions H and S are *2-wise* and *4-wise* independent, respectively [59]. We then represent a Count Sketch in D-dimensional space as a polynomial of degree $D-1$ where each coordinate corresponds to one term of the polynomial. For example, we consider two degree-$(D-1)$ polynomials representing for $C^{(1)}x, C^{(2)}x$:

$$P_x^{(1)}(\omega) = \sum_{i=1}^{d} s_1(i)x_i\omega^{h_1(i)} \text{ and } P_x^{(2)}(\omega) = \sum_{j=1}^{d} s_2(j)x_j\omega^{h_2(j)}.$$

We can fast compute the degree-$(D-1)$ polynomial for $Cx^{(2)}$ using hash functions H and S:

$$\begin{aligned} P_{x^{(2)}}(\omega) &= \sum_{i,j=1}^{d} S(i,j)x_ix_j\omega^{H(i,j)} \\ &= \mathrm{FFT}^{-1}(\mathrm{FFT}(P_x^{(1)}) * \mathrm{FFT}(P_x^{(2)})), \end{aligned}$$

where $(*)$ is the component-wise product operator and FFT uses D interpolation points. In other words, the Count Sketch $Cx^{(2)}$ of $x \otimes x$ can be efficiently computed by Count Sketches $C^{(1)}x, C^{(2)}x$ in $\mathcal{O}(d + D\log D)$ time.

Inspired by the fast convolution of Count Sketches, we are able to efficiently compute the polynomial $P_{x^{(p)}}(\omega)$ for the Count Sketch in D-dimensional space, $Cx^{(p)}$, of the tensor product $x^{(p)}$ of any point $x \in \mathbb{R}^d$ by using independent and *decomposable* hash functions $H : [d^p] \to [D]$ and $S : [d^p] \to \{+1, -1\}$. We decompose H and S as follows:

$$\begin{aligned} H(i_1, \cdots, i_p) &= \sum_{k=1}^{p} h_k(i_k) \bmod D, \\ S(i_1, \cdots, i_p) &= \prod_{k=1}^{p} s_k(i_k), \end{aligned}$$

Algorithm 5 Tensor Sketching(S, p, D)

Require: A dataset S of size n, the number of random features D and the degree of polynomial kernel p

Ensure: Return Count Sketches of the point set S as a random feature mapping f for the polynomial kernel $\kappa(x, y) = \langle x, y \rangle^p$

1: $f(S) \leftarrow \emptyset$
2: Pick p independent hash functions $h_1, \cdots, h_p : [d] \rightarrow [D]$, each from a 2-wise independent family
3: Pick p independent hash functions $s_1, \cdots, s_p : [d] \rightarrow \{+1, -1\}$, each from a 4-wise independent family
4: **for** each data point $x \in S$ **do**
5: Create p different Count Sketches: $C^{(1)}x, \cdots, C^{(p)}x$
6: $(C^{(1)}x, \cdots, C^{(p)}x) \leftarrow \mathrm{FFT}(C^{(1)}x, \cdots, C^{(p)}x)$
7: Obtain $f(x)$ in frequency domain by the component-wise multiplication $C^{(1)}x * \cdots * C^{(p)}x$
8: $f(x) \leftarrow \mathrm{FFT}^{-1}(f(x))$
9: Insert $f(x)$ into $f(S)$
10: **end for**
11: **return** Return $f(S)$

where $h_1, \cdots, h_p : [d] \rightarrow [D]$ and $s_1, \cdots, s_p : [d] \rightarrow \{+1, -1\}$ are chosen independently from *2-wise* and *4-wise* independent family, respectively.

The proposed approach works in $\mathcal{O}(p(d + D \log D))$ time by using $2p$ different and independent hash functions as elaborated above. This idea motivates the intuition for Tensor Sketching approach to approximate polynomial kernels.

4.4.2 Tensor Sketching Approach

We exploit the fast computation of Count Sketches on tensor domains to introduce an efficient algorithm for approximating the polynomial kernel $\kappa(x, y) = (\langle x, y \rangle + c)^p$, for an integer p and $c \geq 0$. It is obvious that we can avoid the constant c by adding an extra dimension of value $\sqrt{c}$ to all data points. So, for simplicity, we solely consider the homogeneous polynomial kernel $\kappa(x, y) = \langle x, y \rangle^p$ for the proposed algorithm and theoretical analysis.

For each point $x \in S \subset \mathbb{R}^d$, Tensor Sketching returns the Count Sketch of size D of the tensor product $x^{(p)}$ as random feature maps in $\mathbb{R}^D$ for the polynomial

kernel. The pseudo-code in Algorithm 5 shows how Tensor Sketching works. We maintain $2p$ independent hash functions $h_1, \cdots, h_p$ and $s_1, \cdots, s_p$ (lines 2 - 3). For each point x, we create p different Count Sketches of size D using these $2p$ different and independent hash functions (line 5). We then compute the Count Sketch of $x^{(p)}$ by the usage of polynomial multiplication (using FFT) (lines 6-8). As a result, we have obtained a random feature mapping f which provides unbiased estimators for the polynomial kernel.

Now, we analyze the complexity of Tensor Sketching. It requires $\mathcal{O}(pd \log D)$ space usage to store $2p$ hash functions. For each point, the running time of computing the Count Sketch of its p-level tensor product is $\mathcal{O}(pd + pD \log D)$ due to applying FFT. Therefore, the total running time of Tensor Sketching is $\mathcal{O}(np(d + D \log D))$. To increase the accuracy of estimates, we choose $D = \mathcal{O}(d)$; therefore, we need $\mathcal{O}(npd \log d)$ operations compared to $\mathcal{O}(nd^2)$ of the previous approaches [41, 60].

4.5 Error Analysis

In this section we analyze the precision of estimate of the kernel $\kappa(x, y) = \langle x, y \rangle^p$, where $x, y \in \mathbb{R}^d$ and p is an integer, showing bounds on the number of random features (D) to achieve a given *absolute* or *relative* precision ε. It is worth noting that the previous approaches [41, 51, 60, 68] only introduced bounds of an absolute error estimate. Often, however, the kernel has small value and a good absolute error approximation is typically a poor relative error estimate. Large errors of estimate might result in either performance degradation or negligible reduction in computational cost.

4.5.1 Relative Error Bound

In contrast to the previous techniques, our approach can be viewed as a specific random projection technique applied to images of data in the explicit polynomial feature space. In fact, Tensor Sketching maintains random projections of images of data in the feature space via independent hash functions of Count Sketches. Therefore, its estimators are unbiased and have tight error bounds.

Given two points $x, y \in \mathbb{R}^d$, we denote by $Cx^{(p)}, Cy^{(p)} \in \mathbb{R}^D$ the Count Sketches of $x^{(p)}$, $y^{(p)} \in \mathbb{R}^{d^p}$, respectively. Lemma 4.3 and 4.4 guarantee that

$$\left\langle x^{(p)}, y^{(p)} \right\rangle = \langle x, y \rangle^p , \quad \|x^{(p)}\| = \|x\|^p, \quad \|y^{(p)}\| = \|y\|^p \ .$$

So applying Lemma 4.1 and 4.2, we have:
Lemma 4.5.

$$\begin{aligned} \mathbf{E}\left[\left\langle Cx^{(p)}, Cy^{(p)} \right\rangle\right] &= \langle x, y \rangle^p , \\ \mathbf{Var}\left[\left\langle Cx^{(p)}, Cy^{(p)} \right\rangle\right] &\leq \frac{1}{D}\left(\langle x, y \rangle^{2p} + \|x\|^{2p} \|y\|^{2p}\right). \end{aligned}$$

While previous works on random feature mappings do not provide bounds on the variance of estimates, the variance of our estimate can be bounded. We make use Chebyshev's inequality to bound the relative error, which depends on the cosine of the angle θ_{xy} between x and y.
Lemma 4.6.

$$\mathbf{P}\left[\left|\left\langle Cx^{(p)}, Cy^{(p)} \right\rangle - \langle x, y \rangle^p\right| \geq \varepsilon \langle x, y \rangle^p\right] \leq \frac{2}{D\varepsilon^2}\left(\frac{1}{\cos\theta_{xy}}\right)^{2p}.$$

Proof. Consider the random variable $X = \left\langle Cx^{(p)}, Cy^{(p)} \right\rangle$, Chebyshev's inequality guarantees that:

$$\begin{aligned} &\mathbf{P}[|X - \mathbf{E}[X]| \geq \varepsilon \mathbf{E}[X]] \leq \frac{\mathbf{Var}[X]}{\varepsilon^2 \mathbf{E}[X]^2} \\ &\leq \frac{1}{D\varepsilon^2} \frac{\langle x, y \rangle^{2p} + \|x\|^{2p} \|y\|^{2p}}{\langle x, y \rangle^{2p}} \\ &= \frac{1}{D\varepsilon^2}\left(\frac{1}{(\cos\theta_{xy})^{2p}} + 1\right) \leq \frac{2}{D\varepsilon^2}\left(\frac{1}{\cos\theta_{xy}}\right)^{2p}. \end{aligned}$$

□

It is obvious that we need more random features to approximate polynomial kernels of large degree p. In addition, the relative error depends on the pairwise angles of data points. So we have to use large D for almost orthogonal data points to achieve a good approximation.

4.5.2 Absolute Error Bound

Following up on the work of Kar and Karnick [41], we assume that the 1-norm of any point of data can be bounded, such that $\|x\|_1 = \sum_{i=1}^{d} x_i \leq R$ for any point x and a nonnegative real R. It is clear that $\|x^{(p)}\|_1 = \|x\|_1^p \leq R^p$. So we first establish the bound of $\left|\left\langle Cx^{(p)}, Cy^{(p)}\right\rangle\right|$ for any pair of points x, y as follows:

Lemma 4.7.

$$\left|\left\langle Cx^{(p)}, Cy^{(p)}\right\rangle\right| \leq R^{2p} \ .$$

Proof. The Hölder inequality says that $\left|\left\langle Cx^{(p)}, Cy^{(p)}\right\rangle\right| \leq \|Cx^{(p)}\|_1 \|Cy^{(p)}\|_\infty$. So it suffices to prove that $\|Cx^{(p)}\|_1 \leq R^p$ for any x due to $\|Cx^{(p)}\|_\infty \leq \|Cx^{(p)}\|_1$. By applying the Cauchy-Schwarz inequality, we have: $\|Cx^{(p)}\|_1 = \sum_{i=1}^{D} |Cx_i^{(p)}| \leq \sum_{i=1}^{d^p} |x_i^{(p)}| \leq R^p$. That proves the claim. □

For any pair of points x, y, we use t different pairs of Count Sketches $\left(C^{(1)}x^{(p)}, C^{(1)}y^{(p)}\right)$, $\cdots$, $\left(C^{(t)}x^{(p)}, C^{(t)}y^{(p)}\right)$. By Hoeffding's inequality, we achieve a tighter absolute error bound than the previous approach [41] as follows:

Lemma 4.8. *Let $X = \frac{1}{t}\sum_{i=1}^{t} X_i$ be an average of the sum of independent random variables $X_i = \left\langle C^{(i)}x^{(p)}, C^{(i)}y^{(p)}\right\rangle$ for each $i \in [t]$, $X_i \in [-R^{2p}, R^{2p}]$ for any nonnegative real R. For any $\varepsilon > 0$,*

$$\Pr[|X - \mathbf{E}[X]| \geq \varepsilon] \leq 2\exp\left(\frac{-t\varepsilon^2}{2R^{4p}}\right) \ .$$

Our absolute error bound depends on the largest value taken by the polynomial kernel in the data space (e.g. R^{2p}). In fact, no algorithm guaranteeing an absolute error can avoid this dependence due to the unbounded nature of the polynomial kernel.

4.5.3 Normalization

Empirically, it has been shown that normalizing a kernel may improve the performance of SVMs. A way to do so is to normalize the data such as $\|x\| = 1$ so that the exact kernel is properly normalized, i.e. $\kappa(x, x) = \langle x, x\rangle^p = 1$. The following lemma shows that Count Sketches can preserve the normalization of kernels.

Lemma 4.9. *Given fixed constants $\varepsilon, \delta < 1$ and a point x such that $\|x\| = 1$, we denote by $Cx^{(p)} \in \mathbb{R}^D$ the Count Sketch of $x^{(p)}$. If $\|x^{(p)}\|_\infty \leq \frac{\varepsilon}{18\sqrt{\log(1/\delta)\log(D/\delta)}}$ and $D \geq 72\log(1/\delta)/\varepsilon^2$, we have that*

$$\mathbf{Pr}\left[\left|\left\langle Cx^{(p)}, Cx^{(p)}\right\rangle - 1\right| \geq \varepsilon\right] \leq 2\delta.$$

Proof. See [73, Appendix B]. □

It is obvious that our kernel approximation can maintain the normalization of kernels within an arbitrarily small factor. In contrast, the Maclaurin expansion based approach [41] does not satisfy this property.

4.6 Experimental Results

We implemented random feature mappings in Matlab-7.11.0 and conducted experiments in a 2.67 GHz core i7 Windows platform with 3GB of RAM. We compared the performance of random feature mappings, including Tensor Sketching (TS) and Random Maclaurin (RM) [41] with non-linear SVMs on 4 real world datasets: Adult [29], Mnist [47], Gisette [15], and Covertype[1] [29]. We used LIBSVM-3.14 [15] for non-linear kernels and LIBLINEAR-1.92 [27] for random feature mappings for classification task. All averages and standard deviations are over 5 runs of the algorithms.

4.6.1 Accuracy of Estimation

This subsection presents the accuracy experiments to evaluate the reliability of our estimation algorithm. We carried out experiments to compare the accuracy of estimators based on the number of random features (D) on two random feature mappings: Tensor Sketching (TS) and Random Maclaurin (RM). We measured the relative error of the approximation of the homogeneous and inhomogeneous polynomial kernels of degree $p = 2, 3, 4$. We took D in ranges [500, 3000] and

[1]We sample 100,000 points for Covertype datasets due to the limit of RAM

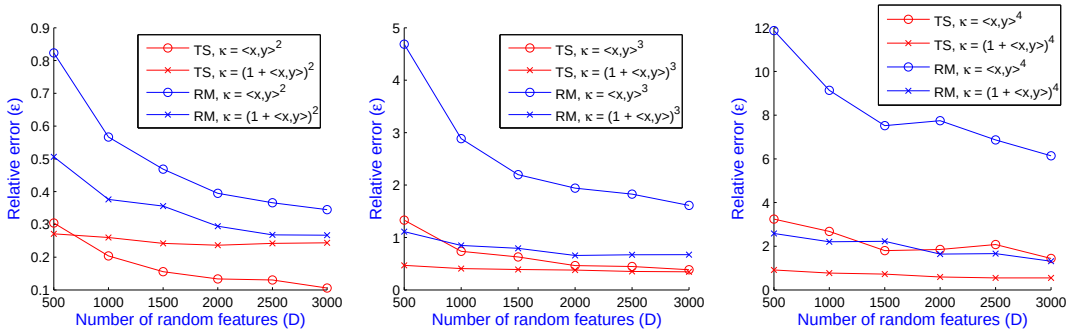

Figure 4.1: Comparison of relative errors between Tensor Sketching (TS) and Random Maclaurin (RM) estimators on the Adult dataset (n = 48,842, d = 123) using different polynomial kernels. (Figures best viewed in color.)

conducted experiments on Adult dataset with size $n = 48,842$ and dimensionality $d = 123$. Figure 4.1 displays the relative error (ε) from expectation of the two approaches on different polynomial kernels.

It is obvious that TS provides a smaller error than the RM approach on those polynomial kernels. The difference is most dramatic on the homogeneous kernels because of the use of Rademacher vectors $\omega_i \in \{+1, -1\}^d$ in RM. In fact, it estimates $\langle x, y\rangle^p$ as $\prod_{i=1}^{p} \langle \omega_i, x\rangle \prod_{i=1}^{p} \langle \omega_i, y\rangle$, which incurs very large variance, especially for large p. Due to the fact that we have to normalize data before applying any kernel method, RM gives small error on inhomogeneous kernels. In this case, the value of Maclaurin expansion concentrates on some low order terms that have small variance of estimate. When the accuracy of kernel machines depends on higher order terms, RM either suffers from low accuracy or needs large D due to large variance of estimate. In contrast, TS is a specific random projection in the polynomial feature space. So it greatly outperforms RM and does not require a large number of random features to achieve a small error. For example, on the inhomogeneous kernels, TS only needs $D = 500$ to achieve $\varepsilon < 1$ while RM requires more than 3000 random features.

4.6.2 Efficiency

This subsection compares the random feature construction time of the two approaches, TS and RM, on two large high-dimensional datasets: Adult ($d = 123$)

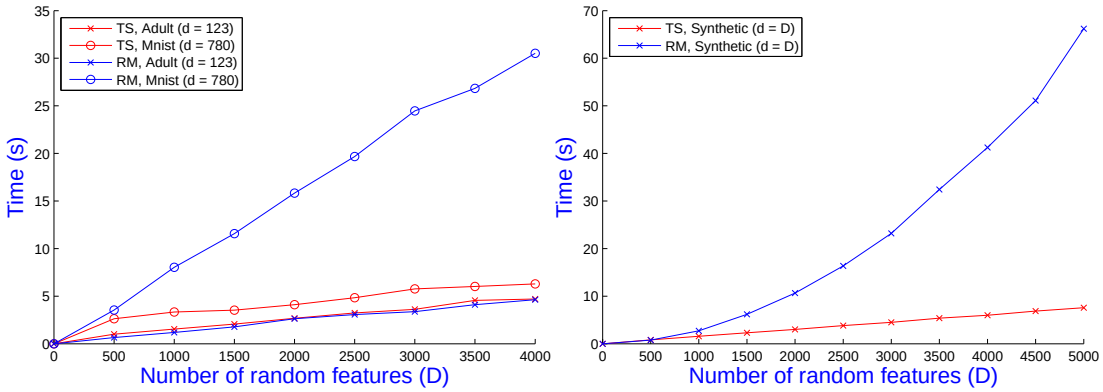

(a) CPU Time (s) on Adult and Mnist datasets

(b) CPU Time (s) on synthetic dataset

Figure 4.2: Comparison of CPU time (s) between Tensor Sketching (TS) and Random Maclaurin (RM) approaches on 3 datasets: (a) Adult ($d = 123$) and Mnist ($d = 780$); (b) Synthetic ($d = D$) using $\kappa = (1 + \langle x, y \rangle)^4$. (Figures best viewed in color.)

and Mnist ($d = 780$). As analyzed above, TS requires $\mathcal{O}(np(d + D \log D))$ time while RM demands $\mathcal{O}(ndD)$ time and much randomness. It is obvious that the running time of TS is faster and less dependent on the original dimensionality of data, a very desirable property since random feature mapping often contributes a significant computational cost in training large-scale high-dimensional datasets.

Figure 4.2.a shows the CPU time requirements in seconds of the two approaches on the kernel $\kappa = (1 + \langle x, y \rangle)^4$ when varying the number of random features D in ranges $[0, 4000]$ and fixing the number of training samples $n = 10,000$. It is clear that the running time of TS approach is almost independent from the dimensionality of data d when using large D. On both Adult ($d = 123$) and Mnist ($d = 779$) datasets, TS approach scales well when increasing D compared to RM on Adult dataset. In contrast, RM shows a linear dependence with d, as depicted on Mnist dataset ($d = 780$). When the dataset (e.g. Mnist) has a smooth decision boundary, RM feature construction time dominates the training time. This property might limit the use of RM.

When the dimensionality of data d increases, we need to increase the number of random features $D = \mathcal{O}(d)$ to boost the accuracy. Figure 4.2.b demonstrates a quadratic running time of RM in terms of dimensionality of data on the synthetic

dataset with setting $d = D$ and $n = 10,000$. This means that RM will be a bottleneck of kernel machines on high-dimensional datasets. The next section will show a significant domination of RM feature mapping when training on the Gisette dataset ($d = 5000$).

4.6.3 Scalability

In this experiment, we compare the performance of random feature mappings (TS, RM) along with LIBLINEAR [27] and non-linear kernel mapping along with LIBSVM [15] for classification tasks on 4 large-scale datasets. We measured the training accuracy and time of these approaches on a variety of polynomial kernels. We note that training time of random feature mapping approaches include time for feature construction and linear SVMs training.

Figure 4.3 and 4.4 demonstrate a comparison of accuracy between TS, RM and non-linear SVMs on degree-2 polynomial kernels. The results impressively show that TS provides higher accuracy than RM on 4 datasets. The most dramatic difference is on the homogeneous kernels due to large error of estimate of RM. Moreover, the accuracy of TS converges faster than RM to that of non-linear kernels when increasing the number of random features D. RM even decreases the accuracy on Gisette dataset because it requires a significantly large number of random features for approximating higher order terms of Maclaurin expansion well.

Figure 4.5 shows the CPU time requirements in seconds of the two approaches in training linear SVMs using LIB-LINEAR on the kernel $\kappa = (1 + \langle x, y \rangle)^2$. It is obvious that TS provides performance benefits on high-dimensional datasets, such as Mnist and Gisette. On Covertype and Adult datasets, RM is slightly faster than TS. This is because RM generates more features for the low order terms of Maclaurin expansion which do not require high computational cost. When p is large, TS significantly outperforms RM, as illustrated in Table 4.1 and 4.2.

It is obvious that RM performs quite poorly on homogeneous kernels on the 4 datasets. Due to the large error of estimate in homogeneous kernels, RM provides low accuracy on 4 datasets, especially in the kernel $\kappa = \langle x, y \rangle^4$. In fact, the large error of estimate produces meaningless results of training linear SVMs (e.g. 41.45

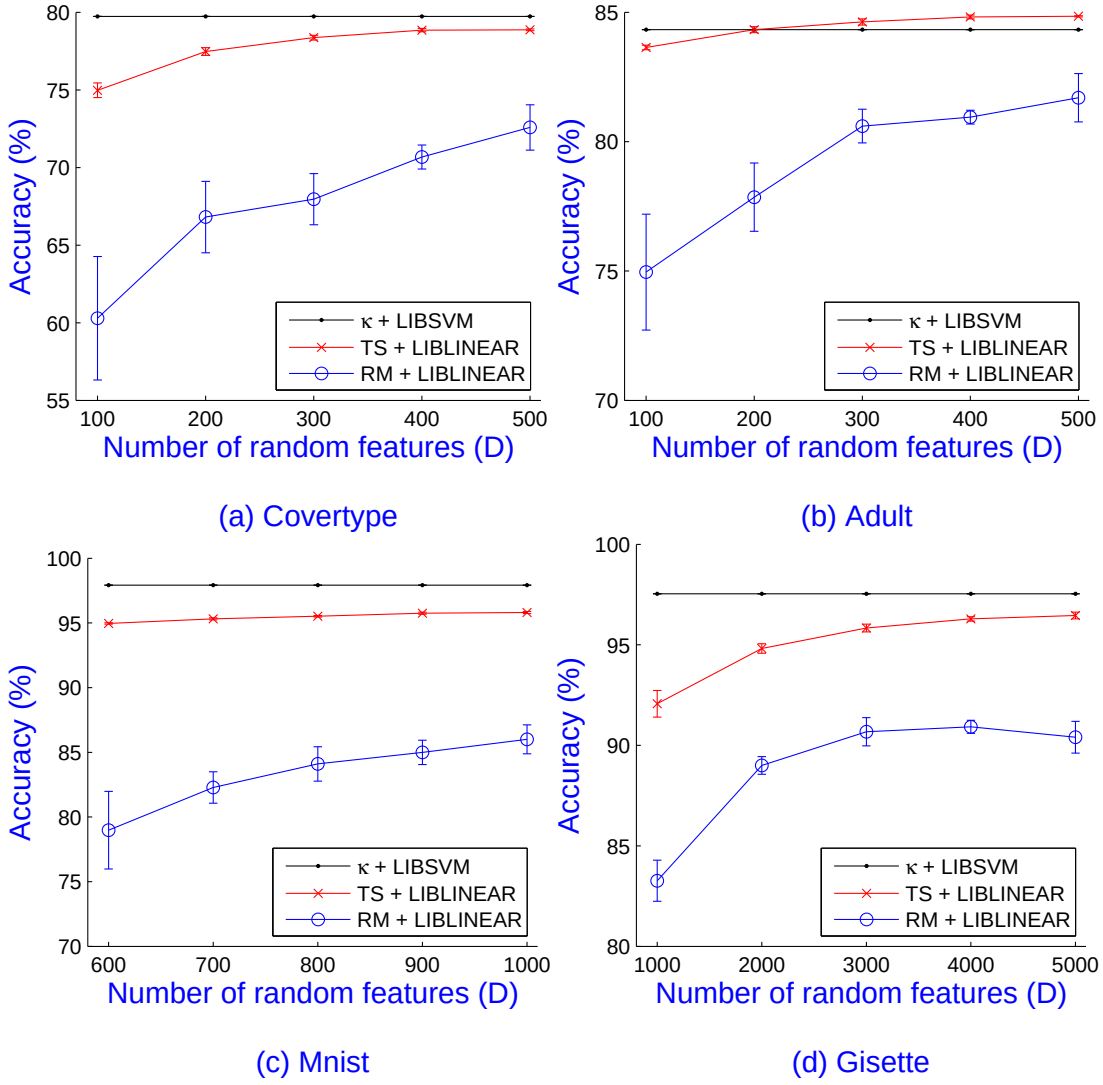

Figure 4.3: Comparison of accuracy of Tensor Sketching (TS), Random Maclaurin (RM) with LIBLINEAR and non-linear kernels with LIBSVM on 4 datasets with the homogeneous kernel $\kappa = \langle x, y \rangle^2$. (Figures best viewed in color.)

% of accuracy on the Mnist dataset). In contrast, TS shows stronger results than both RM and non-linear SVMs because it requires rather small time for feature construction and linear SVMs training while obtaining similar accuracy. TS performs exceptionally well on datasets of non-smooth decision boundaries, including Covertype and Adult, where it can achieve speed-ups of 50 and 1600 times, respectively, compared to non-linear SVMs on the kernel $\kappa = (1 + \langle x, y \rangle)^4$.

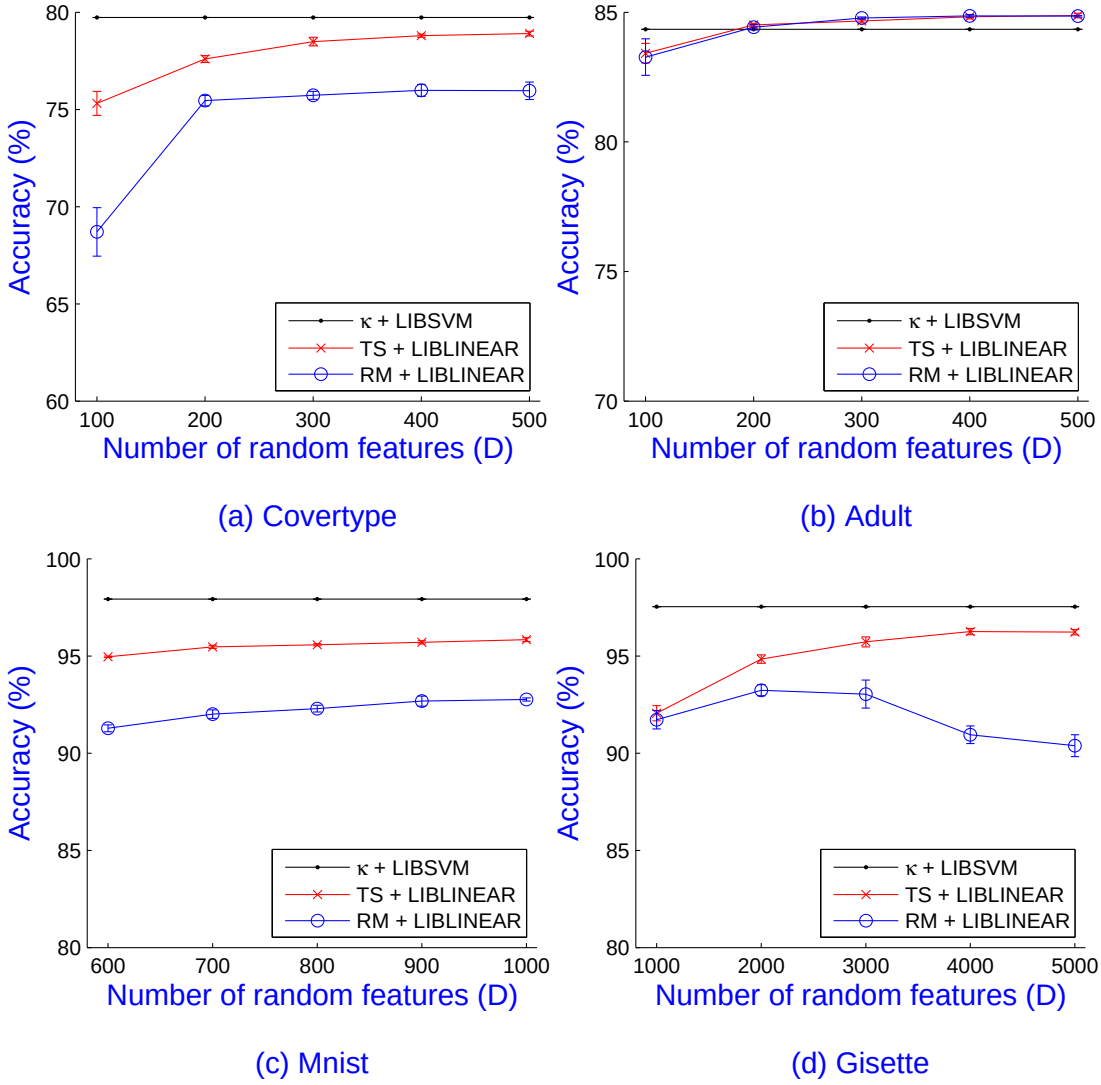

Figure 4.4: Comparison of accuracy of Tensor Sketching (TS), Random Maclaurin (RM) with LIBLINEAR and non-linear kernels with LIBSVM on 4 datasets with the inhomogeneous kernel $\kappa = (1 + \langle x, y \rangle)^2$. (Figures best viewed in color.)

RM works better on inhomogeneous polynomial kernels because the value of Maclaurin expansion concentrates on some low order terms. However it suffers from large computational cost of random mapping in high-dimensional datasets (e.g. Gisette and Mnist). Because these datasets have smooth decision boundaries, their training time is dominated by the random feature construction time. So RM gives similar performance to non-linear SVMs on the Gisette dataset.

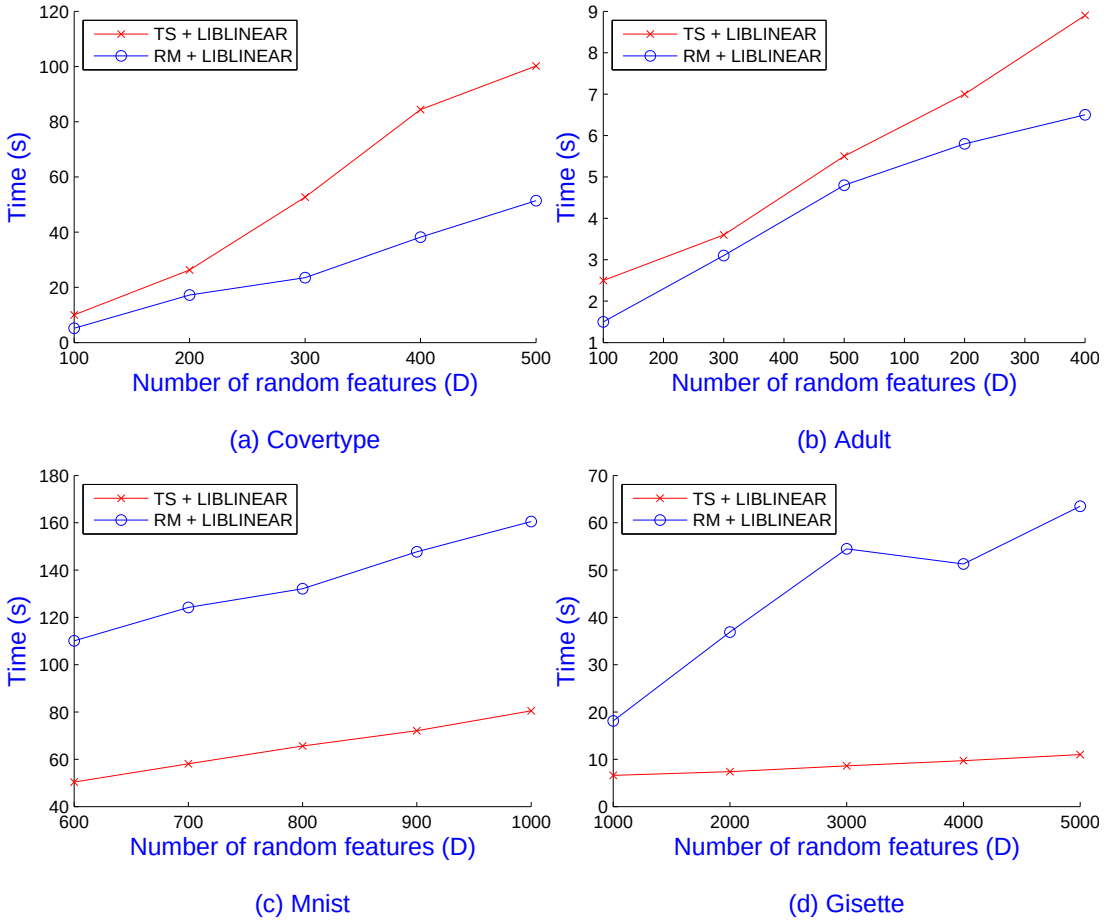

Figure 4.5: Comparison of training time between Tensor Sketching (TS) and Random Maclaurin (RM) with LIBLINEAR on 4 datasets with the inhomogeneous polynomial kernel $\kappa = (1 + \langle x, y \rangle)^2$. (Figures best viewed in color.)

When RM suffers from large error of estimate, it can influence the smoothness of decision boundaries of linear SVMs algorithm and therefore require more training time. This explains the inefficiency of RM compared to non-linear SVMs on Mnist dataset on the kernel $\kappa = (1 + \langle x, y \rangle)^4$.

In contrast, the TS approach gives more stable and better performance than RM and non-linear SVMs approaches on 4 datasets. In particular, it has a slightly lower accuracy but runs much faster than non-linear SVMs. It not only achieves higher accuracy (up to 7%), but also runs faster (up to 13 times) than RM on the Mnist and Gisette datasets. Table 4.3 shows the speedup of TS compared to

Table 4.1: Comparison of Tensor Sketching (TS), Random Maclaurin (RM) feature mappings with LIBLINEAR and non-linear kernels with LIBSVM on 2 datasets (Covertype and Mnist) on many polynomial kernels.

(a) Covertype (n = 100,000, d = 54, D = 500)

Kernel	κ+libsvm	TS+LIBLINEAR	RM+LIBLINEAR
$\langle x, y \rangle^2$	79.73% 11.3 mins	78.87±0.06% 1.6 mins	72.58±1.46% 3.7 secs
$(1 + \langle x, y \rangle)^2$	79.73% 11.5 mins	78.90±0.12% 1.7 mins	75.96±0.45% 0.8 mins
$\langle x, y \rangle^4$	84.01% 1 hour	79.39±0.13% 1.6 mins	**58.55±2.75%** 3.3 secs
$(1 + \langle x, y \rangle)^4$	84.20% **1.5 hours**	79.36±0.19% 1.8 mins	76.76±0.42% 1.6 mins

(b) Mnist (n = 60,000, d = 780, D = 1000)

Kernel	κ+libsvm	TS+LIBLINEAR	RM+LIBLINEAR
$\langle x, y \rangle^2$	97.92% 4.7 mins	95.81±0.08% 1.3 mins	86.00±1.12% 0.5 mins
$(1 + \langle x, y \rangle)^2$	97.93% 4.7 mins	95.84±0.10% 1.3 mins	92.76±0.08% 2.7 mins
$\langle x, y \rangle^4$	97.17% 5 mins	92.49±0.22% 2.1 mins	**41.45±4.81%** 0.5 mins
$(1 + \langle x, y \rangle)^4$	97.31% 5 mins	92.44±0.04% 2.1 mins	90.07±0.65% **17.2 mins**

RM and non-linear SVMs on 4 datasets on the kernel $\kappa = (1 + \langle x, y \rangle)^4$.

The TS random mapping does not show any speedup on low-dimensional datasets (e.g. Covertype, Adult) compared to RM, except for achieving smaller error. However, TS runs 8 times faster than RM in training the Adult dataset due to smaller estimation error. For high-dimensional datasets (e.g. Mnist and Gisette), TS shows speedup on both random mapping and training time. Compared to non-linear kernels, TS achieves significant speedup on Adult and Covertype which have non-smooth decision boundaries.

Table 4.2: Comparison of Tensor Sketching (TS), Random Maclaurin (RM) feature mappings with LIBLINEAR and non-linear kernels with LIBSVM on 2 datasets (Adult and Gisette) on many polynomial kernels.

(a) Adult (n = 48,842, d = 123, D = 200)

Kernel	κ+libsvm	TS+LIBLINEAR	RM+LIBLINEAR
$\langle x, y\rangle^2$	84.33% 0.5 hours	84.33±0.12% 3.6 secs	77.85±1.32% $<$ 1 sec
$(1 + \langle x, y\rangle)^2$	84.34% 0.5 hours	84.51±0.07% 3.8 secs	84.42±0.10% 3.4 secs
$\langle x, y\rangle^4$	79.34% 2 hours	81.09±0.63% 4.3 secs	**58.04±2.37%** $<$ 1 sec
$(1 + \langle x, y\rangle)^4$	79.31% **2 hours**	81.89±0.24% 4.5 secs	84.04±0.46% 14.8 secs

(b) Gisette (n = 7000, d = 5000, D = 5000)

Kernel	κ+libsvm	TS+LIBLINEAR	RM+LIBLINEAR
$\langle x, y\rangle^2$	97.54% 1.4 mins	96.46±0.17% 10.6 secs	90.40±0.79% 1 min
$(1 + \langle x, y\rangle)^2$	97.54% 1.4 mins	96.23±0.14% 10.6 secs	90.38±0.56% 1.1 mins
$\langle x, y\rangle^4$	97.91% 1.8 mins	95.11±0.15% 13.6 secs	**78.89±0.68%** 1.5 mins
$(1 + \langle x, y\rangle)^4$	97.91% 1.8 mins	95.21±0.33% 13.5 secs	88.86±0.57% **2.9 mins**

Table 4.3: Speedup of Tensor Sketching compared to Random Maclaurin and non-linear SVMs on $\kappa = (1 + \langle x, y\rangle)^4$.

Datasets	Random Maclaurin		κ + libsvm
	Mapping	Training	
Adult (D = 200)	__	8×	1600×
Covertype (D = 500)	__	__	50×
Mnist (D = 1000)	2×	9×	2×
Gisette (D = 5000)	9×	25×	8×

Table 4.4: Comparison of Tensor Sketching and Random Maclaurin with H0/1 on $\kappa = (1 + \langle x, y \rangle)^4$.

Datasets	Tensor Sketching	Random Maclaurin with H0/1
Adult $D = 200$	81.89±0.24% 4.5 secs	84.79±0.09% **5.7 secs**
Covertype $D = 500$	79.36±0.19% 1.8 mins	78.88±0.12% **2.2 mins**
Mnist $D = 1000$	92.44±0.04% 2.1 mins	89.19±0.74% **7.8 mins**

4.6.4 Comparison with Heuristic H0/1

In the previous work, the authors [41] introduce a heuristic named H0/1 for fast training. Due to the fact that we have to normalize data before applying any SVM-based learning algorithms, the value of Maclaurin expansion often concentrates on the low order terms. Therefore, we can precompute the first and second terms of the Maclaurin expansion to achieve higher accuracy. For example, consider a Maclaurin expansion of a degree-4 polynomial kernel as follows: $\kappa = (1 + \langle x, y \rangle)^4 = 1 + 4\langle x, y \rangle + 6\langle x, y \rangle^2 + 4\langle x, y \rangle^3 + \langle x, y \rangle^4$. We can easily compute $1 + 4\langle x, y \rangle$ in advance and use D' random features to estimate $6\langle x, y \rangle^2 + 4\langle x, y \rangle^3 + \langle x, y \rangle^4$. This means that H0/1 needs $D = d + D'$ random features and is able to achieve higher accuracy due to the use of D' random features for approximating higher order terms.

However, H0/1 shows some disadvantages: (1) it cannot be used for homogeneous kernels; (2) it is not a dimensionality reduction technique because of using $d + D'$ random features and (3) H0/1 requires longer feature construction times due to the use of more randomness. When d is large, the feature construction time is even larger and often dominates the training time. Table 4.4 shows the comparison between Tensor Sketching and Random Maclaurin with H0/1. Note that we do not use H0/1 on the Gisette dataset because of the large computational cost of random feature construction.

Although RM with H0/1 can offer better accuracy than plain RM, its accuracy is still lower than TS, except on the Adult dataset. In fact, the Adult dataset

works well and achieves higher accuracy (84.92%) on the kernel $\kappa = 1 + 4\langle x, y\rangle$ than with $\kappa = (1 + \langle x, y\rangle)^4$ (79.31%). That explains why the accuracy of RM with H0/1 is exceptionally high. Due to the use of more randomness, the feature construction time of RM with H0/1 is much longer than TS on 3 datasets. In general, H0/1 is only suitable for low-dimensional datasets and works well when the value of polynomial kernel highly concentrates on the first and second terms of Maclaurin expansion.

4.7 Conclusion

In this chapter we have introduced a fast and scalable randomized tensor product technique for approximating polynomial kernels, accelerating the training of kernel machines. By exploiting the connection between tensor product and fast convolution of Count Sketches, our approximation algorithm works in time $\mathcal{O}(n(d + D \log D))$ for n training samples in d-dimensional space and D random features. We present a theoretical analysis of the quality of approximation to gua-rantee the reliability of our estimation algorithm. We show empirically that our approach achieves higher accuracy and often runs orders of magnitude faster than the state-of-the-art approach on large-scale real-world datasets.

An interesting research direction is analyzing and evaluating Tensor Sketching on other learning tasks, such as clustering [20] and multitask learning [73] on large-scale datasets. We also intend to apply Tensor Sketching on other kernels (e.g. Gaussian kernel, sigmoid kernel) by exploiting Taylor-series approximations of these kernels. By applying Tensor Sketching on Taylor-series approximations, we might achieve a substantial speedup in training these kernel machines.

Chapter 5

High Similarity Estimation

Estimating set similarity is a central problem in many computer applications. In this chapter we introduce the ***Odd Sketch****, a compact binary sketch for estimating the Jaccard similarity of two sets. The exclusive-or of two sketches equals the sketch of the symmetric difference of the two sets. This means that Odd Sketches provide a highly space-efficient estimator for sets of high similarity, which is relevant in applications such as web duplicate detection, collaborative filtering, and association rule learning. The method extends to weighted Jaccard similarity, relevant e.g. for TF-IDF vector comparison.*

We present a theoretical analysis of the quality of estimation to guarantee the reliability of Odd Sketch-based estimators. Our experiments confirm this efficiency, and demonstrate the efficiency of Odd Sketches in comparison with b-bit minwise hashing schemes on association rule learning and web duplicate detection tasks.

*This work was published as an article, "****Efficient Estimation for High Similarities using Odd Sketches****" in Proceedings of 23rd International World Wide Web Conference (WWW), 2014.*

5.1 Introduction

Estimating set similarities is a fundamental problem in databases, machine learning, and information retrieval. Given the two sets, $\mathbb{S}_1$ and $\mathbb{S}_2$, where $\mathbb{S}_1, \mathbb{S}_2 \subseteq \Omega = \{0, 1, \ldots, D-1\}$, a challenge is how to quickly compute their Jaccard similarity coefficient J, a normalized measure of set similarity:

$$J(\mathbb{S}_1, \mathbb{S}_2) = \frac{|\mathbb{S}_1 \cap \mathbb{S}_2|}{|\mathbb{S}_1 \cup \mathbb{S}_2|}.$$

One can view large datasets of Web documents as collections of sets where sets and set elements correspond to documents and document words/shingles, respectively. Other examples are datasets encountered in recommender systems, where users and items can be viewed as sets and set elements. Hence, set similarity estimation is one of the key research challenges in many application areas, such as web duplicate detection [12, 14, 34, 53], collaborate filtering [5, 22], and association rule learning [21].

Many applications of set similarity arise in large-scale datasets. For instance, a search engine needs to crawl and index billions of web-pages. Collaborative filtering engines from sites such as Amazon or NetFlix have to deal with tens of millions of users' data. Performing similarity search over such large-scale datasets is very time-consuming. If we are willing to accept an *estimate* of J it turns out that it is possible to get by with much less computation and storage. But how much better can it get? In this work we address the following question:

If each set $\mathbb{S}$ is summarized in a data structure $\mathbb{D}(\mathbb{S})$ of n bits, how precise an estimate of $J(\mathbb{S}_1, \mathbb{S}_2)$ is it possible to make based on $\mathbb{D}(\mathbb{S}_1)$ and $\mathbb{D}(\mathbb{S}_2)$?

Our main finding is that existing solutions, while highly efficient in general, are not optimal when J is close to 1. We present a novel solution, the *Odd Sketch*, that yields improved precision in the high similarity regime.

Although the setting where J is close to 1 has not often been the primary focus when studying similarity measures, there are many applications where this regime is important. Consider a setting where the goal is not just to find a similar item, but to provide a short list and ranking of the most similar items. For example, in

the setting of document similarity, in a sufficiently rich environment there may be hundreds of documents quite similar to another document, and the user wants to see the top ten. For such applications, we require methods that are very accurate for high similarity values J.

5.1.1 Minwise Hashing Schemes

Because minwise hashing is a building block of our approach, and because b-bit minwise hashing is our primary alternative for comparison, we review both briefly.

Minwise Hashing

Minwise hashing is a powerful algorithmic technique to estimate set similarities, originally proposed by Broder et al. [12, 13]. It was used to detect and cluster similar documents in the early AltaVista search engine [14]. Since then, the scheme has been applied successfully in a variety of applications, including similarity search [12, 13, 14], association rule learning [21], compressing social networks [18], advertising diversification [33], tracking Web spam [67], web duplicate detection [48], large-scale learning [49], and more [5, 8, 45].

We now briefly review Broder's minwise hashing scheme. Given a random permutation $\pi : \Omega \mapsto \Omega$, the Jaccard similarity of $\mathbb{S}_1$ and $\mathbb{S}_2$ is

$$J(\mathbb{S}_1, \mathbb{S}_2) = \mathbf{Pr}[\min(\pi(\mathbb{S}_1)) = \min(\pi(\mathbb{S}_2))].$$

Therefore we get an estimator for J by considering a sequence of permutations $\pi_1, \ldots, \pi_k$ and storing the annotated minimum values (called "minhashes").

$$S_1 = \{(i, \min(\pi_i(\mathbb{S}_1))) \mid i = 1, \ldots, k\},$$
$$S_2 = \{(i, \min(\pi_i(\mathbb{S}_2))) \mid i = 1, \ldots, k\}.$$

We estimate J by the fraction $\hat{J} = |S_1 \cap S_2|/k$. This estimator is unbiased, and by independence of the permutations it can be shown that $\mathbf{Var}[\hat{J}] = \frac{J(1-J)}{k}$.

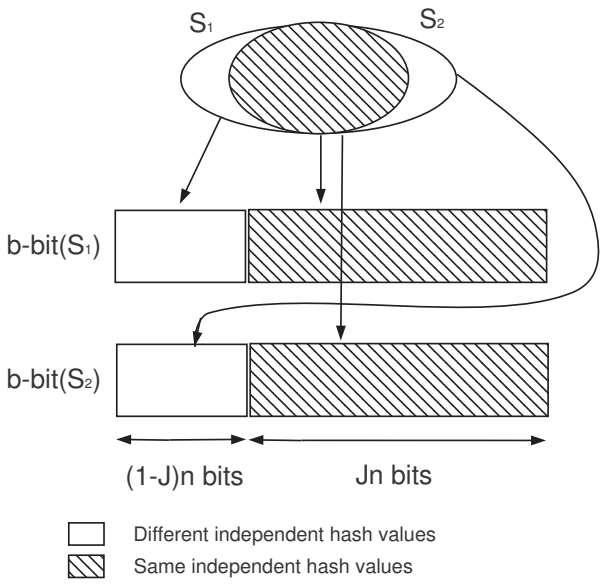

Figure 5.1: Illustration of the b-bit minwise hashing construction. Given a high Jaccard similarity J and two minhashes S_1, S_2, we expect that $|S_1 \cap S_2| = Jn$ (filled space) and $|S_1 \Delta S_2| = 2(1-J)n$ (white space). Due to the same independent hash values in the filled space, the error of the b-bit scheme corresponds to the error of the estimate of $|S_1 \Delta S_2|$. Inaccuracy in just a few bit positions in the white space will yield a large relative error of the estimate of J.

Observe that a minhash can be stored as an array of length k containing the minimum for each $i = 1, \ldots, k$. The hash value $\min(\pi(\mathbb{S}))$ in the minhash is stored as an integer of typically 32 or 64 bits. That means that Broder's scheme might use $32k$ or $64k$ bits of memory to store k hash values for any set $\mathbb{S}$.

b-bit Minwise Hashing

At WWW'10 Li and König [48] proposed b-bit minwise hashing as a space-efficient variant of Broder's minwise hashing scheme. Instead of storing $b = 32$ or $b = 64$ bits for each permutation, this approach suggested using the lowest b bits. It is based on the intuition that the same hash values give the same lowest b bits whereas the different hash values give different lowest b bits with probability $1 - 1/2^b$. Figure 5.1 shows how to construct b-bit minwise sketches.

Let $\min_b(\pi(\mathbb{S}))$ denote the lowest b bits of the hash value $\min(\pi(\mathbb{S}))$. Then

the b-bit minhash S_1^b is obtained from the standard minhash S_1 by replacing min by $\min_b$, reducing space usage to kb. An unbiased estimator $\hat{J}^b$ for $J(\mathbb{S}_1, \mathbb{S}_2)$ and its variance can be computed as follows:

$$\hat{J}^b = \frac{|S_1^b \cap S_2^b|/k - 1/2^b}{1 - 1/2^b} \ , \ \mathbf{Var}[\hat{J}^b] = \frac{1-J}{k}\left(J + \frac{1}{2^b - 1}\right).$$

However, when the Jaccard similarity is high it seems that the b-bit scheme offers less information than it might be able to. As an extreme example, suppose that we get the estimate $\hat{J}^b = 1$, i.e., all the bits of the two summaries are identical. How confident can we be that J is indeed close to 1? For example, even if we actually have $J = 1 - \frac{2}{k}$ it is quite likely that the two summaries will be identical. Somehow, since the two summaries are so highly correlated, differences of just a few bit positions will lead to very different conclusions on how close J is to 1. Thus we might ask: Is it possible to do better, avoiding the limits on accuracy that comes when summaries are highly correlated?

5.1.2 Our Contribution

In this work, we introduce the *Odd Sketch*, a compact binary sketch for estimating the Jaccard similarity of two sets. This binary sketch is similar to a Bloom filter with one hash function [26], constructed on the original minhashes with the "odd" feature that the usual disjunction is replaced by an exclusive-or operation. That is, we hash each element of the minhash into a bit-array data structure. (We will refer to the hash function used for this as the "sketch hash function".) Now, instead of setting a bit to 1, we *flip* a bit according to the sketch hash value of each element in the minhash. We apply the Odd Sketches to minhashes, which means that the Odd Sketch records for each hash value whether it is mapped to by an odd number of elements in the minhash. Figure 5.2 shows a high level illustration of the construction of Odd Sketches.

A key feature of the Odd Sketch is that when we compute the exclusive-or of two Odd Sketches, the result will be equal to the Odd Sketch of the symmetric difference of the minhashes, i.e., the set of elements in one minhash but not the other. This is because the contribution of all identical elements in the minhashes

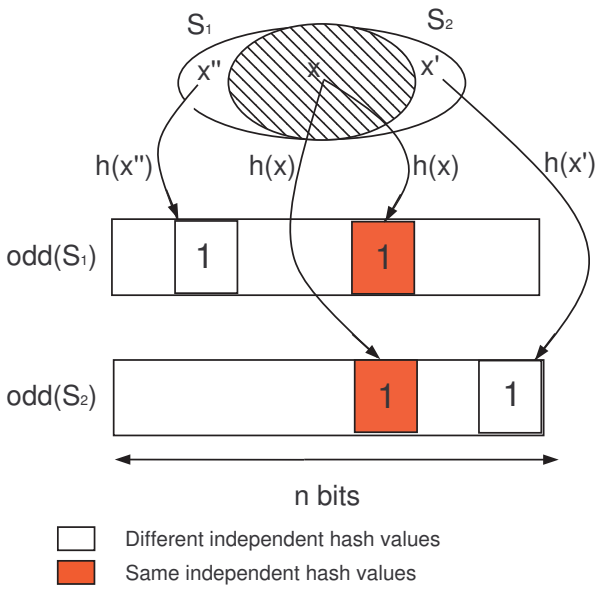

Figure 5.2: Illustration of the Odd Sketch construction. Odd Sketch starts with a 0s bit-vector of size n. We flip a *bit* according to each element of the minhashes S_1 and S_2. The contributions of elements in $S_1 \cap S_2$ cancel out in the exclusive-or $odd(S_1) \oplus odd(S_2)$, so Odd Sketches use all of the n bits to estimate the symmetric difference size $|S_1 \Delta S_2|$. This reduces the variance when J is close to 1.

cancel out. In turn, this means that we are able to base Odd Sketches of size n on minhashes of size significantly above n whenever J is close to 1 and there are many identical values in the minhashes, so that the variance induced by the minhash step is reduced.

The technical difficulty is to provide a good estimator for the size of a set based on its Odd Sketch. We provide a surprisingly simple, asymptotically precise expression for the expected fraction of 1s in an Odd Sketch, and show via concentration around this expectation that the resulting estimator has good precision as long as the fraction of 1s is bounded away from 1/2.

We note that a similar approach has previously been used to estimate the number of distinct elements in a stream, where the usual disjunction was used instead of an exclusive-or operation [6]. One of our contributions is showing that tracking the *parity* of the number of items that hash to a bucket is a useful technique in the context of estimating the size of set differences (rather than the

size of sets).

5.2 Odd Sketches

5.2.1 Construction

The Odd Sketch is a simple, linear sketch of the indicator vector of a set S. Concretely, the sketch consists of an array s of $n > 2$ bits. Let $h : \Omega \mapsto [n]$ be a hash function, which we assume here is fully random. In the Odd Sketch, which we denote by $odd(S)$, the ith bit is given by

$$s_i = \bigoplus_{x \in S} 1_{h(x)=i} \ ,$$

where $0 \leq i < n$. That is, s_i is the parity of the number of set items that hash to the ith location.

To compute the sketch, we start with the zero bit vector of size n. Then we evaluate h on each $x \in S$, and flip the bit $s_{h(x)}$ of the sketch, as shown in the pseudo-code in Algorithm 6.

Algorithm 6 Odd Sketch(S, n)

Require: A set $S \subset \Omega$ and the size of sketch in bits n
1: $s \leftarrow [0]^n$
2: Pick a random hash function $h : \Omega \mapsto [n]$
3: **for** each set element $x \in S$ **do**
4: $\quad s_{h(x)} = s_{h(x)} \oplus 1$
5: **end for**
6: **return** s

Because $odd(S)$ records the parity of the number of elements that hash to a location, it follows that the Odd Sketch of the symmetric set difference $S_1 \Delta S_2$ is the exclusive-or of the Odd Sketches $odd(S_1)$ and $odd(S_2)$.

Lemma 5.1. $odd(S_1) \oplus odd(S_2) = odd(S_1 \Delta S_2)$.

In the following section, we show how to estimate the size of a set from the number of 1s in its Odd Sketch. By Lemma 5.1 we can use this to estimate $|S_1 \Delta S_2|$ from the Odd Sketches of S_1 and S_2. If sets S_1 and S_2 are minhashes of $\mathbb{S}_1$ and $\mathbb{S}_2$, then we can estimate the Jaccard similarity of original two sets from the Odd Sketches of S_1 and S_2.

5.2.2 Estimation

Estimating a Set's Size from Its Odd Sketch

Let m and n denote the size of set S and the size of $odd(S)$ in bits, respectively. Because our hash functions are fully random, we can think about the process of constructing $odd(S)$ as that of independently throwing m balls into n bins, and storing as s_i the parity of the number of balls in bin i. We are interested in generating an estimate $\hat{m}$ for m based on the observation of the number of odd bins in $odd(S)$. In the following we present two estimation approaches for the estimate $\hat{m}$. The first one is based on the Markov chain model and the second one relies on the standard *Poisson approximation* to the balls and bins setting. Both approaches yield the same estimate when n is sufficiently large.

Consider the parity of number of balls landing in any specific bin (say the first) as a simple two-state Markov chain model. The first/second state corresponds to the even/odd parity. The probability of changing states is $1/n$. Let p_i be the probability that any specific bin has an odd number of balls after i balls have been thrown. A simple induction based on Markov chains yields

$$p_i = \frac{1 - (1 - 2/n)^i}{2}.$$

It helps to now introduce some notation. Let X_i be a 0-1 random variable corresponding to the parity of the number of balls that land in the ith bin after throwing m balls, and let $X = \sum_i X_i$. We have shown that

$$\mathbf{E}[X] = n\frac{1 - (1 - 2/n)^m}{2}.$$

Hence, a seemingly reasonable approximation for m if we see z odd bins in the sketch is to assume that $z \approx \mathbf{E}[X]$, in which case

$$z \approx n\frac{1-(1-2/n)^m}{2},$$

and solving we obtain an estimate $\hat{m}$ by

$$\hat{m} = \frac{\ln(1-2z/n)}{\ln(1-2/n)}. \tag{5.1}$$

This approximation is reasonable if X is sharply concentrated around its expectation, which we show later.

The second estimation approach leverages the standard *Poisson approximation* to the balls and bins setting and provides a pratical estimate. That is, when m balls are thrown into n bins, this is very approximately the same as independently giving each bin a number of balls that is Poisson distributed with mean $\mu = m/n$. (We discuss this further below; also, see [54, Section 5.4].) Lemma 5.2 provides the relationship between the Poisson distribution with mean μ and the parity of the distribution.

Lemma 5.2. *(Schuster and Philippou [63]) Let Q be a random variable that has Poisson distribution with mean μ. The probability p that Q is odd is $(1-e^{-2\mu})/2$.*

Proof. The probability that Q is odd is given by

$$\begin{aligned} p &= \sum_{i \text{ odd}} \frac{e^{-\mu}\mu^i}{i!} = e^{-\mu} \sum_{i \text{ odd}} \frac{\mu^i}{i!} \\ &= e^{-\mu}\frac{e^{\mu}-e^{-\mu}}{2} = \frac{1-e^{-2\mu}}{2} \ . \end{aligned}$$

□

Let Y_i be the parity of the number of balls that land in the ith bin in the setting where the number of balls are independently Poisson distributed with mean $\mu = m/n$ in each bin, and let $Y = \sum_i Y_i$ be the number of bins with an

odd number of balls. Then

$$\mathbf{E}[Y] = np = n\frac{1 - e^{-2m/n}}{2}.$$

Hence, a seemingly reasonable approximation for m if we see z odd bins in the sketch is to assume that $z \approx \mathbf{E}[Y]$, in which case we obtain an estimate $\hat{m}$ as

$$\hat{m} = -\frac{n}{2}\ln\left(1 - 2z/n\right). \tag{5.2}$$

Since the Y_i are independent and identically distributed, standard Chernoff bounds provide that $z \approx \mathbf{E}[Y]$ with high probability, as we clarify further below. We note that when n is sufficiently large in practice, we have $\ln(1 - 2/n) \approx -2/n$. In this case, the estimate is approximately the estimate derived from equation 5.1.

Estimating Jaccard Similarity from Odd Sketches

Suppose we construct Odd Sketches $odd(S_1), odd(S_2)$ from the minhashes S_1 and S_2 derived from $\mathbb{S}_1$ and $\mathbb{S}_2$. Recall that, when we construct sets S_1 and S_2, if we think of the sets as random variables before instantiating them, we have

$$\mathbf{E}[|S_1 \Delta S_2|] = 2k(1 - J),$$

where k is the number of independent permutations and J is the Jaccard similarity of $\mathbb{S}_1$ and $\mathbb{S}_2$. Moreover, $|S_1 \Delta S_2|$ should be closely concentrated around its expectation, since each permutation independently gives a match with probability J. Once we have instantiated S_1 and S_2, given $odd(S_1)$ and $odd(S_2)$, we can estimate $|S_1 \Delta S_2|$ for the S_1 and S_2 we derived, using equation 5.2. For notational convenience we will think of $odd(S_1)$ and $odd(S_2)$ as the sets of bit positions containing 1, which means that their exclusive-or corresponds exactly to the symmetric difference. If we use $|S_1 \hat{\Delta} S_2|$ to denote our estimate of $|S_1 \Delta S_2|$, then

$$|S_1 \hat{\Delta} S_2| = -\frac{n}{2}\ln(1 - 2\,|odd(S_1)\Delta odd(S_2)|/n).$$

Here $|odd(S_1)\Delta odd(S_2)|$ refers to the number of 1s in the structure. Using $|S_1\hat{\Delta}S_2|$ as a proxy for $\mathbf{E}[|S_1\Delta S_2|]$, the Jaccard similarity can be estimated as follows:

$$\begin{aligned}\hat{J}^{odd} &= 1 - \frac{|S_1\hat{\Delta}S_2|}{2k} \\ &= 1 + \frac{n}{4k}\ln\left(1 - \frac{2\,|odd(S_1)\Delta odd(S_2)|}{n}\right).\end{aligned}$$

Both Odd Sketches and b-bit minwise hashing can be viewed as variations of the original minwise hashing scheme that reduce the number of bits used. The quality of their estimators is dependent on the quality of the original minwise estimators. In practice, both Odd Sketches and b-bit minwise hashing need to use more permutations but less storage space than the original minwise hashing scheme.

5.2.3 Analysis

In the previous section, we assumed that the number of odd bins in our data structure was closely concentrated around its expectation to justify various approximations. Here we justify this assumption. This is straightforward in the Poisson setting where bin parities are independent; we show how to handle the dependencies that exist in the balls-and-bins model. We also directly calculate the variance of the number of odd bins for both the Poisson and balls-and-bins setting.

Concentration

Recall our notation: we throw $m = \mu n$ balls into n bins, so that the average number of balls per bin is μ. We let X_i be the parity of the number of balls that land in the ith bin and $X = \sum_i X_i$ be the number of odd bins. Similarly, let Y_i be the parity of the number of balls that land in the ith bin in the setting where the number of balls are independently Poisson-distributed, and let $Y = \sum_i Y_i$. We show that X and Y are closely concentrated around their means.

We use the standard approach of passing to the setting where each bin obtains independently a Poisson distributed number of balls with mean μ. This is justified by, for example, [54, Corollary 5.9] where the following is shown:

Lemma 5.3. *[Corollary 5.9 of [54]] Any event that takes placed with probability p when each bin obtains an independently distributed Poisson number of balls with mean μ takes place with probability at most $pe\sqrt{m}$ when $m = \mu n$ balls are thrown into n bins.*

Since Y is the sum of independent 0-1 random variables, applying a Chernoff bound [54, Exercise 4.13] to Y yields

$$\mathbf{Pr}(|Y - \mathbf{E}[Y]| \geq \epsilon n) \leq 2e^{-2n\epsilon^2}.$$

Hence, from Lemma 5.3 we have

$$\mathbf{Pr}(|X - \mathbf{E}[Y]| \geq \epsilon n) \leq (2e\sqrt{m})e^{-2n\epsilon^2}.$$

Denote by $\bar{X} = \frac{1}{n}X$ the fraction of bins with an odd number of balls. We find

$$\begin{aligned}\mathbf{Pr}(|\bar{X} - \frac{1}{n}\mathbf{E}[Y]| \geq \epsilon) &\leq (2e\sqrt{m})e^{-2n\epsilon^2} \ , \\ \mathbf{Pr}(|\bar{X} - p| \geq \epsilon) &\leq (2e\sqrt{m})e^{-2n\epsilon^2},\end{aligned}$$

where $p = \left(1 - e^{-2m/n}\right)/2$. The true expected fraction of odd bins is $\mathbf{E}[X]/n = \frac{1-(1-2/n)^m}{2}$, which differs from p by an $o(1)$ amount.

Since m corresponds to the symmetric difference between two minhashes, we have $m \leq 2k$. Hence, by choosing $n > c\epsilon^{-2}\log k$ for some constant c, our estimator closely concentrates around its mean with probability $1 - k^{-\omega(1)}$.

Variance Bound

We note that the variance on the number of odd bins for the Poisson setting is trivial to calculate, since the bins are independent. Letting $p = \left(1 - e^{-2m/n}\right)/2$,

the standard result (on variance of biased coin flips) gives that the variance is $np(1-p)$.

For the balls and bins case there are dependencies among the bin loads that make the variance calculation more difficult. Recall that p_i is the probability that any specific bin has an odd number of balls after i balls have been thrown, and

$$p_i = \frac{1-(1-2/n)^i}{2},$$

so each $X_i = 1$ with probability $(1-(1-2/n)^m)/2$. To calculate the variance, we first calculate $\mathbf{E}[X^2]$; the standard expansion gives

$$\begin{aligned}
\mathbf{E}[X^2] &= \mathbf{E}[(\sum_i X_i)^2] \\
&= \sum_i \mathbf{E}[X_i^2] + 2\sum_{i<j} \mathbf{E}[X_i X_j] \\
&= \sum_i \mathbf{E}[X_i] + 2\sum_{i<j} \mathbf{E}[X_i X_j].
\end{aligned}$$

where we have used the fact that $(X_i)^2 = X_i$ since X_i only takes on the values 0-1. The first summation is just $\mathbf{E}[X]$.

To calculate the second summation, by symmetry it suffices to consider a specific pair of variables, say X_1 and X_2. We consider the total number of balls that land in the combination of bins 1 and 2. If this number is odd, then clearly $X_1X_2 = 0$. If this number is 0, then clearly $X_1X_2 = 0$. If this number is even, but more than 0, then $X_1X_2 = 1$ with probability exactly 1/2. To see this, consider the last ball that lands in either bin 1 or bin 2. One of these bins must have an odd number of balls. If the new ball lands in the other bin, then both have an odd number of balls; this happens with probability 1/2. It follows that $\mathbf{E}[X_1X_2]$ is half the probability that bins 1 and 2 considered together obtain an even and positive number of balls. As with the calculation for p_i, a simple induction based on the two-state Markov chain model shows that after i balls have been thrown, the probability q_i that the first two bins have an even number of balls greater

than 0 is

$$q_i = \frac{1 + (1 - 4/n)^i - 2(1 - 2/n)^i}{2}.$$

Hence the second sum is

$$\binom{n}{2} \frac{1 + (1 - 4/n)^m - 2(1 - 2/n)^m}{2}.$$

The variance is then $\mathbf{E}[X^2] - \mathbf{E}[X]^2$, or

$$\binom{n}{2} \frac{1 + (1 - 4/n)^m - 2(1 - 2/n)^m}{2} + \frac{n(1 - (1 - 2/n)^m)}{2} - \left(\frac{n(1 - (1 - 2/n)^m)}{2}\right)^2.$$

Simplifying, this is

$$n^2 \frac{(1 - 4/n)^m - (1 - 2/n)^{2m}}{4} + n \frac{1 - (1 - 4/n)^m}{4}.$$

While this is easily seen to be $\mathcal{O}(n^2)$, the coefficient

$$\frac{(1 - 4/n)^m - (1 - 2/n)^{2m}}{4}$$

of the n^2 term above is in fact $O(1/n^2)$ when $m = \mu n$. (Note that both expressions in the numerator converge to and are approximately $e^{-4m/n}$. By examining the asymptotics carefully one can show the coefficient is $\mathcal{O}(1/n^2)$.) Hence the variance here is also $\mathcal{O}(n)$. Indeed, the second term is

$$n \frac{1 - (1 - 4/n)^m}{4} \approx n \frac{1 - e^{-4m/n}}{4} = np(1 - p),$$

which is the variance for the Poisson setting, and the first term is negative. Again, by considering the asymptotic expansions carefully one obtains that the variance in the Poisson case is larger than in the case where there are exactly m balls thrown for large enough n, as one might naturally expect.

Accuracy of the Estimator

In the previous sections we bounded the variance and gave strong tail bounds for the fraction z/n of 1s in an Odd Sketch. Recall that its expected value is $p_m = \frac{1-(1-2/n)^m}{2}$ derived from the Markov chain and its practical estimate is $p = \frac{1-e^{-2m/n}}{2}$ derived from the Poisson approximation. What remains is to bound the error resulting from applying the estimator from equation (5.2), repeated here for convenience:

$$\hat{m} = -\frac{n}{2}\ln\left(1 - 2z/n\right).$$

Defining the function $f(x) = -\frac{n}{2}\ln(1-2x)$, we have $\hat{m} = f(z/n)$. There are two sources of inaccuracy: The first is that the estimator has a bias since the expected number of 1s, $np_m = n\frac{1-(1-2/n)^m}{2}$, differs from the practical estimate $np = n\frac{1-e^{-2m/n}}{2}$. However, it can be confirmed by an easy computation that the difference can be at most 1, so this is not significant.

The second, and more significant, source of error is that when z/n deviates from its expectation p_m, $f(z/n)$ will deviate from $f(p_m)$. Informally, an if z/n deviates from its expectation by ε, this will give an error of roughly $f'(z/n)\cdot\varepsilon$, as long as ε is small enough, where $f'(x) = \frac{n}{1-2x}$ is the derivative of f. It is clear that a small error can be magnified significantly if z/n is close to $1/2$, since $f'(x)$ goes to infinity as $x \to 1/2$. Therefore we choose parameters such that p, the practical estimate of z/n, is bounded away from $1/2$ ($p \approx 0.3$ gives the best results, as we see when we discuss our experiments). By the results in section 5.2.3 this means that with high probability (wrt. n) we will have $z/n < 0.4$ (say). As long as this is the case, since f' is monotonely increasing, we have that the error is bounded by $f'(0.4)|z/n - p_m| = 5n$. This bound is pessimistic, but shows that the estimation error is (with high probability) proportional to the error in the estimate of p_m. In turn, this implies that the variance of the estimator is $\mathcal{O}(n)$.

5.2.4 Weighted Similarity

Odd Sketches work with any notion of similarity that can be transformed to Hamming distance of two vectors. In particular, it works with any similarity measure that can be captured using the probability that two minhashes are identical. For

example, the Jaccard similarity of two vectors $v, w \in \mathbf{R}^d$ with nonnegative entries can be defined as:

$$J(v,w) = \frac{\sum_i \min(v_i, w_i)}{\sum_i \max(v_i, w_i)},$$

generalizing standard Jaccard similarity which corresponds to 0-1 vectors. Hash functions that result in minhash equality with probability $J(v,w)$ can be found in [32, 38, 52].

5.3 Experimental Results

We implemented b-bit minwise hashing and Odd Sketch in Matlab, and conducted experiments on a 2.67 GHz Core i7 Windows machine with 3GB of RAM. We compared the performance of b-bit minwise hashing and Odd Sketch on association rule learning and web duplication detection tasks. All results are the averages of 10 runs of the algorithms.

5.3.1 Parameter Setting

It is obvious that the performance of both b-bit minwise and Odd Sketch depends on the number of independent permutations used in the original minwise hashing scheme. The b-bit minwise scheme uses $k_b = n/b$ permutations where the storage space is n bits and $b \geq 1$ is the number of bits per permutation. Since larger k_b provides higher accuracy, setting $b = 1$ turns out to achieve the smallest variance, as will be clear from our empirical evaluation.

In the Odd Sketch setting, the number of independent permutations k_{odd} is dependent on the sketch size n and the user-defined similarity threshold J_0. Typically, we are interested in retrieving pairs of sets such that $J > J_0$ (and perhaps subject these pairs to additional filtering). Moreover, we want to choose k_{odd} as large as possible to reduce the error from the original minwise hashing step. It seems difficult to mathematically establish the optimal way of choosing k_{odd}, but we conducted experiments that indicate that the smallest variance is achieved when the exclusive-or of two odd sketches with similarity J_0 contains around 30% 1s.

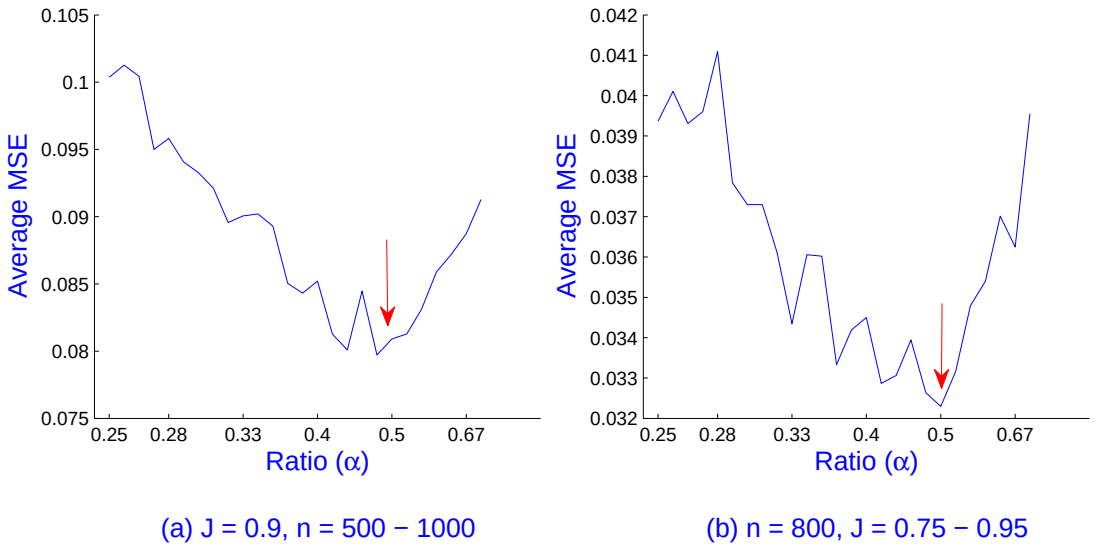

Figure 5.3: Comparison of the average MSE on different ratios α on the synthetic dataset: (a) Fix $J = 0.9$ and change $n = 500 - 1000$ bits; (b) Fix $n = 800$ bits and change $J = 0.75 - 0.95$.

Our estimator needs the fraction of 1s in $odd(S_1 \Delta S_2)$ to be smaller than $1/2$. If a fraction of more than $1/2$ is observed this is (with high probability) a sign of very low Jaccard similarity, so we may estimate $J = 0$. Recall that the process of constructing $odd(S_1 \Delta S_2)$ corresponds to throwing $|S_1 \Delta S_2|$ balls into n bins. It turns out that if we choose k_{odd} such that $|S_1 \Delta S_2| \approx n/2$ we get the most accurate estimate when similarity is around J. In other words, we choose the parameter k_{odd} such that the ratio $\alpha = \frac{2k_{odd}(1-J_0)}{n} \approx \frac{1}{2}$.

We conducted experiments to evaluate this choice of ratio α. We compared the mean square error (MSE, incorporating both variance and bias) of our estimator $\hat{J}^{odd}$ for different ratios of $\alpha = \frac{2k_{odd}(1-J_0)}{n}$ in $[0.25, 1]$, and for different sketch sizes $n \in [500, 1000]$ bits. For each choice we found that $\alpha = 1/2$ gave the smallest observed MSE. Figure 5.3 displays the average MSE of $\hat{J}^{odd}$, averaged over variety of values of J and n. It illustrates that Odd Sketch achieves the highest accuracy when using the ratio $\alpha = 0.5$. So we can choose $k_{odd} = \frac{n}{4(1-J_0)}$ given a threshold J_0. When we are interested in $J_0 \geq 0.75$, we can set $k_{odd} > n$. This means that Odd Sketch can use more independent permutations than b-bit schemes.

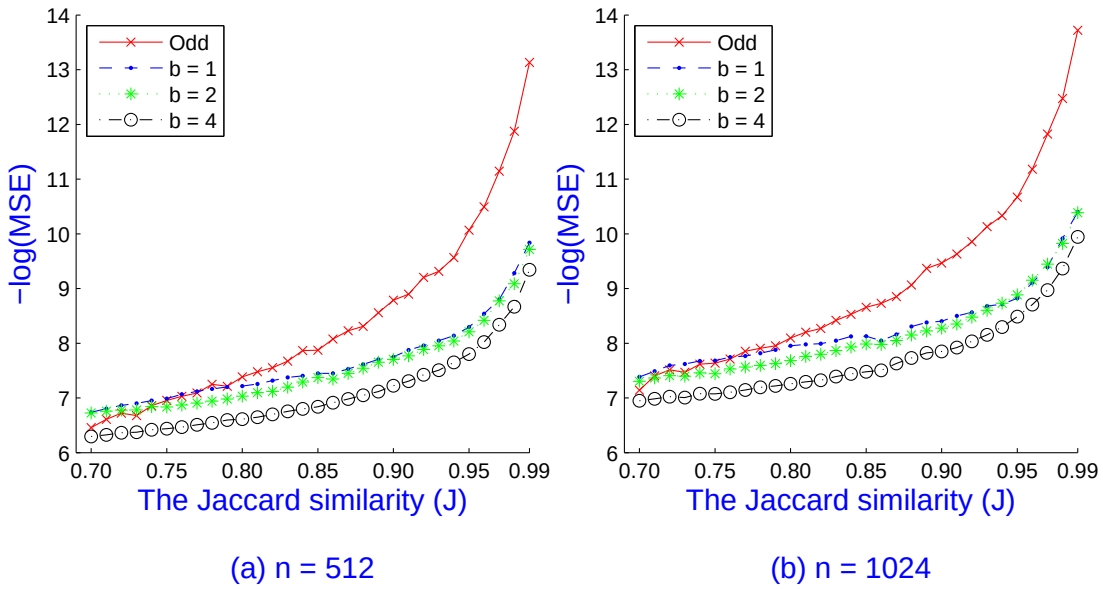

(a) n = 512 (b) n = 1024

Figure 5.4: Comparison of the negative log of mean square error (MSE) of Odd Sketch and b-bit minwise hashing for different Jaccard similarity. In these experiments Odd Sketch used $k_{odd} = \frac{n}{4(1-J)}$ permutations, and b-bit minwise hashing used $k_b = \frac{n}{b}$.

In fact, even for the inferior choice of $k_{odd} = n$, Odd Sketch can achieve better performance than 1-bit minwise hashing when $J_0 > 0.75$.

5.3.2 Accuracy of Estimation

This subsection shows experiments to further evaluate the accuracy of our estimation algorithm. We carried out experiments to compare the accuracy of b-bit minwise hashing and Odd Sketch. In the b-bit schemes, we set $k_b = n/b$ to achieve a space usage of n bits. For the Odd Sketch, we set $k_{odd} = \frac{n}{4(1-J)}$. We again measured the mean square error (MSE) of estimators of both approaches. We varied n in $\{512, 1024\}$ bits and conducted experiments on synthetic datasets. (But note that since we apply hashing the outcome is independent of the particular set elements, and we expect the same result on any real-life dataset.) This dataset is very high-dimensional ($D = 10,000$) and highly sparse (sparsity $> 99.9\%$).

Figure 5.4 shows the negative log of MSE ($-\log(\text{MSE})$) of estimators of the

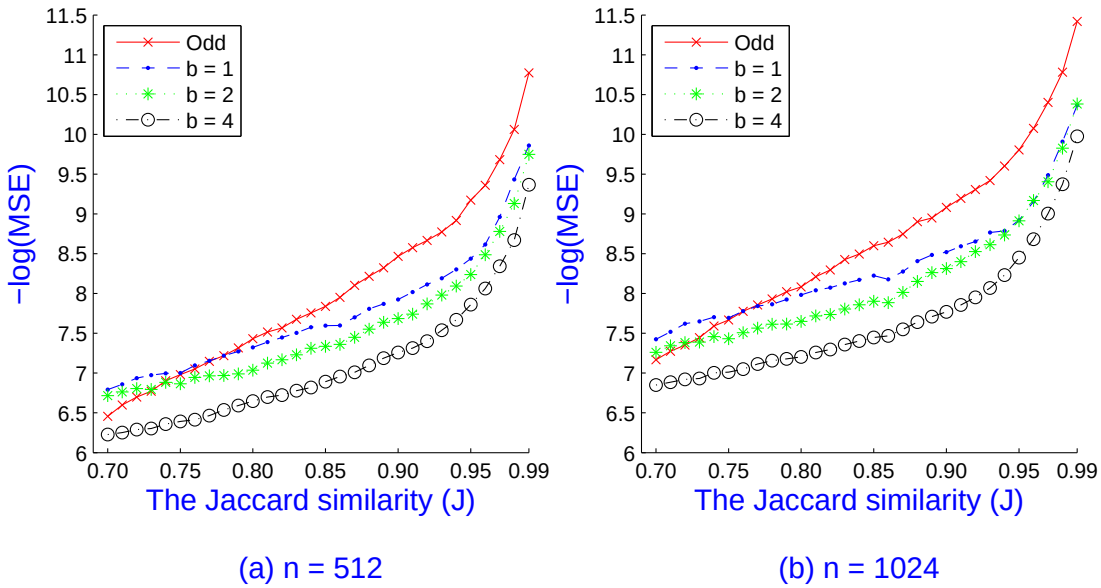

(a) n = 512 (b) n = 1024

Figure 5.5: Comparison of the negative log of mean square error (MSE) of Odd Sketch and b-bit minwise hashing for different Jaccard similarities. Here, Odd Sketch uses $k_{odd} = n$, and b-bit minwise hashing uses $k_b = \frac{n}{b}$ permutations.

two approaches for different values J. We note that the MSE is always smaller than 1 in our experiments, so larger $-\log(\text{MSE})$ is better. For high Jaccard similarities $J \geq 0.8$, Odd Sketch provides a smaller error than the b-bit minwise approach. The difference is more dramatic when J is very high because Odd Sketch makes use of a larger number of independent permutations than the b-bit minwise schemes. This figure also shows that the 1-bit scheme has superior performance compared to the b-bit schemes for $b > 1$. We note that b-bit schemes for $b > 1$ require additional bit-manipulation to pack b bits of hash values into 64-bit (or 32-bit) words. In contrast, both Odd Sketch and 1-bit schemes only need the XOR and bit-counting operations to compare two summaries.

One might argue that Odd Sketch requires a more expensive preprocessing step than b-bit minwise hashing due to the use of larger number of permutations in the minwise hashing step. But even with $k_{odd} = n$, where the hashing cost is identical to that of 1-bit minwise hashing, Odd Sketch still provides better accuracy when $J > 0.75$, as shown in Figure 5.5.

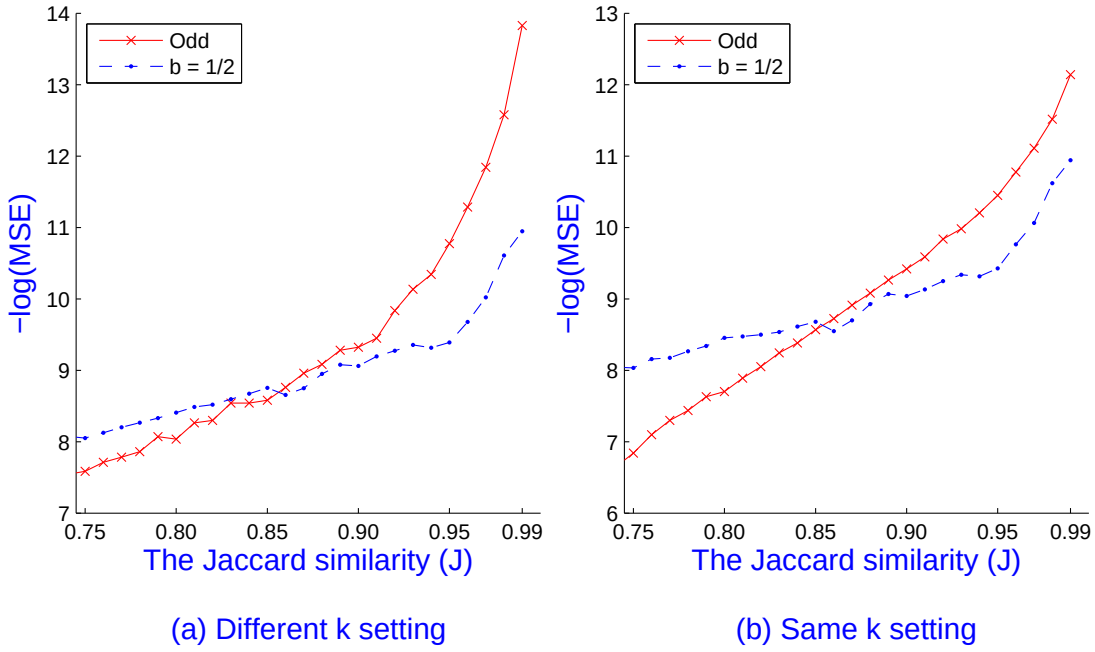

Figure 5.6: Comparison of the negative log of mean square error (MSE) of Odd Sketch and $\frac{1}{2}$-bit minwise hashing for different Jaccard similarities: (a) Different number of permutations: $k_{odd} = \frac{n}{4(1-J)}$ and $k_{\frac{1}{2}} = 2n$; (b) Same number of permutations: $k_{odd} = k_{\frac{1}{2}} = 2n$.

When the target similarity is very high, the authors of b-bit minwise hashing also discussed the idea of combining any 2 bits of a 1-bit minhash by XOR operations to increase the amount of information in each bit. This approach is called $\frac{1}{2}$-bit minwise hashing, and similar to Odd Sketch has a nonlinear estimator. The $\frac{1}{2}$-bit scheme uses $k_{\frac{1}{2}} = 2n$ permutations.

We carried out experiments to compare the mean square errors of estimators of Odd Sketch and $\frac{1}{2}$-bit minwise hashing, as shown in Figure 5.6. The figure shows that Odd Sketch achieves a considerably smaller error than $\frac{1}{2}$-bit minwise hashing when $J > 0.85$ for both choices of k. It also shows that Odd Sketch with the best choice of k_{odd} provides higher accuracy than for $k_{odd} = 2n$.

We conclude the accuracy evaluation of Odd Sketch by depicting the empirical cumulative distribution function (cdf) of estimators. Figure 5.7 shows the empirical cdfs of Odd Sketch, 1-bit scheme and $\frac{1}{2}$-bit scheme on 10,000 estima-

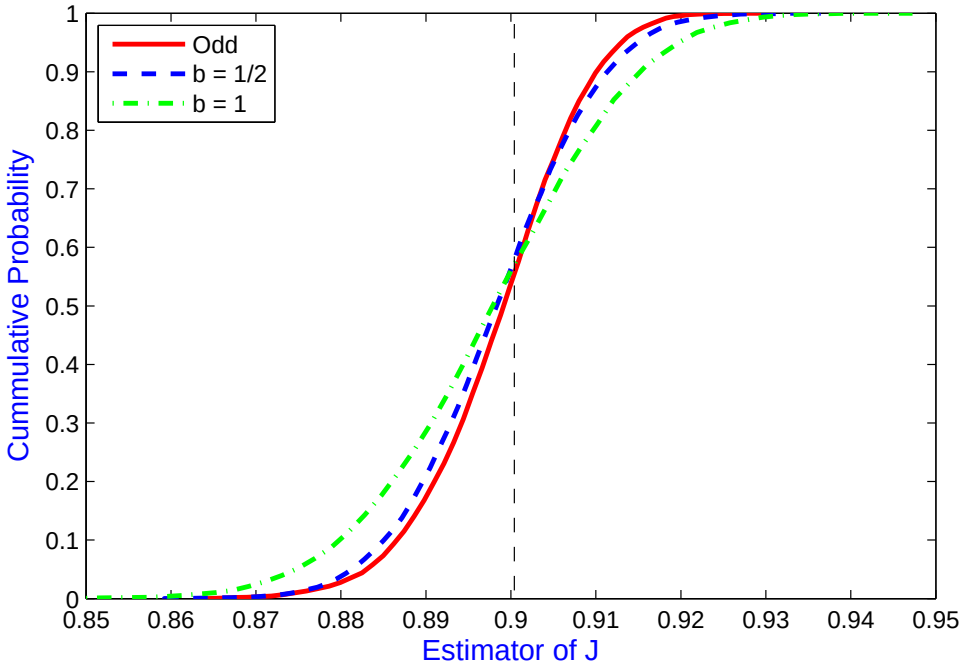

Figure 5.7: Comparison of the empirical cumulative distribution function (cdf) of estimators based on Odd Sketch, 1-bit scheme, and $\frac{1}{2}$-bit scheme with $J = 0.9$.

tors of the Jaccard similarity $J = 0.9$. The slope of cdf of Odd Sketch is steeper than that of $\frac{1}{2}$-bit scheme and significantly steeper than that of 1-bit scheme. This means that Odd Sketch provides superior performance compared to b-bit minwise hashing when the target similarity is high.

5.3.3 Association Rule Learning

Cohen et al. [21] used minwise hashing to generate the candidate sets of high Jaccard similarity in the context of learning pairwise associations. This subsection compares the performance of Odd Sketch and b-bit schemes in this setting. Since $b = 1$ provides the highest accuracy among $b \geq 1$, we only used the 1-bit scheme in our experiment. For a more clear comparison, we used the same number of permutations for the two approaches. We measured the precision-recall ratio of both approaches on detecting the pairwise items that have Jaccard similarity larger

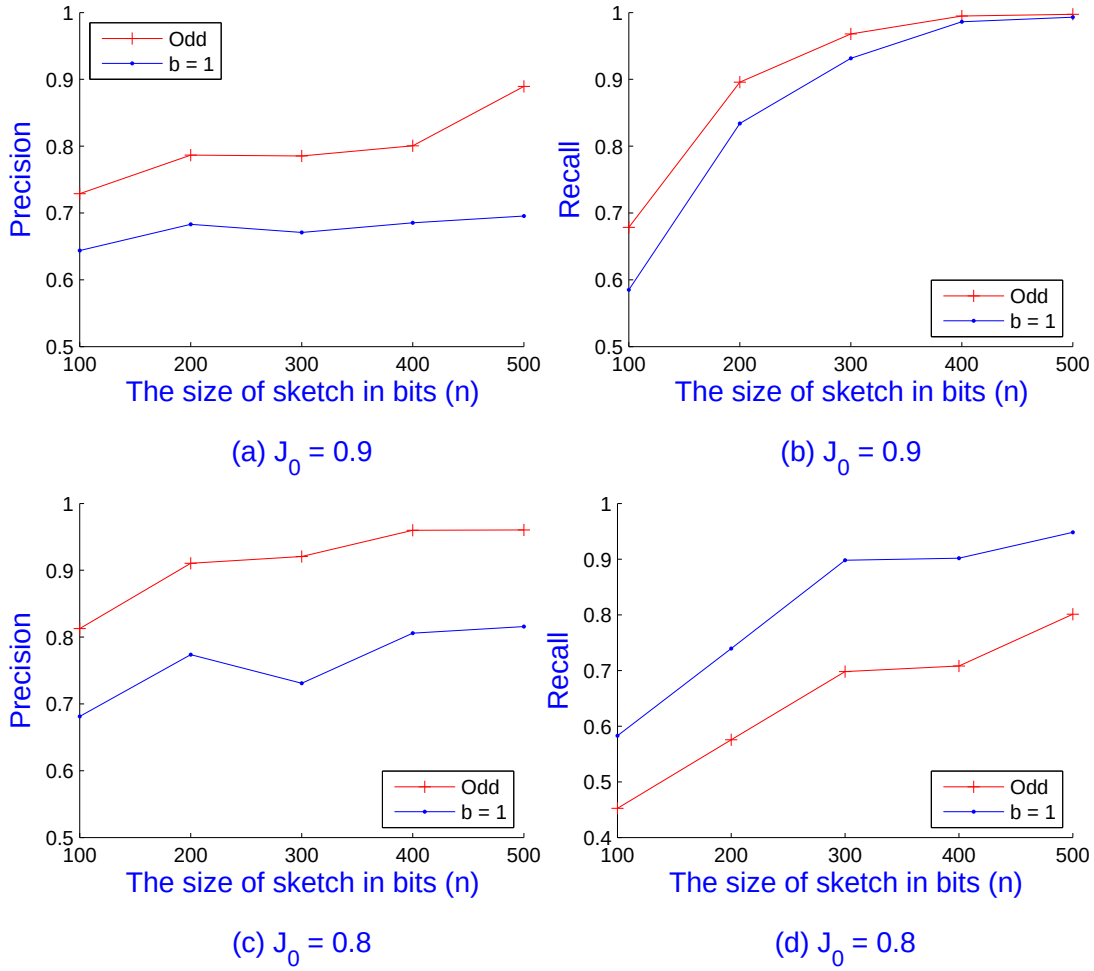

Figure 5.8: Comparison of the precision-recall ratio between Odd Sketches and 1-bit scheme on the mushroom dataset.

than a threshold J_0. We conducted experiments on the large public datasets[1]: mushroom ($N = 8124; D = 119$) and connect ($N = 67,557; D = 127$). Due to the similar results on both datasets, we only report the representative results of mushroom dataset here.

Figure 5.8 shows the precision-recall ratio of the Odd Sketch and the 1-bit scheme. For the high target threshold $J_0 = 0.9$, the Odd Sketch provides significantly higher precision and recall ratio (up to 10% better) than 1-bit minwise hashing. For $J_0 = 0.8$, the Odd Sketch is still better in precision but slightly

[1]http://fimi.ua.ac.be/data/

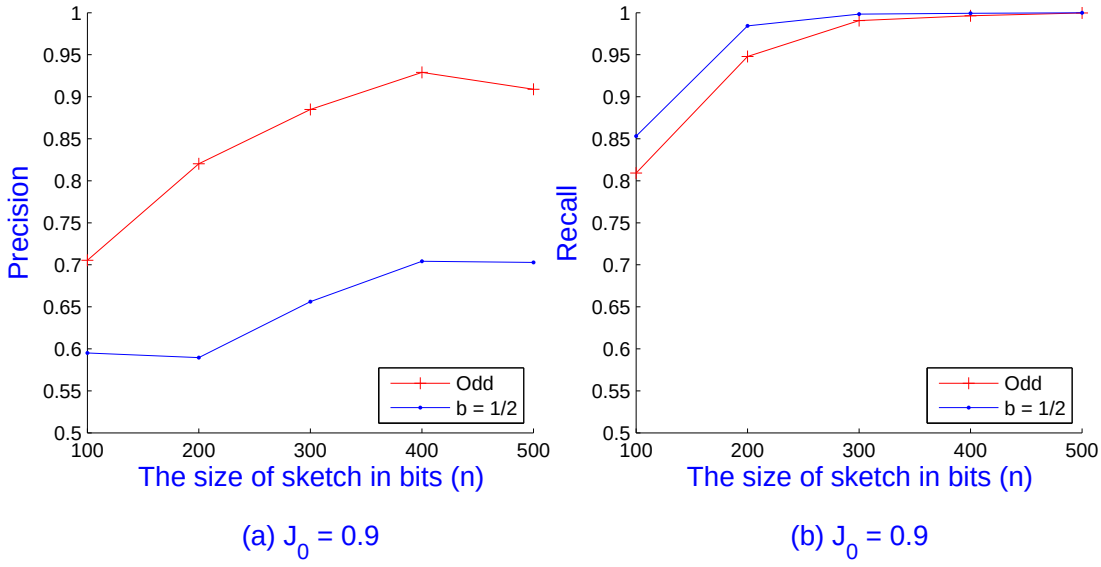

Figure 5.9: Comparison of the precision-recall ratio between Odd Sketches and $\frac{1}{2}$-bit scheme on the mushroom dataset with $J_0 = 0.9$.

worse in recall.

Figure 5.9 demonstrates the superiority of Odd Sketch compared to $\frac{1}{2}$-bit minwise hashing with respect to precision. The Odd Sketch achieved up to 20% higher precision while providing similar recall.

5.3.4 Web Duplicate Detection

In this experiment, we compare the performance of the two approaches on web duplicate detection tasks on the bag of words dataset[1]. We picked three datasets, including KOS blog entires ($D = 6906; N = 3430$), Enron Emails ($D = 28,102; N = 39,861$), and NYTimes articles ($D = 102,660; N = 300,000$). We computed all pairwise Jaccard similarities among documents, and retrieved every pair with $J > J_0$. For the sake of comparison, we used the same number of permutations and considered the thresholds $J_0 = 0.85$ and $J_0 = 0.90$. We again used the precision-recall ratio as our standard measure.

[1] `http://archive.ics.uci.edu/ml/datasets/Bag+of+Words`

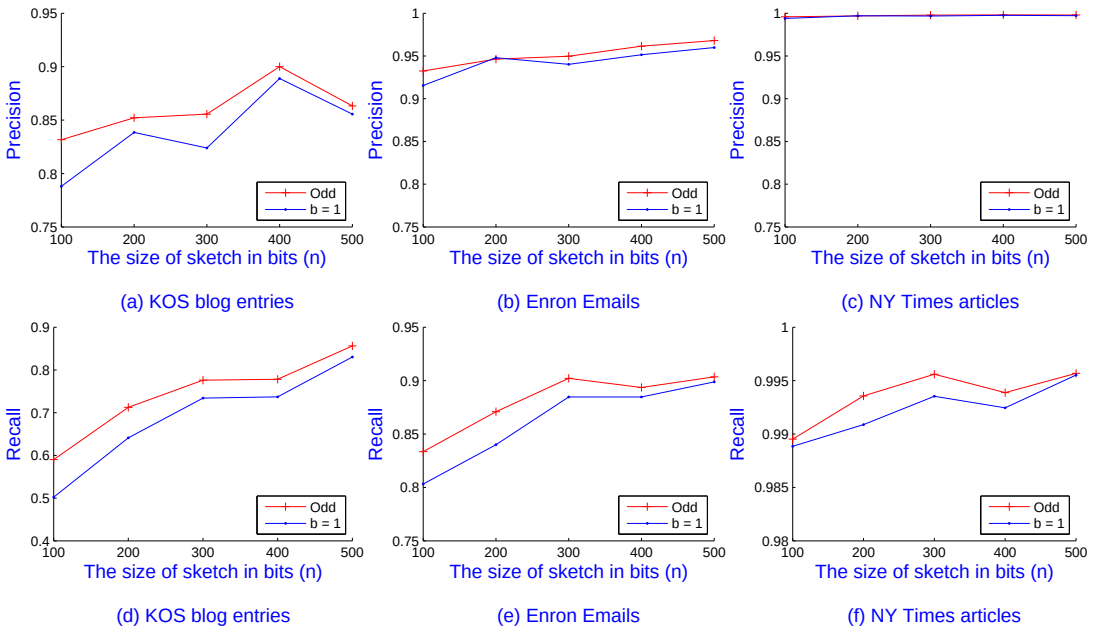

Figure 5.10: Comparison of the precision-recall ratio between Odd Sketches and 1-bit minwise hashing with $J_0 = 0.85$ on the three datasets: KOS blog entries, Enron Emails and NYTimes articles.

Figures 5.10 and 5.11 show the precision-recall ratio for the Odd Sketch and 1-bit minwise hashing on three datasets with $J_0 = 0.85$ and $J_0 = 0.9$, respectively. The Odd Sketch obtains higher relative precision ratio or at least is comparable to 1-bit scheme when $J_0 = 0.85$. It achieves up to 7% and 1% higher than the 1-bit scheme on KOS blog entries and Enron Emails, respectively. For $J_0 = 0.9$, the precision ratios are almost the same on three datasets. However, Odd Sketch greatly outperforms in the recall ratio. The Odd Sketch's relative recall is approximately 15% higher than the 1-bit scheme on the KOS blog entries when $J_0 = 0.85$ and $J_0 = 0.9$. The difference in relative recall is not significant on the other datasets. These relative gaps are around 5% and less 1% on Enron Emails and NYTimes articles, respectively.

Figure 5.12 shows the observed precision-recall graphs of the Odd Sketch and the $\frac{1}{2}$-bit scheme. We again set $k_{odd} = k_1 = 2n$ for the sake of fair comparison. Both approaches achieve very high precision (higher than 90%) on the three datasets. The Odd Sketch still obtains higher precision than the $\frac{1}{2}$-bit scheme although the difference is not dramatic. The gap of both schemes in the recall

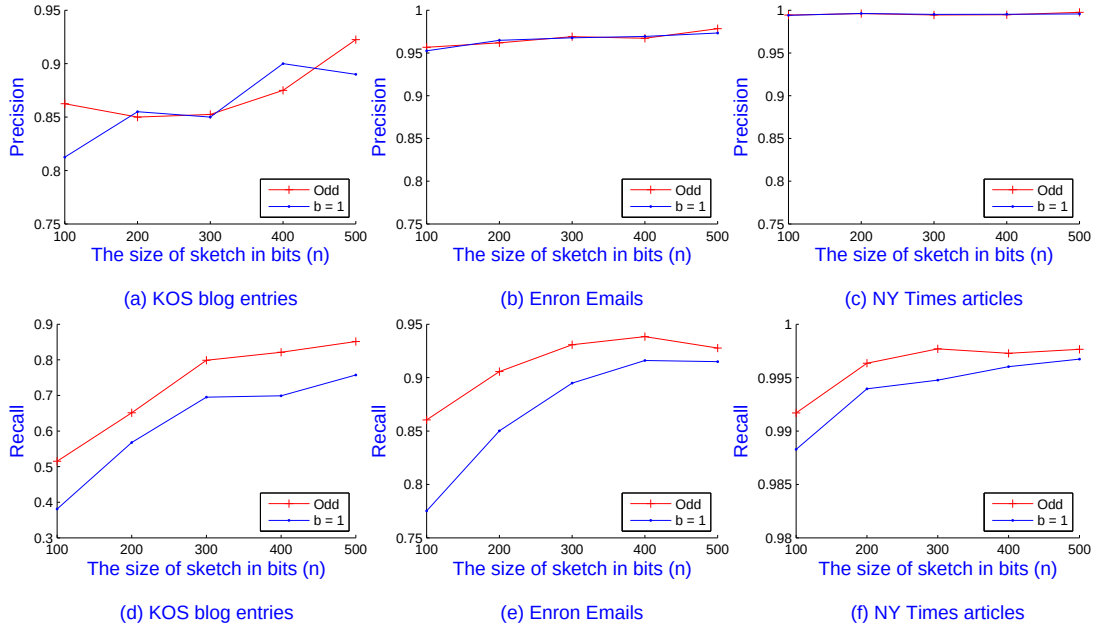

Figure 5.11: Comparison of the precision-recall ratio between Odd Sketches and 1-bit minwise hashing with $J_0 = 0.9$ on the three datasets: KOS blog entries, Enron Emails and NYTimes articles.

ratio is considerable on KOS blog entries and Enron Emails. The most dramatic difference is around 4% when $n = 200$. On the NYTimes articles dataset, the ratio curves of both schemes are overlapping when $n \geq 200$.

5.4 Conclusion

In this chapter, we proposed the *Odd Sketch*, a compact binary sketch for estimating the Jaccard similarity of two sets. By combining the minwise hashing technique with a hash table where only the parity of the number of items hashed to bucket is stored, Odd Sketches can be combined with just an exclusive-or operation to allow a simple estimation of the Jaccard similarity that provides a highly space-efficient solution, particularly for the high similarity regime. We presented a theoretical analysis of the quality of estimate. Our experiments on synthetic and real world datasets demonstrate the efficiency of Odd Sketches in comparison with b-bit minwise hashing schemes on association rule learning and

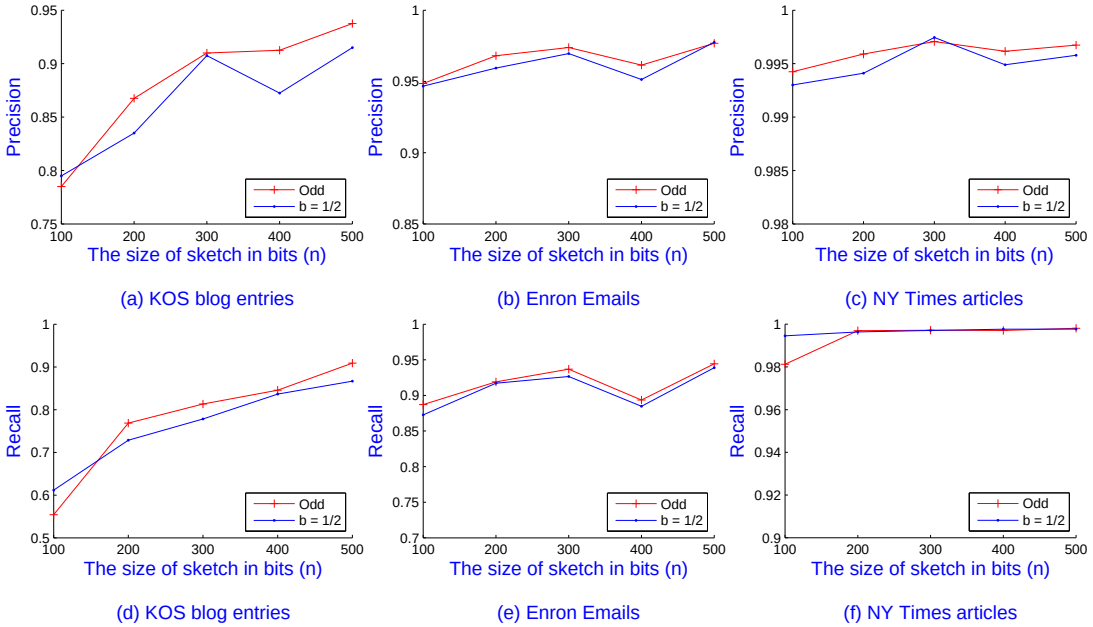

Figure 5.12: Comparison of the precision-recall ratio between Odd Sketches and $\frac{1}{2}$-bit minwise hashing with $J_0 = 0.9$ on the three datasets: KOS blog entries, Enron Emails and NYTimes articles.

web duplicate detection tasks. We expect that there are many other additional applications where Odd Sketches can be similarly applied.

Chapter 6

Conclusions

Big data analytics have been growing demands for not only novel platform system architectures but also computational algorithms to address the fast-paced big data needs. Designing and evaluating scalable and efficient algorithms that are able to handle complex big data analysis tasks without excessive use of computational resources have become a major research topic in computer science fields, such as data mining, machine learning, information retrieval, etc. Not surprisingly, in a wide range of data-intensive applications, randomized algorithms are substantially more efficient than the best known deterministic solutions. The use of randomization often leads to simpler and faster algorithms with little or no loss in performance. In addition, in most cases, the randomized algorithms can be organized to exploit parallel computing environments where existing deterministic algorithms fail to run at all.

In the thesis, we continued the line of research on exploiting randomization in big data analytics. We investigated the fundamental data analysis problems including angle-based outlier detection, large-scale SVM classification and high similarity estimation. We showed how to apply advanced randomized techniques, e.g. sampling and sketching, to solve these fundamental tasks. By taking advantage of benefits of randomized techniques, our proposed randomized algorithms are very scalable, compact and fast solutions. The experiments on large-scale real world data sets demonstrated the efficiency and scalability of our approaches on

such problems in large-scale data analysis. In short, the thesis is an exhibition of the power of randomization in big data analytics.

In future we hope to exploit the power of randomization not only on the algorithmic aspects but also on the platform system architectures for big data analytics. That means that the designed randomized algorithms should fit well into the MapReduce paradigm for massive scalability across hundreds or thousands of servers in a Hadoop cluster. Therefore we can achieve significant parallel and sequential speedups.

In closing, randomization not only plays an important role in algorithm design, but also provides a powerful framework to address a wide range of data-intensive applications in modern massive data set analysis.

Appendix A

CW Trick

We describe the pseudo-code of CW-trick to generate 4-wise independent random variables. This trick will use the Mersenne prime $\mathbf{PRIME} = 2^{31} - 1$ to generate 4-wise independent random variable.

Algorithm 7 CW-trick(x, a, b, c, d, e)

Ensure: Return a 4-wise independent random variable

1: $h = hash31(hash31(hash31(hash31(x, a, b), x, c), x, d), x, e)$
2: $h = h\&\mathbf{PRIME}$
3: **return** h

Algorithm 8 hash31(x, a, b)

Ensure: Return a 2-wise independent random variable

1: $h = a * x + b$
2: $h = h + h >> 31$
3: **return** $h\&\mathbf{PRIME}$

Appendix B

Count Sketch-based estimator

Lemma B.1. *Given two points $x, y \in \mathbb{R}^d$, we denote by $Cx, Cy \in \mathbb{R}^k$ the respective Count Sketches of x, y on the 2-wise hash function $h : [d] \to [k]$ and 4-wise hash function $s : [d] \to \{+1, -1\}$, we have*

$$\begin{aligned}\mathbf{E}[\langle Cx, Cy\rangle] &= \langle x, y\rangle\,,\\ \mathbf{Var}[\langle Cx, Cy\rangle] &= \frac{1}{k}\left(\sum_{i\neq j} x_i^2 y_j^2 + \sum_{i\neq j} x_i y_i x_j y_j\right).\end{aligned}$$

Proof. Consider a random variable $\xi_{ij} = 1$ iff $i = j$, and 0 otherwise, for any $i, j, k, l \in [d]$, we have

$$\langle Cx, Cy\rangle = \sum_{i,j} x_i y_j s(i)s(j)\xi_{h(i),h(j)} = \langle x, y\rangle + \sum_{i\neq j} x_i y_j s(i)s(j)\xi_{h(i),h(j)}.$$

Recall that $h : [d] \to [k]$ is 2-wise independent and $s : [d] \to \{+1, -1\}$ is 4-wise independent. Applying the independence property of these hash functions, we can verify that

$$\mathbf{E}\left[\langle Cx, Cy\rangle\right] = \langle x, y\rangle\,.$$

For the variance, we compute $\mathbf{E}\big[\langle Cx, Cy\rangle^2\big]$ by expanding $\langle Cx, Cy\rangle^2$ as follows:

$$\begin{aligned}
\langle Cx, Cy\rangle^2 &= \left(\langle x, y\rangle + \sum_{i\neq j} x_i y_j s(i)s(j)\xi_{h(i),h(j)}\right)\left(\langle x, y\rangle + \sum_{k\neq l} x_k y_l s(k)s(l)\xi_{h(k),h(l)}\right) \\
&= \langle x, y\rangle^2 + \langle x, y\rangle\left(\sum_{i\neq j} x_i y_j s(i)s(j)\xi_{h(i),h(j)} + \sum_{k\neq l} x_k y_l s(k)s(l)\xi_{h(k),h(l)}\right) \\
&+ \left(\sum_{i\neq j} x_i y_j s(i)s(j)\xi_{h(i),h(j)}\right)\left(\sum_{k\neq l} x_k y_l s(k)s(l)\xi_{h(k),h(l)}\right) \\
&= \langle x, y\rangle^2 + \langle x, y\rangle\left(\sum_{i\neq j} x_i y_j s(i)s(j)\xi_{h(i),h(j)} + \sum_{k\neq l} x_k y_l s(k)s(l)\xi_{h(k),h(l)}\right) \\
&+ \sum_{\substack{i\neq j,k\neq l\\ i=k,j=l}} x_i^2 y_j^2 \xi^2_{h(i),h(j)} + \sum_{\substack{i\neq j,k\neq l\\ i=l,j=k}} x_i x_j y_i y_j \xi^2_{h(i),h(j)} \\
&+ \sum_{\substack{i\neq j,k\neq l\\ i=k,j\neq l}} x_i^2 y_j y_l s(j)s(l)\xi_{h(i),h(j)}\xi_{h(i),h(l)} + \sum_{\substack{i\neq j,k\neq l\\ i=l,j\neq k}} x_i x_k y_i y_j s(j)s(k)\xi_{h(i),h(j)}\xi_{h(k),h(i)} \\
&+ \sum_{\substack{i\neq j,k\neq l\\ i\neq k,j=l}} x_i x_k y_j^2 s(i)s(k)\xi_{h(i),h(j)}\xi_{h(k),h(j)} + \sum_{\substack{i\neq j,k\neq l\\ i\neq l,j=k}} x_i x_j y_j y_l s(i)s(l)\xi_{h(i),h(j)}\xi_{h(j),h(l)} \\
&+ \sum_{i\neq j\neq k\neq l} x_i y_j x_k y_l s(i)s(j)s(k)s(l)\xi_{h(i),h(j)}\xi_{h(k),h(l)}.
\end{aligned}$$

Applying the independence property of hash functions again, we get

$$\mathbf{E}[\langle Cx, Cy\rangle^2] = \langle x, y\rangle^2 + \frac{1}{k}\left(\sum_{i\neq j} x_i^2 y_j^2 + \sum_{i\neq j} x_i y_i x_j y_j\right).$$

Using the fact that $\mathbf{Var}[X] = \mathbf{E}[X^2] - \mathbf{E}[X]^2$ proves the claim of variance. □

Bibliography

[1] D. Achlioptas. Database-friendly random projections. In *Proceedings of PODS'01*, pages 274–281, 2001.

[2] C. C. Aggarwal and P. S. Yu. Outlier detection for high dimensional data. In *Proceedings of SIGMOD'01*, pages 37–46, 2001.

[3] N. Ailon and B. Chazelle. Approximate nearest neighbors and the fast johnson-lindenstrauss transform. In *Proceedings of STOC'06*, pages 557–563, 2006.

[4] N. Alon, Y. Matias, and M. Szegedy. The space complexity of approximating the frequency moments. In *Proceedings of STOC'96*, pages 20–29, 1996.

[5] Y. Bachrach, E. Porat, and J. S. Rosenschein. Sketching techniques for collaborative filtering. In *Proceedings of IJCAI'09*, pages 2016–2021, 2009.

[6] Z. Bar-Yossef, T. Jayram, R. Kumar, D. Sivakumar, and L. Trevisan. Counting distinct elements in a data stream. In *RANDOM*, pages 1–10. Springer, 2002.

[7] S. D. Bay and M. Schwabacher. Mining distance-based outliers in near linear time with randomization and a simple pruning rule. In *Proceedings of KDD'03*, pages 29–38, 2003.

[8] M. Bendersky and W. B. Croft. Finding text reuse on the web. In *Proceedings of WSDM'09*, pages 262–271, 2009.

[9] K. S. Beyer, J. Goldstein, R. Ramakrishnan, and U. Shaft. When is "nearest neighbor" meaningful? In *Proceedings of ICDT'99*, pages 217–235, 1999.

[10] V. Braverman, K.-M. Chung, Z. Liu, M. Mitzenmacher, and R. Ostrovsky. AMS without 4-wise independence on product domains. In *Proceedings of STACS'10*, pages 119–130, 2008.

[11] M. M. Breunig, H.-P. Kriegel, R. T. Ng, and J. Sander. LOF: Identifying density-based local outliers. In *Proceedings of SIGMOD'00*, pages 93–104, 2000.

[12] A. Z. Broder. On the resemblance and containment of documents. *Sequences'97*, pages 21–29, 1997.

[13] A. Z. Broder, M. Charikar, A. M. Frieze, and M. Mitzenmacher. Min-wise independent permutations (extended abstract). In *Proceedings of STOC'98*, pages 327–336, 1998.

[14] A. Z. Broder, S. C. Glassman, M. S. Manasse, and G. Zweig. Syntactic clustering of the web. *Computer Networks*, 29(8-13):1157–1166, 1997.

[15] C.-C. Chang and C.-J. Lin. LIBSVM: A library for support vector machines. *ACM Transactions on Intelligent Systems and Technology*, 2:27:1–27:27, 2011.

[16] M. Charikar. Similarity estimation techniques from rounding algorithms. In *Proceedings of STOC'02*, pages 380–388, 2002.

[17] M. Charikar, K. Chen, and M. Farach-Colton. Finding frequent items in data streams. In *Proceedings of ICALP'02*, pages 693–703, 2002.

[18] F. Chierichetti, R. Kumar, S. Lattanzi, M. Mitzenmacher, A. Panconesi, and P. Raghavan. On compressing social networks. In *Proceedings of KDD'09*, pages 219–228, 2009.

[19] R. Chitta, R. Jin, T. C. Havens, and A. K. Jain. Approximate kernel k-means: solution to large scale kernel clustering. In *Proceedings of KDD'11*, pages 895–903, 2011.

[20] R. Chitta, R. Jin, and A. K. Jain. Efficient kernel clustering using random fourier features. In *Proceedings of ICDM'12*, pages 161–170, 2012.

[21] E. Cohen, M. Datar, S. Fujiwara, A. Gionis, P. Indyk, R. Motwani, J. D. Ullman, and C. Yang. Finding interesting associations without support pruning. *IEEE Trans. Knowl. Data Eng.*, 13(1):64–78, 2001.

[22] A. Das, M. Datar, A. Garg, and S. Rajaram. Google news personalization: scalable online collaborative filtering. In *Proceedings of WWW'07*, pages 271–280, 2007.

[23] S. Dasgupta and A. Gupta. An elementary proof of the Johnson-Lindenstrauss lemma. Technical report, International Computer Science Institute, Berkeley, US, 1999.

[24] J. Dean and S. Ghemawat. MapReduce: Simplified data processing on large clusters. In *Proceedings of OSDI'04*, pages 137–150, 2004.

[25] P. Drineas and M. W. Mahoney. On the Nyström method for approximating a gram matrix for improved kernel-based learning. *Journal of Machine Learning Research*, 6:2153–2175, 2005.

[26] D. Eppstein, M. T. Goodrich, F. Uyeda, and G. Varghese. What's the difference?: efficient set reconciliation without prior context. In *Proceedings of SIGCOMM'11*, pages 218–229, 2011.

[27] R.-E. Fan, K.-W. Chang, C.-J. Hsieh, X.-R. Wang, and C.-J. Lin. LIBLINEAR: A library for large linear classification. *Journal of Machine Learning Research*, 9:1871–1874, 2008.

[28] S. Fine and K. Scheinberg. Efficient SVM training using low-rank kernel representations. *Journal of Machine Learning Research*, 2:243–264, 2001.

[29] A. Frank and A. Asuncion. UCI machine learning repository, 2010.

[30] A. Ghoting, S. Parthasarathy, and M. E. Otey. Fast mining of distance-based outliers in high-dimensional datasets. *Data Mining and Knowledge Discovery*, 16(3):349–364, 2008.

[31] M. X. Goemans and D. P. Williamson. Improved approximation algorithms for maximum cut and satisfiability problems using semidefinite programming. *Journal of the ACM*, 42(6):1115–1145, 1995.

[32] S. Gollapudi and R. Panigrahy. Exploiting asymmetry in hierarchical topic extraction. In *Proceedings of CIKM'06*, pages 475–482, 2006.

[33] S. Gollapudi and A. Sharma. An axiomatic approach for result diversification. In *Proceedings of WWW'09*, pages 381–390, 2009.

[34] M. R. Henzinger. Finding near-duplicate web pages: a large-scale evaluation of algorithms. In *Proceedings of SIGIR'06*, pages 284–291, 2006.

[35] A. Hinneburg, C. C. Aggarwal, and D. A. Keim. What is the nearest neighbor in high dimensional spaces? In *Proceedings of VLDB'00*, pages 506–515, 2000.

[36] P. Indyk and A. McGregor. Declaring independence via the sketching of sketches. In *Proceedings of SODA'08*, pages 737–745, 2008.

[37] P. Indyk and R. Motwani. Approximate nearest neighbors: Towards removing the curse of dimensionality. In *Proceedings of STOC'98*, pages 604–613, 1998.

[38] S. Ioffe. Improved consistent sampling, weighted minhash and l1 sketching. In *Proceedings of ICDM'10*, pages 246–255, 2010.

[39] T. Joachims. Training linear SVMs in linear time. In *Proceedings of KDD'06*, pages 217–226, 2006.

[40] W. B. Johnson and J. Lindenstrauss. Extensions of Lipschitz mappings into a Hilbert space. *Contemporary mathematics*, 26(189-206):1, 1984.

[41] P. Kar and H. Karnick. Random feature maps for dot product kernels. In *Proceedings of AISTATS'12*, pages 583–591, 2012.

[42] E. M. Knorr and R. T. Ng. Algorithms for mining distance-based outliers in large datasets. In *Proceedings of VLDB'98*, pages 392–403, 1998.

[43] H.-P. Kriegel, M. Schubert, and A. Zimek. Angle-based outlier detection in high-dimensional data. In *Proceedings of KDD'08*, pages 444–452, 2008.

[44] H.-P. Kriegel, M. Schubert, and A. Zimek. Outlier detection techniques. In *Tutorial at KDD'10*, 2010.

[45] K. Kutzkov, A. Bifet, F. Bonchi, and A. Gionis. STRIP: stream learning of influence probabilities. In *Proceedings of KDD'13*, pages 275–283, 2013.

[46] Q. V. Le, T. Sarlós, and A. J. Smola. Fastfood - computing hilbert space expansions in loglinear time. In *Proceedings of ICML'13*, pages 244–252, 2013.

[47] Y. LeCun, L. Bottou, Y. Bengio, and P. Haffner. Gradient-based learning applied to document recognition. *Proceedings of the IEEE*, 86:2278–2324, 1998.

[48] P. Li and A. C. König. b-bit minwise hashing. In *Proceedings of WWW'10*, pages 671–680, 2010.

[49] P. Li, A. Shrivastava, J. L. Moore, and A. C. König. Hashing algorithms for large-scale learning. In *Advances in NIPS'11*, pages 2672–2680, 2011.

[50] V. Mahadevan, W. Li, V. Bhalodia, and N. Vasconcelos. Anomaly detection in crowded scenes. In *Proceedings of CVPR'10*, pages 1975–1981, 2010.

[51] S. Maji and A. C. Berg. Max-margin additive classifiers for detection. In *Proceedings of ICCV'09*, pages 40–47, 2009.

[52] M. Manasse, F. McSherry, and K. Talwar. Consistent weighted sampling. *MSR-TR-2010-73 technical report*, 2010.

[53] G. S. Manku, A. Jain, and A. D. Sarma. Detecting near-duplicates for web crawling. In *Proceedings of WWW'07*, pages 141–150, 2007.

[54] M. Mitzenmacher and E. Upfal. *Probability and Computing: Randomized Algorithms and Probabilistic Analysis*. Cambridge University Press, 2005.

[55] E. Müller, M. Schiffer, and T. Seidl. Statistical selection of relevant subspace projections for outlier ranking. In *Proceedings of ICDE'11*, pages 434–445, 2011.

[56] E. Osuna, R. Freund, and F. Girosi. An improved training algorithm for support vector machines. In *Proceedings of NNSP'97*, pages 276–285, 1997.

[57] R. Pagh. Compressed matrix multiplication. In *Proceedings of ICTS'12*, pages 442–451, 2012.

[58] S. Papadimitriou, H. Kitagawa, P. B. Gibbons, and C. Faloutsos. LOCI: Fast outlier detection using the local correlation integral. In *Proceedings of ICDE'03*, pages 315–326, 2003.

[59] M. Pătraşcu and M. Thorup. The power of simple tabulation hashing. In *Proceedings of STOC'11*, pages 1–10, 2011.

[60] A. Rahimi and B. Recht. Random features for large-scale kernel machines. In *Advances in NIPS'07*, pages 1177–1184, 2007.

[61] S. Ramaswamy, R. Rastogi, and K. Shim. Efficient algorithms for mining outliers from large data sets. In *Proceedings of SIGMOD'00*, pages 427–438, 2000.

[62] B. Schökopf and A. J. Smola. *Learning with kernels: Support vector machines, regularization, Optimization, and Beyond*. MIT Press, 2001.

[63] E. F. Schuster and A. N. Philippou. The odds in some odd-even games. *The American Mathematical Monthly*, 82:646–648, 1975.

[64] S. Shalev-Shwartz, Y. Singer, and N. Srebro. Pegasos: Primal estimated sub-gradient solver for SVM. In *Proceedings of ICML'07*, pages 807–814, 2007.

[65] A. J. Smola and B. Schökopf. Sparse greedy matrix approximation for machine learning. In *Proceedings of ICML'00*, pages 911–918, 2000.

[66] M. Thorup and Y. Zhang. Tabulation-based 5-independent hashing with applications to linear probing and second moment estimation. *SIAM J. Comput.*, 41(2):293–331, 2012.

[67] T. Urvoy, E. Chauveau, P. Filoche, and T. Lavergne. Tracking web spam with html style similarities. *TWEB*, 2(1), 2008.

[68] A. Vedaldi and A. Zisserman. Efficient additive kernels via explicit feature maps. In *Proceedings of CVPR'10*, pages 3539–3546, 2010.

[69] S. S. Vempala. *The Random Projection Method*. American Mathematical Society, 2003.

[70] S. Vempati, A. Vedaldi, A. Zisserman, and C. V. Jawahar. Generalized RBF feature maps for efficient detection. In *Proceedings of BMVC'10*, pages 1–11, 2010.

[71] Y. Wang, S. Parthasarathy, and S. Tatikonda. Locality sensitive outlier detection: A ranking driven approach. In *Proceedings of ICDE'11*, pages 410–421, 2011.

[72] M. N. Wegman and L. Carter. New hash functions and their use in authentication and set equality. *Journal of Computer and System Sciences*, 22(3):265–279, 1981.

[73] K. Q. Weinberger, A. Dasgupta, J. Langford, A. J. Smola, and J. Attenberg. Feature hashing for large scale multitask learning. In *Proceedings of ICML'09*, pages 1113–1120, 2009.

[74] R. Wheeler and J. S. Aitken. Multiple algorithms for fraud detection. *Knowledge Based Systems*, 13(2-3):93–99, 2000.

[75] C. K. I. Williams and M. Seeger. Using the Nyström method to speed up kernel machines. In *Advances in NIPS'01*, pages 682–688, 2001.

[76] T. Yang, Y.-F. Li, M. Mahdavi, R. Jin, and Z.-H. Zhou. Nyström method vs random fourier features: A theoretical and empirical comparison. In *Advances in NIPS'12*, pages 485–493, 2012.